



KASCADE-Grande

W.D. APEL¹, J.C. ARTEAGA-VELÁZQUEZ², K. BEKK¹, M. BERTAINA³, J. BLÜMER^{1,4}, H. BOZDOĞ¹, I.M. BRANCUS⁵, P. BUCHHOLZ⁶, E. CANTONI^{3,7}, A. CHIAVASSA³, F. COSSAVELLA^{4,13}, K. DAUMILLER¹, V. DE SOUZA⁸, F. DI PIERRO³, P. DOLL¹, R. ENGEL¹, J. ENGLER¹, M. FINGER⁴, D. FUHRMANN⁹, P.L. GHIA⁷, H.J. GILS¹, R. GLASSTETTER⁹, C. GRUPEN⁶, A. HAUNGS¹, D. HECK¹, J.R. HÖRANDEL¹⁰, D. HUBER⁴, T. HUEGE¹, P.G. ISAR^{1,14}, K.-H. KAMPERT⁹, D. KANG⁴, H.O. KLAGES¹, K. LINK⁴, P. ŁUCZAK¹¹, M. LUDWIG⁴, H.J. MATHES¹, H.J. MAYER¹, M. MELISSAS⁴, J. MILKE¹, B. MITRICA⁵, C. MORELLO⁷, G. NAVARRA^{3,15}, J. OEHLISCHLÄGER¹, S. OSTAPCHENKO^{1,16}, S. OVER⁶, N. PALMIERI⁴, M. PETCU⁵, T. PIEROG¹, H. REBEL¹, M. ROTH¹, H. SCHIELER¹, F.G. SCHRÖDER¹, O. SIMA¹², G. TOMA⁵, G.C. TRINCHERO⁷, H. ULRICH¹, A. WEINDL¹, J. WOCHLE¹, M. WOMMER¹, J. ZABIEROWSKI¹¹

¹ *Institut für Kernphysik, KIT - Karlsruher Institut für Technologie, Germany*

² *Universidad Michoacana, Instituto de Física y Matemáticas, Morelia, Mexico*

³ *Dipartimento di Fisica Generale dell' Università Torino, Italy*

⁴ *Institut für Experimentelle Kernphysik, KIT - Karlsruher Institut für Technologie, Germany*

⁵ *National Institute of Physics and Nuclear Engineering, Bucharest, Romania*

⁶ *Fachbereich Physik, Universität Siegen, Germany*

⁷ *Istituto di Fisica dello Spazio Interplanetario, INAF Torino, Italy*

⁸ *Universidade São Paulo, Instituto de Física de São Carlos, Brasil*

⁹ *Fachbereich Physik, Universität Wuppertal, Germany*

¹⁰ *Dept. of Astrophysics, Radboud University Nijmegen, The Netherlands*

¹¹ *Soltan Institute for Nuclear Studies, Lodz, Poland*

¹² *Department of Physics, University of Bucharest, Bucharest, Romania*

¹³ *now at: Max-Planck-Institut Physik, München, Germany;* ¹⁴ *now at: Institute Space Sciences, Bucharest, Romania;* ¹⁵ *deceased;* ¹⁶ *now at: Univ Trondheim, Norway*
 haungs@kit.edu

Abstract: Contributions of the KASCADE-Grande Collaboration to the 32nd International Cosmic Ray Conference, Beijing, August, 2011.

Keywords: KASCADE-Grande, Cosmic Rays, air showers, 10^{16} - 10^{18} eV

Contents

- | | |
|--|--|
| <p>1. page 3: Cosmic Ray Measurements with KASCADE-Grande</p> <p>2. page 7: A study of the mass composition of cosmic rays based on an event-by-event assignment with KASCADE-Grande data</p> <p>3. page 11: Study of the ratio muon size to shower size as a mass sensitive parameter of KASCADE-Grande</p> <p>4. page 15: The cosmic ray elemental composition based on measurement of the N_μ/N_{ch} ratio with KASCADE-Grande</p> | <p>5. page 19: KASCADE-Grande measurements of energy spectra for elemental groups of cosmic rays</p> <p>6. page 23: Primary energy reconstruction from the S(500) observable recorded with the KASCADE-Grande Array</p> <p>7. page 27: Tests of hadronic interaction models with the KASCADE-Grande muon data</p> <p>8. page 31: A direct measurement of the muon component of air showers by the KASCADE-Grande Experiment</p> <p>9. page 35: On the primary mass sensitivity of muon pseudorapidities measured with KASCADE-Grande</p> <p>10. page 39: Gamma-Ray Source Studies using a Muon Tracking Detector (MTD)</p> |
|--|--|



Cosmic Ray Measurements with KASCADE-Grande

A. HAUNGS¹, W.D. APEL¹, J.C. ARTEAGA-VELÁZQUEZ², K. BEKK¹, M. BERTAINA³, J. BLÜMER^{1,4}, H. BOZDOĞ¹, I.M. BRANCUS⁵, P. BUCHHOLZ⁶, E. CANTONI^{3,7}, A. CHIAVASSA³, F. COSSAVELLA^{4,13}, K. DAUMILLER¹, V. DE SOUZA⁸, F. DI PIERRO³, P. DOLL¹, R. ENGEL¹, J. ENGLER¹, M. FINGER⁴, D. FUHRMANN⁹, P.L. GHIA⁷, H.J. GILS¹, R. GLASSTETTER⁹, C. GRUPEN⁶, D. HECK¹, J.R. HÖRANDEL¹⁰, D. HUBER⁴, T. HUEGE¹, P.G. ISAR^{1,14}, K.-H. KAMPERT⁹, D. KANG⁴, H.O. KLAGES¹, K. LINK⁴, P. ŁUCZAK¹¹, M. LUDWIG⁴, H.J. MATHES¹, H.J. MAYER¹, M. MELISSAS⁴, J. MILKE¹, B. MITRICA⁵, C. MORELLO⁷, G. NAVARRA^{3,15}, J. OEHLSCHLÄGER¹, S. OSTAPCHENKO^{1,16}, S. OVER⁶, N. PALMIERI⁴, M. PETCU⁵, T. PIEROG¹, H. REBEL¹, M. ROTH¹, H. SCHIELER¹, F.G. SCHRÖDER¹, O. SIMA¹², G. TOMA⁵, G.C. TRINCHERO⁷, H. ULRICH¹, A. WEINDL¹, J. WOCHLE¹, M. WOMMER¹, J. ZABIEROWSKI¹¹

¹ *Institut für Kernphysik, KIT - Karlsruher Institut für Technologie, Germany*

² *Universidad Michoacana, Instituto de Física y Matemáticas, Morelia, Mexico*

³ *Dipartimento di Fisica Generale dell' Università Torino, Italy*

⁴ *Institut für Experimentelle Kernphysik, KIT - Karlsruher Institut für Technologie, Germany*

⁵ *National Institute of Physics and Nuclear Engineering, Bucharest, Romania*

⁶ *Fachbereich Physik, Universität Siegen, Germany*

⁷ *Istituto di Fisica dello Spazio Interplanetario, INAF Torino, Italy*

⁸ *Universidade São Paulo, Instituto de Física de São Carlos, Brasil*

⁹ *Fachbereich Physik, Universität Wuppertal, Germany*

¹⁰ *Dept. of Astrophysics, Radboud University Nijmegen, The Netherlands*

¹¹ *Soltan Institute for Nuclear Studies, Lodz, Poland*

¹² *Department of Physics, University of Bucharest, Bucharest, Romania*

¹³ *now at: Max-Planck-Institut Physik, München, Germany;* ¹⁴ *now at: Institute Space Sciences, Bucharest, Romania;* ¹⁵ *deceased;* ¹⁶ *now at: Univ Trondheim, Norway*
haungs@kit.edu

Abstract: The detection of high-energy cosmic rays above a few hundred TeV is realized by the observation of extensive air-showers. By using the multi-detector setup of KASCADE-Grande, energy spectrum, elemental composition, and anisotropies of high-energy cosmic rays in the energy range from below the knee up to 1 EeV are investigated. The most distinct feature of the spectrum, the knee, is thought to be the beginning of the end of the galactic origin of cosmic rays. As the highest energies (above the ankle) are most probably of extragalactic origin, between 10 PeV to 1 EeV one expects the transition of galactic to extragalactic origin. KASCADE-Grande is dedicated to explore this transition region. The estimation of energy and mass of the high-energy primary particles is based on the combined investigation of the charged particle, the electron, and the muon components measured by the detector arrays of Grande and KASCADE. The latest analysis results have shown that a knee-like structure in the all-particle energy spectrum at 83 PeV is due to a decrease of flux of the heavy mass component. In this contribution an overview is given on various different analysis methods to verify this finding.

Keywords: KASCADE-Grande, 10-1000PeV, spectrum and composition

KASCADE-Grande: Main parts of the experiment are the Grande array spread over an area of $700 \times 700 \text{ m}^2$, the original KASCADE array covering $200 \times 200 \text{ m}^2$ with unshielded and shielded detectors, and additional muon tracking devices. This multi-detector system allows us to investigate the energy spectrum, composition, and anisotropies of cosmic rays in the energy range up to 1 EeV. The estimation of energy and mass of the primary particles is based on the combined investigation of the charged particle, the elec-

tron, and the muon components measured by the detector arrays of Grande and KASCADE.

The multi-detector experiment KASCADE [1] (located at 49.1°n , 8.4°e , 110 m a.s.l.) was extended to KASCADE-Grande in 2003 by installing a large array of 37 stations consisting of 10 m^2 scintillation detectors each (fig. 1). KASCADE-Grande [2] provides an area of 0.5 km^2 and operates jointly with the existing KASCADE detectors. The joint measurements with the KASCADE muon track-

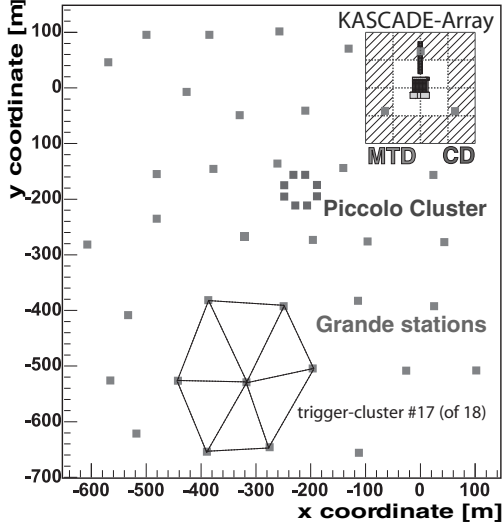


Figure 1: Layout of the KASCADE-Grande experiment: The original KASCADE (with Array, Muon Tracking Detector and Central Detector), the distribution of the 37 stations of the Grande array, and the small Piccolo cluster for fast trigger purposes are shown. The outer 12 clusters of the KASCADE array consist of μ - and e/γ -detectors, the inner 4 clusters of e/γ -detectors, only.

ing devices are ensured by an additional cluster (Piccolo) close to the center of KASCADE-Grande for fast trigger purposes. For results of the muon tracking devices see references [3, 4]. While the Grande detectors are sensitive to charged particles, the KASCADE array detectors measure the electromagnetic component and the muonic component separately. These muon detectors enable to reconstruct the total number of muons on an event-by-event basis also for Grande triggered events.

Basic shower observables like the core position, angle-of-incidence, and total number of charged particles are provided by the measurements of the Grande stations. A core position resolution of ≈ 5 m, a direction resolution of $\approx 0.7^\circ$, and a resolution of the total particle number in the showers of $\approx 15\%$ is achieved. The total number of muons (N_μ resolution $\approx 25\%$) is calculated using the core position determined by the Grande array and the muon densities measured by the KASCADE muon array detectors. Full efficiency for triggering and reconstruction of air-showers is reached at primary energy of $\approx 10^{16}$ eV, slightly varying on the cuts needed for the reconstruction of the different observables [2].

The strategy of the KASCADE-Grande data analysis to reconstruct the energy spectrum and elemental composition of cosmic rays is to use the multi-detector set-up of the experiment and to apply different analysis methods to the same data sample. This has advantages in various aspects: One would expect the same results by all methods when the measurements are accurate enough, when the reconstructions work without failures, and when the Monte-

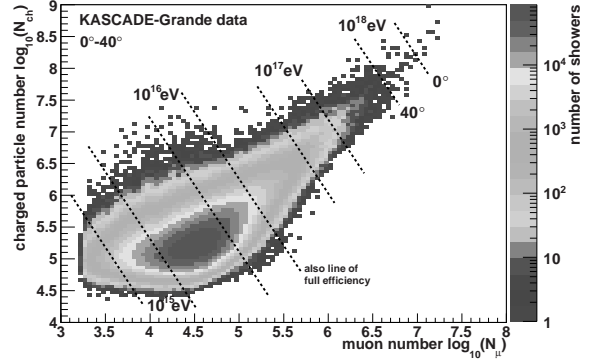


Figure 2: Two-dimensional distribution of the shower sizes charged particle number and total muon number as measured by KASCADE-Grande. All quality cuts are applied, i.e. these data are the basis for the mass composition studies.

Carlo simulations describe correctly and consistently the shower development and detector response.

The main air-shower observables of KASCADE-Grande, shower size and total number of muons, could be reconstructed with high precision and low systematic uncertainties and are used in the following for the data analysis (fig. 2).

The all-particle energy spectrum: In a first step of the analysis, we reconstructed the all-particle energy spectrum. Applying various reconstruction methods to the KASCADE-Grande data the obtained all-particle energy spectra are compared for cross-checks of the reconstruction, for studies of systematic uncertainties and for testing the validity of the underlying hadronic interaction models. By combining both observables and using the hadronic interaction model QGSJet-II, a composition independent all-particle energy spectrum of cosmic rays is reconstructed in the energy range of 10^{16} eV to 10^{18} eV within a total uncertainty in flux of 10-15%.

Despite the overall smooth power law behavior of the resulting all-particle spectrum, there are some structures observed, which do not allow to describe the spectrum with a single slope index [5]. There is a feature in the spectrum showing a small break at around $8 \cdot 10^{16}$ eV. The power law index of $\gamma = -2.95 \pm 0.05$ is obtained by fitting the range before this break. Applying a second power law above the break an index of $\gamma = -3.24 \pm 0.08$ is obtained (see figure 3). With a statistical significance of more than 2 sigma the two power laws are incompatible with each other. This slight slope change occurs at an energy where the rigidity dependent knee of the iron component would be expected (KASCADE QGSJet based analysis assigns the proton knee to an energy of $2 - 4 \cdot 10^{15}$ eV). Despite the fact, that the discussed spectrum is based on the QGSJet-II hadronic interaction model, there is confidence that the found structures of the energy spectrum remain stable. Tests with EPOS as well as investigations of the spec-

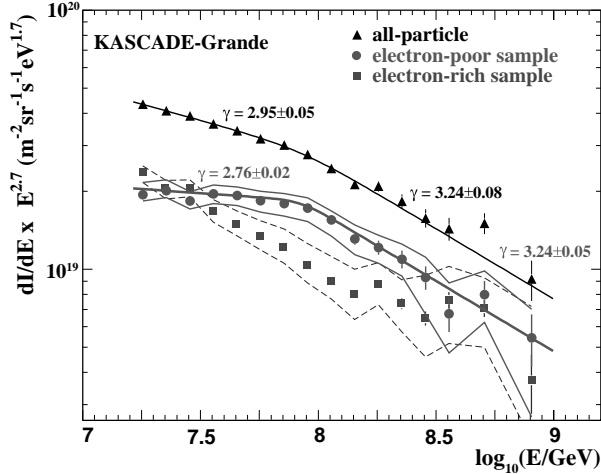


Figure 3: Reconstructed all-particle energy spectrum together with the spectra of the electron-poor and electron-rich components. Fits on the spectra and resulting slopes are also indicated.

tra of the pure (and independently obtained) observables shower size and total muon number, confirmed the structures [5].

Composition: A conclusion on the origin of the found structures in the all-particle spectrum is not possible without investigating the composition in detail in this energy range. The basic goal of the KASCADE-Grande experiment is the determination of the chemical composition in the primary energy range $10^{16} - 10^{18}$ eV. Like for the reconstruction of the energy, again several methods using different observables are applied to the registered data in order to study systematic uncertainties. However, the influence of predictions of the hadronic interaction models has a much larger influence on the composition than on the primary energy. As it is well known from KASCADE data analysis [6] that the relative abundances of the individual elements or elemental groups are very dependent on the hadronic interaction model underlying the analyses the strategy is to derive the energy spectra of the individual mass groups. The structure or characteristics of these spectra are found to be much less affected by the differences of the various hadronic interaction models than the relative abundance. The present goal is to verify the structure found in the all-particle energy spectrum at around 100 PeV in the individual mass group spectra and to assign it to a particular mass.

The main observables taken into account for composition studies at KASCADE-Grande are the shower size (N_{ch} , or the subsequently derived electron number N_e) and the muon shower size (N_μ). Figure 2 displays the correlation of these two observables, i.e. this distribution is the basis of the composition analysis with KASCADE-Grande data. For all the methods it is crucial to verify the sensitivity of the observables to different primary particles and the reproducibility of the measurements with the hadronic interac-

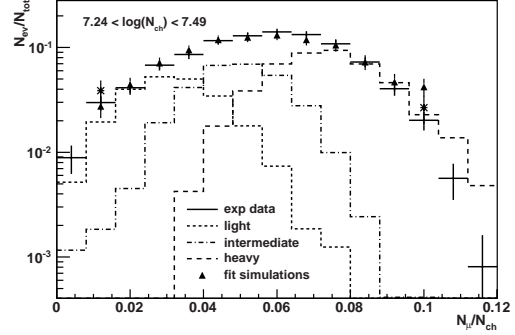


Figure 4: Shower size ratio distributions for a certain bin in charged particle number. Shown is the measured distribution as well as the simulated ones for three primary mass groups and the resulting sum.

tion model in use as a function of sizes and the atmospheric depth. So far, in the composition analysis we concentrate on interpreting the data with the hadronic interaction model QGSJet-II (and FLUKA as low energy interaction model).

Four methods of composition studies at KASCADE-Grande are discussed in the following, all showing the same result: The knee-like structure in the all-particle spectrum is due to the decrease of the flux of the heavy component of primary cosmic particles.

- **Charged particle – muon number ratio [7]:** The total number of charged particles N_{ch} and the total number of muons N_μ of each recorded event are considered and the distribution of N_μ/N_{ch} is studied in different intervals of N_{ch} (corresponding to different energy intervals) and zenith angle. The experimental distribution of the observable N_μ/N_{ch} is taken into account and fitted with a linear combination of elemental contributions from simulations, where we distinguish three groups: light, medium and heavy primaries. By this way the means and the widths of the distributions as two mass sensitive observables are taken into account (see as an example figure 4). The width of the data distribution is in all ranges of N_{ch} so large that always three mass groups are needed to describe them. Using the Monte Carlo simulations the corresponding energy of each mass group and shower size bin is assigned to obtain the spectra of the individual mass groups. Investigating the spectra of these individual mass groups, it is obvious that the break seen in the all particle spectrum is due to heavy primary masses.
- **The Y-cut method [8]:** Here, the shower ratio $Y_{CIC} = \log N_\mu / \log N_{ch}$ between the muon and the charged particle numbers, both corrected for atmospheric attenuation by the Constant Intensity Cut method (CIC), is used as parameter to separate the KASCADE-Grande data into different mass groups. MC simulations performed with CORSIKA on the

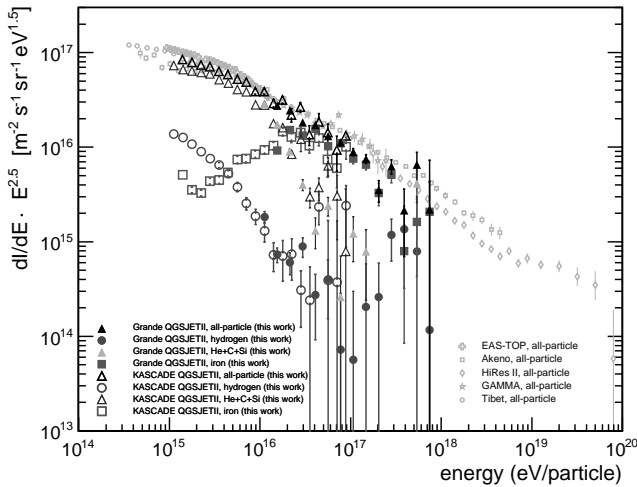


Figure 5: KASCADE and KASCADE-Grande reconstructed energy spectra of individual mass groups.

framework of FLUKA/QGSJET-II are employed to obtain the expected Y_{CIC} distributions as a function of the energy for different cosmic ray primaries as a basis for the separation. Then the Y_{CIC} -parameter is used to divide the KASCADE-Grande data into electron-rich and electron-poor events, i.e. generated by light and heavy primaries. The results confirm the findings above.

- The k-parameter method [9]: Using the above mentioned reconstruction of the energy spectrum by correlating the size of the charged particles N_{ch} and muons N_{μ} on an event-by-event basis, the mass sensitivity is minimized by means of the parameter $k(N_{ch}, N_{\mu})$. On the other hand, the evolution of k as a function of energy keeps track of the evolution of the composition, and allows an event-by-event separation between light and heavy primaries. Using k as separation parameter for different mass groups, where the exact values of k have to be determined with help of simulations, directly the energy spectra of the mass groups are obtained. Figure 3 shows the resulting spectra. As the significance of the break of the all-particle spectrum increases significantly when enhancing heavy primaries, it is obvious that this structure is introduced by heavy primaries.
- The Gold-unfolding method [10]: This method is based on the unfolding of the two-dimensional shower size spectrum (fig. 2) in a similar way as it was developed for the KASCADE data analysis [6]. Due to the fact that the accuracies in reconstructing the shower sizes for KASCADE-Grande are not as high as in case of KASCADE, for comparing both results, primary masses are combined to light (H), medium (He+C+Si) and heavy (Fe) spectra. The resulting individual mass group spectra can be combined to provide a solution for the entire energy

range from 1 PeV to 1 EeV. This analysis was performed for the combination of N_{ch} with N_{μ} [10] as well as for the combination N_e with N_{μ} . Figure 5 shows the results for the latter case [11]. The obtained spectra are compared with the results using KASCADE data in the lower energy range, both using the hadronic interaction model QGSJet II with FLUKA. The agreement in the overlapping energy range of the spectra is remarkable. The knee-like feature in the iron component is found at an energy which is about 26 times higher than the proton knee in case of KASCADE.

Summarizing, by these first composition studies it is seen that the knee-like feature in the energy spectrum at about $8 \cdot 10^{16}$ eV is due to a kink in the spectrum of the heavy component of primary cosmic particles. In addition, at least three primary elements are needed to describe the experimental data over the entire energy range accessible by KASCADE-Grande, i.e. up to 1 EeV. Furthermore, it was found that QGSJet-II, the hadronic interaction model in use, can fairly well reproduce the data and, in particular, provides a consistent solution on the elemental composition, independent of the method in use. One has to remark, that using another hadronic interaction model would probably lead to significant changes in the relative abundances of the elemental groups as different models predict different shower sizes for a certain energy and mass of the primary cosmic ray. But, we are confident that the obtained spectral form for the heavy and light component of the cosmic ray spectrum will remain unchanged.

Acknowledgement: KASCADE-Grande is supported by the BMBF of Germany, the MIUR and INAF of Italy, the Polish Ministry of Science and Higher Education and the Romanian Authority for Scientific Research.

References

- [1] T. Antoni et al. (KASCADE Collaboration), NIM A **513** (2003) 429.
- [2] W.-D. Apel et al. (KASCADE-Grande Collaboration), NIM A **620** (2010) 202.
- [3] P. Doll et al. (KASCADE-Grande Collaboration), ICRC 2011, these proceedings, #0274.
- [4] J. Zabierowski et al. (KASCADE-Grande Collaboration), ICRC 2011, these proceedings, #0273.
- [5] W.-D. Apel et al. (KASCADE-Grande Collaboration), Astrop. Phys. (2011), submitted.
- [6] T. Antoni et al. (KASCADE Collaboration), Astrop. Phys. **24** (2005) 1.
- [7] E. Cantoni et al. (KASCADE-Grande Collaboration), ICRC 2011, these proceedings, #0504.
- [8] J.C. Arteaga-Velazquez et al. (KASCADE-Grande Collaboration), ICRC 2011, these proceedings, #0739.
- [9] M. Bertaina et al. (KASCADE-Grande Collaboration), ICRC 2011, these proceedings, #0312.
- [10] D. Fuhrmann et al. (KASCADE-Grande Collaboration), ICRC 2011, these proceedings, #0280.
- [11] M. Finger, PhD-thesis Karlsruhe Institute of Technology (2011).



A study of the mass composition of cosmic rays based on an event-by-event assignment with KASCADE-Grande data

M. BERTAINA¹, W.D. APEL², J.C. ARTEAGA-VELÁZQUEZ³, K. BEKK², J. BLÜMER^{2,4}, H. BOZDOG², I.M. BRANCUS⁵, P. BUCHHOLZ⁶, E. CANTONI^{1,7}, A. CHIAVASSA¹, F. COSSAVELLA^{4,13}, K. DAUMILLER², V. DE SOUZA⁸, F. DI PIERRO¹, P. DOLL², R. ENGEL², J. ENGLER², M. FINGER⁴, D. FUHRMANN⁹, P.L. GHIA⁷, H.J. GILS², R. GLASSTETTER⁹, C. GRUPEN⁶, A. HAUNGS², D. HECK², J.R. HÖRANDEL¹⁰, D. HUBER⁴, T. HUEGE², P.G. ISAR^{2,14}, K.-H. KAMPERT⁹, D. KANG⁴, H.O. KLAGES², K. LINK⁴, P. ŁUCZAK¹¹, M. LUDWIG⁴, H.J. MATHES², H.J. MAYER², M. MELISSAS⁴, J. MILKE², B. MITRICA⁵, C. MORELLO⁷, G. NAVARRA^{1,15}, J. OEHLISCHLÄGER², S. OSTAPCHENKO^{2,16}, S. OVER⁶, N. PALMIERI⁴, M. PETCU⁵, T. PIEROG², H. REBEL², M. ROTH², H. SCHIELER², F.G. SCHRÖDER², O. SIMA¹², G. TOMA⁵, G.C. TRINCHERO⁷, H. ULRICH², A. WEINDL², J. WOCHOLE², M. WOMMER², J. ZABIEROWSKI¹¹

¹ *Dipartimento di Fisica Generale dell' Università Torino, Italy*

² *Institut für Kernphysik, KIT - Karlsruher Institut für Technologie, Germany*

³ *Universidad Michoacana, Instituto de Física y Matemáticas, Morelia, Mexico*

⁴ *Institut für Experimentelle Kernphysik, KIT - Karlsruher Institut für Technologie, Germany*

⁵ *National Institute of Physics and Nuclear Engineering, Bucharest, Romania*

⁶ *Fachbereich Physik, Universität Siegen, Germany*

⁷ *Istituto di Fisica dello Spazio Interplanetario, INAF Torino, Italy*

⁸ *Universidade São Paulo, Instituto de Física de São Carlos, Brasil*

⁹ *Fachbereich Physik, Universität Wuppertal, Germany*

¹⁰ *Dept. of Astrophysics, Radboud University Nijmegen, The Netherlands*

¹¹ *Soltan Institute for Nuclear Studies, Lodz, Poland*

¹² *Department of Physics, University of Bucharest, Bucharest, Romania*

¹³ *now at: Max-Planck-Institut Physik, München, Germany;* ¹⁴ *now at: Institute Space Sciences, Bucharest, Romania;* ¹⁵ *deceased;* ¹⁶ *now at: Univ Trondheim, Norway*
bertaina@to.infn.it

Abstract: The cosmic ray energy spectrum between 10^{16} eV and 10^{18} eV is reconstructed in KASCADE-Grande by correlating the size of the charged particles (N_{ch}) and muons (N_{μ}) on an event-by-event basis. In the energy assignment, the mass sensitivity is minimized by means of a parameter $k(N_{ch}, N_{\mu})$. On the other hand, the evolution of k as a function of energy keeps track of the evolution of the composition, and allows an event-by-event separation between electron rich and electron poor primaries. A first result on the evolution of k and its connection with the shape of the energy spectrum, is presented in the framework of the QGSJet II-03 interaction model.

Keywords: Composition, energy spectrum, 10^{16} - 10^{18} eV, KASCADE-Grande.

1 Introduction

The study of the energy spectrum and of the chemical composition of cosmic rays are fundamental tools to understand origin, acceleration and propagation of cosmic rays. The energy range between 10^{16} eV and 10^{18} eV is quite important from astrophysical point of view because it is expected that in this energy range the transition between galactic and extra-galactic origin of cosmic rays will occur. The results obtained at lower energies by KASCADE [1] and EAS-TOP [2] as well as by other experiments suggest that the knee in the primary energy spectrum around $3 - 4 \times$

10^{15} eV is due to the break in the spectra of light elements. Moreover, KASCADE results seem to indicate that a rigidity dependent mechanism is responsible for such knees. Therefore, a knee of the heaviest components would be expected in the range of 10^{16} eV to 10^{18} eV. Various theories with different assumptions try to explain the rather smooth behavior of the cosmic ray energy spectrum in this energy range (i.e. [3, 4]). In order to discriminate between the different models, a very precise measurement of the possible structures of the energy spectrum and of the evolution of the composition is needed.

2 The Technique

The technique employed to derive the all-particle energy spectrum and the abundance of electron-rich (e.r.) and electron-poor (e.p.) primaries is based on the correlation between the size of the charged particles (N_{ch}) and muons (N_{μ}) on an event-by-event basis. The method itself has been described in detail in [5].

A sample of Monte Carlo data was simulated including the full air shower development in the atmosphere, the response of the detector and its electronics as well as their uncertainties. In this way, the parameters reconstructed from simulation are obtained in the same way as for real data. The EAS events were generated with an isotropic distribution with spectral index $\gamma = -3$ and were simulated with CORSIKA [6] and the hadronic Monte Carlo generators FLUKA [7] and QGSJet II-03 [8]. Sets of simulated events were produced in the energy range from 10^{15} eV to 10^{18} eV with high statistics and for five elements: H, He, C, Si and Fe, representative for different mass groups (≈ 353.000 events per primary). Few events up to $3 \cdot 10^{18}$ eV were also generated in order to cross-check the reconstruction behavior at the highest energies.

Grande stations [9] are used to provide core position and angle-of-incidence, as well as the total number of charged particles in the shower, by means of a maximum likelihood procedure comparing the measured number of particles with the one expected from a modified NKG lateral distribution function [10] of charged particles in the EAS. The total number of muons is calculated using the core position determined by the Grande array and the muon densities measured by the KASCADE muon array detectors. The total number of muons N_{μ} in the shower disk (above the energy threshold of 230 MeV) is derived from a maximum likelihood estimation assuming a lateral distribution function based on the one proposed by Lagutin and Raikin [11]. The reconstruction procedures and obtained accuracies of KASCADE-Grande observables are described in detail in reference [9].

For the reconstructed events, we restricted ourselves to events with zenith angles lower than 40° . Additionally, only air showers with cores located in a central area on KASCADE-Grande were selected. With this cut on the fiducial area, border effects are discarded and possible under- and overestimations of the muon number for events close to and far away from the center of the KASCADE array are reduced. All of these cuts were applied also to the Monte Carlo simulations to study the effects and to optimize the cuts. Full efficiency for triggering and reconstruction of air-showers is reached at primary energy of $\approx 10^{16}$ eV, slightly depending on the cuts needed for the reconstruction of the different observables [9].

The analysis presented here is finally based on 1173 days of data and the cuts on the sensitive central area and zenith angle correspond to a total acceptance of $A = 1.976 \cdot 10^9$ cm²·sr, and an exposure of $N = 2.003 \cdot 10^{17}$ cm²·s·sr, respectively.

With Monte Carlo simulations a formula is obtained to

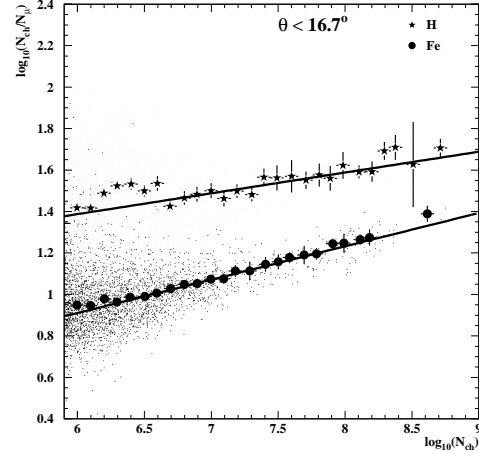


Figure 1: Scatter plot of the reconstructed N_{ch}/N_{μ} vs. N_{ch} for H and Fe primaries for the first angular bin. The full dots and error bars indicate the mean and its statistical error of the distribution of the individual events (small dots). The fits result in parameters c and d of expression 3.

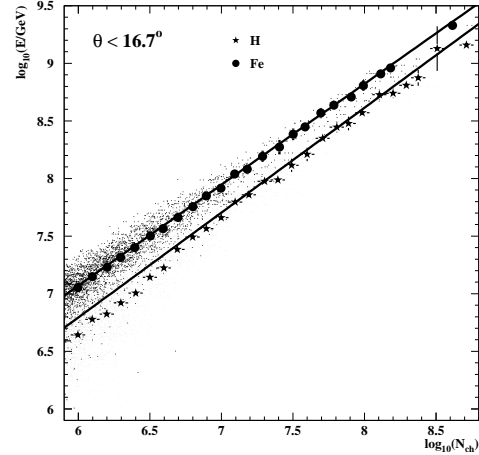


Figure 2: Scatter plot of E vs. N_{ch} for Fe and H primaries. The fits result in parameters a and b of expression 1.

calculate the primary energy per individual shower on the basis of N_{ch} and N_{μ} . The formula takes into account the mass sensitivity in order to minimize the composition dependence in the energy assignment, and at the same time, provides an event-by-event separation between e.r. and e.p. candidates. The formula is defined for 5 different zenith angle intervals ($\theta < 16.7$, $16.7 \leq \theta < 24.0$, $24.0 \leq \theta < 29.9$, $29.9 \leq \theta < 35.1$, $35.1 \leq \theta < 40.0$) independently, to take into account the shower attenuation in atmosphere. Data are combined only at the very last stage to obtain a unique power law spectrum and mass composition. The energy assignment is defined as $E = f(N_{ch}, k)$ (see equation 1), where N_{ch} is the size of the charged particle component and the parameter k is defined through the ratio of the sizes of the N_{ch} and muon (N_{μ}) components: $k = g(N_{ch}, N_{\mu})$ (see equation 2). The main aim of the k variable is to take into account the average differences in the N_{ch}/N_{μ} ratio among different primaries with same N_{ch} and the shower to

Table 1: Parameters of the calibration functions.

Angles[deg]	a		b		c		d	
	H	Fe	H	Fe	H	Fe	H	Fe
0.0 – 16.7	0.910	0.876	1.333	1.817	0.100	0.161	0.786	-0.055
16.7 – 24.0	0.894	0.878	1.495	1.923	0.081	0.179	0.884	-0.254
24.0 – 29.9	0.937	0.889	1.301	1.935	0.104	0.156	0.677	-0.170
29.9 – 35.1	0.934	0.881	1.458	2.099	0.109	0.171	0.543	-0.351
35.1 – 40.0	0.919	0.875	1.748	2.287	0.105	0.156	0.412	-0.348

shower fluctuations for events of the same primary mass:

$$\log_{10}(E[\text{GeV}]) = [a_H + (a_{Fe} - a_H) \cdot k] \cdot \log_{10}(N_{ch}) + b_H + (b_{Fe} - b_H) \cdot k \quad (1)$$

$$k = \frac{\log_{10}(N_{ch}/N_\mu) - \log_{10}(N_{ch}/N_\mu)_H}{\log_{10}(N_{ch}/N_\mu)_{Fe} - \log_{10}(N_{ch}/N_\mu)_H} \quad (2)$$

$$\log_{10}(N_{ch}/N_\mu)_{H,Fe} = c_{H,Fe} \cdot \log_{10}(N_{ch}) + d_{H,Fe}. \quad (3)$$

The k parameter is, by definition of eq. (2), a number centered around 0 for H showers and 1 for Fe ones if expressed as a function of N_{ch} , while slightly shifted when reported as a function of energy (see Fig. 4). The complete list of parameters a - d can be found in table 1.

Figs. 1, 2 show the scatter plots with the parametrizations

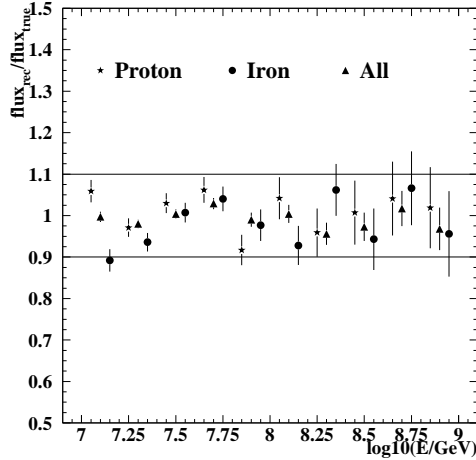


Figure 3: Ratio between the reconstructed and true simulated energy spectra for H, Fe and all mixed primaries summing up all angular bins.

defined for H and Fe in the first angular bin, while Fig. 3 shows the capability of reproducing simulated energy spectra. Pure spectra of H, Fe and a mixture of 5 different primaries with 20% abundance each are shown as examples. The true flux is always reproduced within 10% uncertainty.

3 Results

Fig. 4 shows, for the sum of the first two angular bins, the evolution of the k parameter as a function of the reconstructed energy obtained by simulating with QGSJet II-03 model pure H, He, C, Si, Fe primary spectra, as well as for the experimental data. Similar behavior is obtained also for the other angular bins. The error bars indicate the average

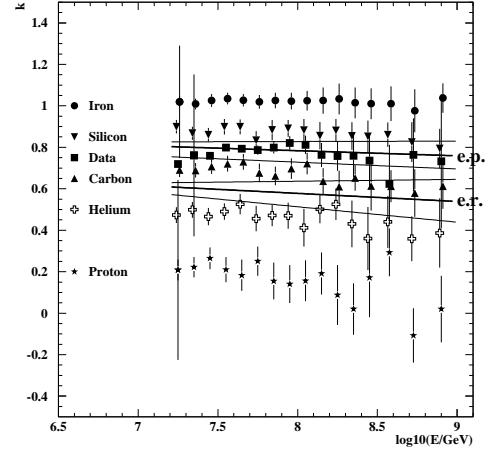


Figure 4: Evolution of the k parameter as a function of the reconstructed energy for experimental data compared with pure primary spectra for the angular range 0-24°. The error bars assign statistical as well as reconstruction uncertainties of k .

dispersion of the k parameter among different bins, which include statistical errors, and systematic uncertainty of equations 3 in each angular bin. Fig. 4 shows also two thick straight lines which are used to classify events into different mass groups. The classification is done for each angular bin, independently, to avoid possible systematic effects among the bins. The top thick line represents the separation between e.p. and intermediate samples and it is defined by fitting the $k_{e.p.}(E) = (k_{Si}(E) + k_C(E))/2$ points which are obtained by averaging the values of k for Si and C components. In analogy, the bottom thick line represents the separation line between intermediate and e.r. samples and it is defined by fitting the $k_{e.r.}(E) = (k_C(E) + k_{He}(E))/2$ points which are obtained by averaging the values of k for C and He components. In the following, e.p. events will be defined as those having a k value higher than the top thick line and e.r. events those with k below the bottom thick line. The region in between, which is dominated mainly by CNO and highly contaminated by Si and He, will be defined as the intermediate sample. Such an assignment is, therefore, chosen on an event-by-event basis. Naturally, the absolute abundances of the events in the three classes depend on the location of the straight lines. For that reason, two thin lines with different slopes bracket the range of possible positions of each thick line. They represent the uncertainties in defining these energy-dependent selection cuts.

Fig. 5 shows the flux of the three components classified as previously explained. The reconstructed spectrum of the e.p. sample shows a distinct knee-like feature around 8×10^{16} eV. Applying a fit of two power laws with a smooth transition [13] results in a statistical significance of 3.5σ that the entire spectrum cannot be fitted with a single power law. The change of the spectral slope is $\Delta\gamma = -0.48$ from $\gamma = -2.76 \pm 0.02$ to $\gamma = -3.24 \pm 0.05$ with the break position at $\log_{10}(E/\text{eV}) = 16.92 \pm 0.04$. Applying

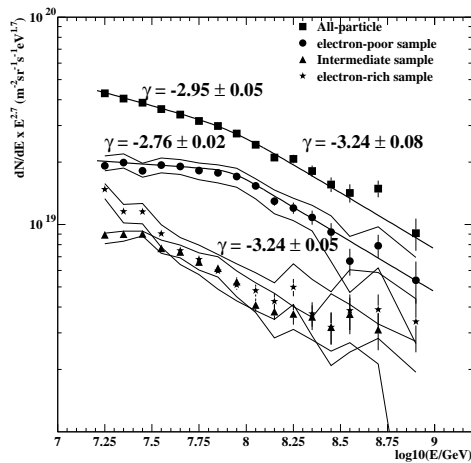


Figure 5: Reconstructed energy spectrum of the e.r., e.p. and intermediate samples as classified in the text together with the all-particle spectrum.

the same function to the all-particle spectrum results in a statistical significance of only 2.1σ that a fit of two power laws is needed to describe the spectrum. Here the change of the spectral slope is from $\gamma = -2.95 \pm 0.05$ to $\gamma = -3.24 \pm 0.08$, but with the break position again at $\log_{10}(E/\text{eV}) = 16.92 \pm 0.10$. The spectrum of the e.r. sample is compatible with a single power law ($\gamma \sim -3.37$).

The error bands in the spectra show that the result is independent from the particular choice of the selection-cut lines. However, in order to further validate the present result, parallel shifts of the cut-line of the e.p. sample have been applied. Specifically, by shifting the cut line to higher values of k , the e.p. sample is enhanced, and its flux diminishes, while shifting the cut line towards lower values of k , the e.p. sample becomes more contaminated by e.r. events and the flux increases. Fig. 6 indicates that shifting up the line cut keeps the knee-like structure unchanged, while shifts down tend to smooth out the structure. This result confirms that the structure seen in the spectrum is caused by the e.p. component, and that the conclusion is essentially independent of the particular hadronic interaction model used in the analysis.

4 Conclusions

A first result on the evolution of the k parameter, which is sensitive to the evolution of the average mass composition has been derived using an event-by-event approach, based on QGSJet II-03 model. It shows that the e.p. component shows a knee-like structure at $(8.3 \pm 0.8) \times 10^{16}$ eV and the change of slope is about $\Delta\gamma \sim 0.5$ through the break. The change of slope of $\Delta\gamma \sim 0.3$ observed in the all-particle spectrum is located in the same energy range where the change of slope of the e.p. component occurs, indicating that it reflects the knee in the e.p. component. The e.r. component has a much steeper spectrum compared to the e.p. one. In the framework of the QGSJet-

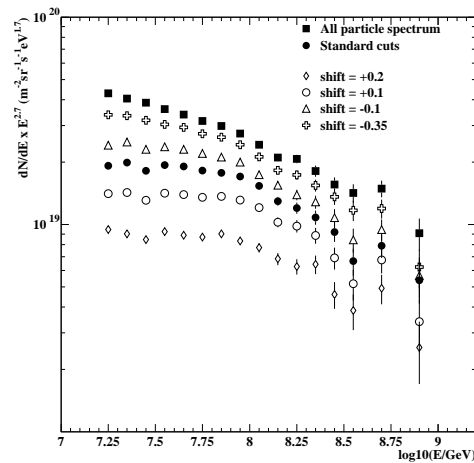


Figure 6: Effect of the shift of the cut line of the e.p. component on its energy spectrum.

II-03 model, the e.p. component is the most dominant one in the energy range $10^{16} - 10^{18}$ eV. This result is in agreement with those obtained by other analyses of KASCADE-Grande data [14, 15, 16].

Acknowledgement: KASCADE-Grande is supported by the BMBF of Germany, the MIUR and INAF of Italy, the Polish Ministry of Science and Higher Education (this work in part by grant for 2009-2011) and the Romanian Authority for Scientific Research.

References

- [1] W.-D. Apel et al. (KASCADE Collaboration), *Astrop. Phys.* **24** (2005) 1.
- [2] M. Aglietta et al. (EAS-TOP Coll.), *Astrop. Phys.* **21** (2004) 583.
- [3] V. Berezhinsky, A. Gazizov, S. Grigorieva, *Phys. Rev D* **74** (2006) 043005.
- [4] A.M. Hillas, *J. Phys. G: Nucl. Part. Phys.* **31** (2005) 95.
- [5] M. Bertaina et al. (KASCADE-Grande Coll.), *Proc. 31th ICRC, Lodz (Poland) #icrc0323* (2009).
- [6] D. Heck et al., Report FZKA 6019, Forschungszentrum Karlsruhe (1998).
- [7] A. Fassò et al., Report CERN-2005-10, INFN/TC-05/11, SLAC-R-773 (2005).
- [8] S.S. Ostapchenko, *Nucl. Phys. B (Proc. Suppl.)* **151** (2006) 143&147; S. Ostapchenko, *Phys. Rev. D* **74** (2006) 014026.
- [9] W.-D. Apel et al. (KASCADE-Grande Collaboration), *NIM A* **620** (2010) 202.
- [10] W.-D. Apel et al. (KASCADE Coll.), *Astrop. Phys.* **24** (2006) 467.
- [11] A. A. Lagutin and R. I. Raikin, *Nucl. Phys. Proc. Suppl.*, **97** (2001) 274.
- [12] M. Bertaina et al. (KASCADE-Grande Collaboration), *Proc. of the 22nd ECRS, Turku, Finland* (2010).
- [13] T. Antoni et al. (KASCADE Collaboration), *Astrop. Phys.* **16** (2002) 245.
- [14] J.-C. Arteaga, A. Chiavassa et al. (KASCADE-Grande Collaboration), *this Conference Proc.*, #0739
- [15] E. Cantoni, A. Chiavassa et al. (KASCADE-Grande Collaboration), *this Conference Proc.*, #0504.
- [16] D. Fuhrmann et al. (KASCADE-Grande Collaboration), *this Conference Proc.*, #0280.



Study of the ratio muon size to shower size as a mass sensitive parameter of KASCADE-Grande

J.C. ARTEAGA-VELÁZQUEZ¹, A. CHIAVASSA², W.D. APEL³, F. BALESTRA², K. BEKK³, M. BERTAINA², J. BLÜMER^{3,4}, H. BOZDOG³, I.M. BRANCUS⁵, P. BUCHHOLZ⁶, E. CANTONI^{2,7}, F. COSSAVELLA^{4,13}, K. DAUMILLER³, V. DE SOUZA⁸, F. DI PIERRO², P. DOLL³, R. ENGEL³, J. ENGLER³, M. FINGER⁴, D. FUHRMANN⁹, P.L. GHIA⁷, H.J. GILS³, R. GLASSTETTER⁹, C. GRUPEN⁶, A. HAUNGS³, D. HECK³, J.R. HÖRANDEL¹⁰, D. HUBER⁴, T. HUEGE³, P.G. ISAR^{3,14}, K.-H. KAMPERT⁹, D. KANG⁴, H.O. KLAGES³, K. LINK⁴, P. ŁUCZAK¹¹, M. LUDWIG⁴, H.J. MATHES³, H.J. MAYER³, M. MELISSAS⁴, J. MILKE³, B. MITRICA⁵, C. MORELLO⁷, G. NAVARRA^{2,15}, J. OEHLISCHLÄGER³, S. OSTAPCHENKO^{3,16}, S. OVER⁶, N. PALMIERI⁴, M. PETCU⁵, T. PIEROG³, H. REBEL³, M. ROTH³, H. SCHIELER³, F.G. SCHRÖDER³, O. SIMA¹², G. TOMA⁵, G.C. TRINCHERO⁷, H. ULRICH³, A. WEINDL³, J. WOCHLE³, M. WOMMER³, J. ZABIEROWSKI¹¹

¹ *Universidad Michoacana, Instituto de Física y Matemáticas, Morelia, Mexico*

² *Dipartimento di Fisica Generale dell' Università Torino, Italy*

³ *Institut für Kernphysik, KIT - Karlsruher Institut für Technologie, Germany*

⁴ *Institut für Experimentelle Kernphysik, KIT - Karlsruher Institut für Technologie, Germany*

⁵ *National Institute of Physics and Nuclear Engineering, Bucharest, Romania*

⁶ *Fachbereich Physik, Universität Siegen, Germany*

⁷ *Istituto di Fisica dello Spazio Interplanetario, INAF Torino, Italy*

⁸ *Universidade São Paulo, Instituto de Física de São Carlos, Brasil*

⁹ *Fachbereich Physik, Universität Wuppertal, Germany*

¹⁰ *Dept. of Astrophysics, Radboud University Nijmegen, The Netherlands*

¹¹ *Soltan Institute for Nuclear Studies, Lodz, Poland*

¹² *Department of Physics, University of Bucharest, Bucharest, Romania*

¹³ *now at: Max-Planck-Institut Physik, München, Germany;* ¹⁴ *now at: Institute Space Sciences, Bucharest, Romania;* ¹⁵ *deceased;* ¹⁶ *now at: Univ Trondheim, Norway*
 arteaga@ifm.umich.mx; achiavas@to.infn.it

Abstract: In this work, the shower ratio $Y^{CIC} = \log N_{\mu} / \log N_{ch}$ between the muon and the charged numbers, both corrected by atmospheric attenuation with the Constant Intensity Cut method (CIC), is studied as a parameter to separate the KASCADE-Grande data into different mass groups. MC simulations performed with CORSIKA on the framework of FLUKA/QGSJet II are employed to obtain the expected Y^{CIC} distributions as a function of the energy for different cosmic ray primaries as a basis for the separation. Then the Y^{CIC} parameter is used to divide the KASCADE-Grande data into “electron rich” and “electron poor” events. The fraction of events generated by H (Fe) primaries and classified as “electron rich” (“electron poor”) and its dependence on the primary energy is discussed. Finally, the energy spectra of these samples are reconstructed. A knee-like structure is found around 10^{17} in the “electron poor” sample associated with the heavy component of cosmic rays.

Keywords: KASCADE-Grande, energy spectrum, cosmic ray composition

1 Introduction

In order to understand the origin, nature, propagation and acceleration mechanism of galactic cosmic rays, detailed measurements with enough statistics on their energy spectrum, composition and arrival directions are needed. The task is complicated since at high energies ($\gtrsim 1$ PeV), cosmic rays must be studied indirectly by means of extensive air showers (EAS) detected with Earth-bound experiments. Information about composition and primary energy requires the simultaneous observation of several EAS

parameters, such as the muon and the electron particle contents at ground level. By combining the informations from both EAS observables, the KASCADE experiment was able to separate for the first time the cosmic ray energy spectra of different mass groups in the so called *knee* energy region (around 10^{15} eV) [1]. The picture of the galactic cosmic ray spectrum is still incomplete due to the lack of statistics in the interval $10^{16} - 10^{18}$ eV, where a *knee* in the heavy component of cosmic rays is predicted by several models. To explore this energy regime KASCADE was upgraded to KASCADE-Grande, a multidetector-setup with

enhanced area also designed to measure with precision the charged, muon and electron contents of air showers for cosmic ray studies [2]. In this paper we present an analysis based on the ratio between the muon and the charged particle numbers in EAS. This ratio is exploited to divide the events in two samples: the *electron poor* and the *electron rich* events. The two samples can be identified with EAS generated by primaries belonging to different mass groups (i.e. light and heavy elements). The technique is illustrated by applying it to the KASCADE-Grande data to reconstruct the light and heavy spectra of cosmic rays.

2 The KASCADE-Grande experiment

KASCADE-Grande, located in Karlsruhe, Germany (110 m a.s.l.), is a cosmic ray detector designed to measure EAS within the energy interval of $10^{16} - 10^{18}$ eV. Two detector arrays of different sizes are the main components of the experiment [2]. The first one is composed by 37 plastic scintillator detectors and covers a surface of 700×700 m². It is aimed to provide measurements of the charged particle number (N_{ch}), core position and arrival direction of air showers [2]. The penetrating component (N_{μ}) is measured with the aid of a smaller array of 200×200 m² integrated by 252 e/γ and shielded detectors [3, 2]. The electron shower size is obtained from the difference between N_{ch} and N_{μ} parameters.

3 Simulations and data selection

To perform the present analysis, MC simulations must be invoked. FLUKA [4] and QGSJet II-03 [5] were employed to describe the hadronic interactions at low and high energies, respectively. CORSIKA [6] was used to describe the EAS development and GEANT 4 to simulate the response of the KASCADE-Grande experiment to the passage of the air shower. Both simulated and experimental data are saved with identical output formats and analyzed with the same reconstruction program. MC data was generated for H, He, C, Si and Fe nuclei. Events were sampled from an isotropic distribution with spectral index $\gamma = -2$. The simulated data was weighted to emulate a $\gamma = -3$ energy spectrum.

With the aid of Monte Carlo simulations, quality cuts were investigated. They were carefully selected to reduce the systematic uncertainties on the muon and charged particle numbers. First, the experimental data sample was built out of events successfully reconstructed with the KASCADE-Grande procedure and collected during stable periods of data acquisition. Only EAS detected with more than 35 active stations were considered in this work. Then border effects were avoided by picking events with shower cores located inside a central area of 1.37×10^5 m² in the Grande array. Finally, the analysis was restricted to EAS with arrival zenith angles lower than 30° , $\log N_{ch} > 6$ and $\log N_{\mu} > 5.1$. The N_{μ} value is corrected for systematic effects by means of a proper correction function

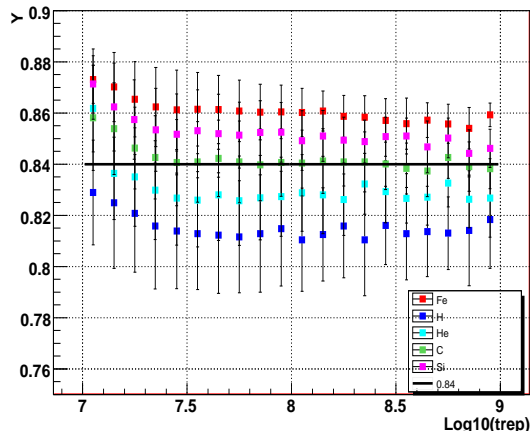


Figure 1: Estimations of the Y^{CIC} ratio for five different primaries shown as a function of the reconstructed energy. The results are obtained by means of a full EAS (based on the QGSJet II-03 high energy hadronic interaction model) and detector simulation.

parameterized out of MC simulations. With the above selection cuts, the effective time of observation is equivalent to 1173 days. Full efficiency ($\gtrsim 95\%$) is achieved for $\log(E/\text{GeV}) \geq 7.4$.

4 The Y^{CIC} ratio

The KASCADE-Grande (N_{μ}, N_{ch}) data offers a unique opportunity to investigate the chemical composition of galactic cosmic rays. Several methods can be envisaged for this enterprise. The one described in this contribution relies on the classification of the EAS on the basis of the Y^{CIC} ratio, a parameter defined as

$$Y^{CIC} = \log N_{\mu}(\theta_{ref}) / \log N_{ch}(\theta_{ref}). \quad (1)$$

In the above formula, the EAS observables, N_{μ} and N_{ch} , have been corrected event by event for attenuation effects in the atmosphere in such a way that they correspond to the shower sizes at a reference zenith angle, θ_{ref} . The correction is achieved by applying the Constant Intensity Cut Method (CIC) as described in references [7] and [8]. This procedure allows to combine data collected from different zenith angles in a model independent way. Here, θ_{ref} was chosen to 22° .

The Y^{CIC} parameter is a sensitive quantity to the composition of primary cosmic rays. The point can be better appreciated by looking at figure 1. There the mean values of Y^{CIC} are plotted as a function of the reconstructed energy for five single primaries (see [10] for details about the energy estimation), the error bars represent the RMS of the Y^{CIC} distributions. We can notice that at a fixed energy, the Y^{CIC} ratio grows with the mass of the primary particle. The effect can be understood as a result of the fact that the physics of hadronic interactions favors the production

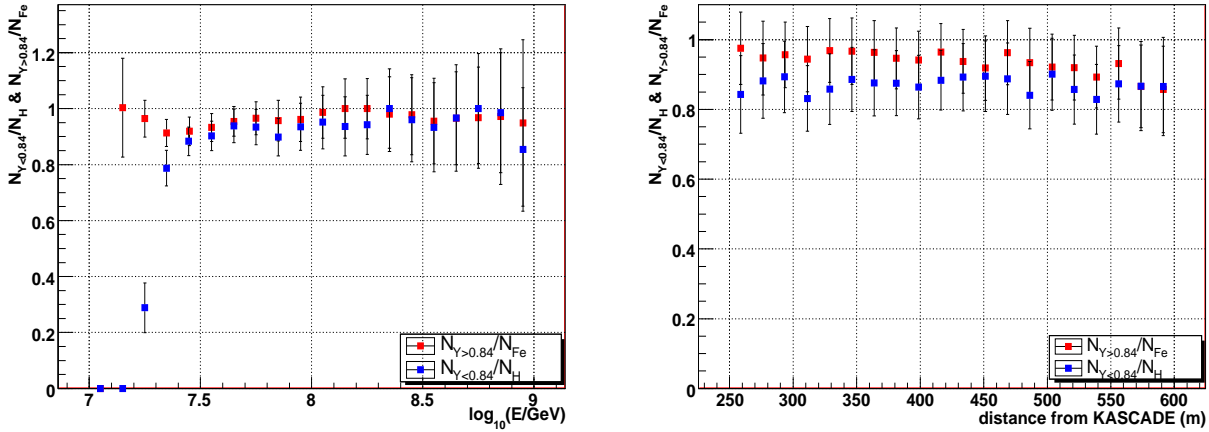


Figure 2: Fraction of hydrogen (iron) events classified as *electron rich* (*electron poor*) using the cut $Y_{cut}^{CIC} = 0.84$. The fractions for protons (stars) and iron nuclei (dots) are plotted against the reconstructed primary energy and the distance of the core position to the center of KASCADE. These results are obtained with a full EAS simulation based on the QGSJet II-03 interaction model.

of more secondary charged pions, and hence of muons, for heavy nuclei. This implies a lower production of electrons and charged particles in general when increasing the mass number of the parent nuclei. As seen in figure 1, the Y^{CIC} distributions are almost energy independent in the region of 100% efficiency. Taking advantage of the overall behavior of Y^{CIC} and in a first attempt to study the primary composition of cosmic rays in KASCADE-Grande by means of this parameter a cut is applied on the data at $Y_{cut}^{CIC} = 0.84$. Therefore the events are divided into two different sets for a subsequent analysis: the *electron rich* and *electron poor* groups corresponding to events with $Y^{CIC} < 0.84$ and $Y^{CIC} \geq 0.84$, respectively. From figure 1, it is clear that the first set covers the mean Y^{CIC} values for light mass elements, here H and He, while the second set contains the region for heavy mass nuclei, such as Si and Fe. In this way the *electron rich* and *electron poor* samples become representative of the light and heavy mass groups.

We remind that the Y^{CIC} distributions were obtained in the framework of the QGSJet II-03 hadronic model. However other hadronic interaction models, such as EPOS 1.99 [9], were investigated. Through these studies it was observed that the mean values of Y^{CIC} still do not depend on the primary energy, while their absolute values are modified. Thus, in the case of the EPOS 1.99 hadronic interaction model, the optimal separation between light and heavy mass groups is $Y_{cut}^{CIC} = 0.86$.

The separation into different mass groups employing the Y^{CIC} cut is not completely clean due to the size of the fluctuations inside each energy bin. Using MC simulations we have evaluated, for each element, the fraction of events selected as *electron rich* or *electron poor*. For simplicity, only the results obtained for hydrogen and iron nuclei are shown in figure 2 as a function of the reconstructed energy (left panel) and the core position (right panel). For energies greater than $\log(E/\text{GeV}) \geq 7.4$ (i.e. 100% ef-

iciency) the fraction of events properly classified through the Y^{CIC} ratio is almost energy independent and greater than 80%. This fraction is somewhat higher for iron primaries because of the lower shower fluctuations for heavy nuclei. It is not surprising to find out that their corresponding curves are approximately constant (in the energy range of full detection efficiency) over the whole effective area since the selection cuts on the EAS parameters were explicitly chosen to guarantee that measured shower parameters do not depend on the experimental conditions, such as the core distance from the KASCADE array center (i.e. mean distance of the muon detectors from the shower core).

These results show that possible distortions introduced in the reconstructed energy spectra of the different event samples, separated using the Y_{cut}^{CIC} value, are minimized. In the next section, the method is used to get insight into the composition of the primary cosmic ray flux.

5 Applications: Energy spectra for two mass groups

Once the experimental data is divided into *electron poor* and *electron rich* groups using the above procedure above, the primary energy of each event is estimated following [10]. After the energy derivation, the energy spectrum is reconstructed for each electron group leading to the energy spectra for the light and heavy components of the cosmic ray primary flux, which are presented in figure 3. The all-particle spectrum is also shown, and it is estimated as the direct sum of the two mass group spectra here estimated. The plots are not corrected for migration effects.

From figure 3 an outstanding feature is immediately appreciated in the heavy component of cosmic rays which corresponds to a *knee*-like structure. This feature also appears in more detailed analyses of the KASCADE-Grande

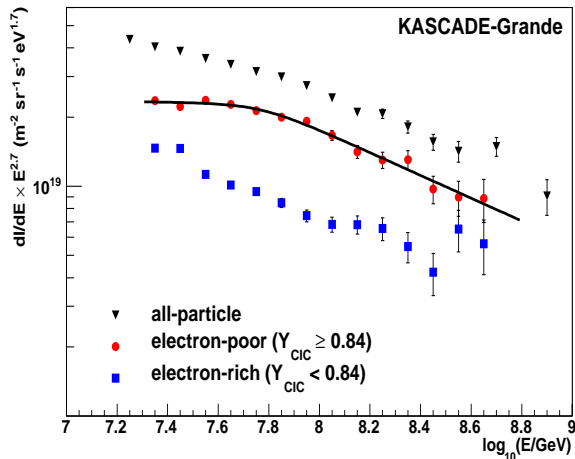


Figure 3: Light and heavy energy spectra derived from the KASCADE-Grande (N_μ, N_{ch}) data using the Y_{CIC} ratio as a mass estimator. The all-particle cosmic ray energy spectrum (squares) derived by adding the individual mass group fluxes is also shown.

data [12, 13, 14]. A fit with a broken power-law spectrum to the *electron poor* spectrum indicates a change of slope $\Delta\gamma = -0.47$ at $\log_{10}(E/\text{GeV}) = 7.77 \pm 0.06$ from $\gamma = -2.72 \pm 0.02$ to $\gamma = -3.19 \pm 0.02$. As seen in figure 4, the knee-like feature is a structure which does not depend on the position of the Y_{cut}^{CIC} , i.e., it is inherent to the cosmic ray data.

In figure 3, it can be noticed that the all-particle energy spectrum shows also a break. From a fit with a broken power-law spectrum, the position of the break is found around $\log_{10}(E/\text{GeV}) = 7.92 \pm 0.10$, but the change of slope is smaller for this case: $\Delta\gamma = -0.29$, from $\gamma = -2.95 \pm 0.05$ to $\gamma = -3.24 \pm 0.08$. It is seen that this feature arises as a consequence of the knee in the heavy component, but is less pronounced due to the contribution of the light group, which is not zero for $\log(E/\text{GeV}) \geq 7.4$.

6 Conclusions

In this contribution, the potential of the Y^{CIC} ratio as a mass sensitive parameter was studied. It was shown that the classification of EAS data into *electron rich* and *electron poor* events by applying the cut $Y_{cut}^{CIC} = 0.84$ can lead to the separation of the light and heavy mass groups in the cosmic ray flux. The fraction of events generated by hydrogen (iron) primaries and classified as *electron rich* (*electron poor*) does not depend on the primary energy and (in the frame of the QGSJet II-03 interaction model) is greater than 80%. Properly choosing the selection cuts on the EAS parameters the separation efficiency can be expected to be constant with energy, core position and zenith angle avoiding the introduction of distortions to the corresponding energy spectra. By applying the Y^{CIC} method, the energy spectra of the light and heavy mass groups were obtained.

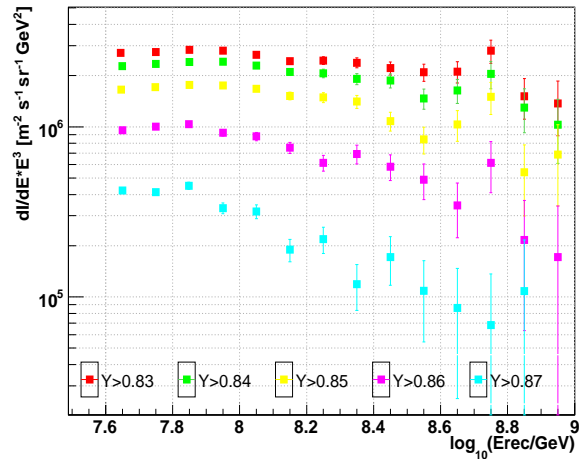


Figure 4: Energy spectra for the *electron poor* sample obtained for different Y^{CIC} cuts.

The results show that the heavy component presents a knee around $\log_{10}(E/\text{GeV}) = 7.77 \pm 0.06$ and that the contribution to the all-particle energy spectrum from the light component is different from zero.

Acknowledgment: KASCADE-Grande is supported by the BMBF of Germany, the MIUR and INFN of Italy, the Polish Ministry of Science and Higher Education and the Romanian Authority for Scientific Research. This study was partly supported by the DAAD-Proalmex program (2009-2010) and CONACYT.

References

- [1] W.-D. Apel *et al.* (KASCADE Collaboration), *Astrop. Phys.* **24** (2005) 1.
- [2] W.-D. Apel *et al.* (KASCADE-Grande Collaboration), *NIM A* **620** (2010) 202.
- [3] T. Antoni *et al.* (KASCADE Collaboration), *NIM A* **513** (2003) 429.
- [4] A. Fassò *et al.*, Report CERN-2005-10, INFN/TC-05/11, SLAC-R-773 (2005).
- [5] S.S. Ostapchenko, *Nucl. Phys. B (Proc. Suppl.)* **151** (2006) 143&147; S. Ostapchenko, *Phys. Rev. D* **74** (2006) 014026.
- [6] D. Heck *et al.*, Report FZKA 6019, Forschungszentrum Karlsruhe (1998).
- [7] D. Kang *et al.*, KASCADE-Grande Coll., Proc. 31st ICRC, icrc1044, (2009).
- [8] J.C. Arteaga *et al.*, KASCADE-Grande Coll., Proc. 31st ICRC, icrc0805, (2009).
- [9] K. Werner, F.M. Liu, T. Pierog, *Phys. Rev. C* **74** (2006) 044902.
- [10] M. Bertaina *et al.*, KASCADE-Grande Coll., *Astrophys. Space Sci. Trans.* **7**, 229 (2011).
- [11] J.C. Arteaga *et al.*, KASCADE-Grande Coll., Proc. *XVI ISVHECRI*, astro-ph/1009.4716v1 (2010).
- [12] M. Bertaina, KASCADE-Grande Coll., these proceedings.
- [13] D. Fuhrmann and M. Finger *et al.*, KASCADE-Grande Coll., these proceedings.
- [14] E. Cantoni, KASCADE-Grande Coll., these proceedings. Proc. *XVI ISVHECRI*, astro-ph/1009.4716v1 (2010).



The cosmic ray elemental composition based on measurement of the N_μ/N_{ch} ratio with KASCADE-Grande

E. CANTONI^{1,7}, W.D. APEL², J.C. ARTEAGA-VELÁZQUEZ³, K. BEKK², M. BERTAINA¹, J. BLÜMER^{2,4}, H. BOZDOG², I.M. BRANCUS⁵, P. BUCHHOLZ⁶, A. CHIAVASSA¹, F. COSSAVELLA^{4,13}, K. DAUMILLER², V. DE SOUZA⁸, F. DI PIERRO³, P. DOLL², R. ENGEL², J. ENGLER², M. FINGER⁴, D. FUHRMANN⁹, P.L. GHIA⁷, H.J. GILS², R. GLASSTETTER⁹, C. GRUPEN⁶, A. HAUNGS², D. HECK², J.R. HÖRANDEL¹⁰, D. HUBER⁴, T. HUEGE², P.G. ISAR^{2,14}, K.-H. KAMPERT⁹, D. KANG⁴, H.O. KLAGES², K. LINK⁴, P. ŁUCZAK¹¹, M. LUDWIG⁴, H.J. MATHES², H.J. MAYER², M. MELISSAS⁴, J. MILKE², B. MITRICA⁵, C. MORELLO⁷, G. NAVARRA^{1,15}, J. OEHLISCHLÄGER², S. OSTAPCHENKO^{2,16}, S. OVER⁶, N. PALMIERI⁴, M. PETCU⁵, T. PIEROG², H. REBEL², M. ROTH², H. SCHIELER², F.G. SCHRÖDER², O. SIMA¹², G. TOMA⁵, G.C. TRINCHERO⁷, H. ULRICH², A. WEINDL², J. WOCHLE², M. WOMMER², J. ZABIEROWSKI¹¹

¹ *Dipartimento di Fisica Generale dell' Università Torino, Italy*

² *Institut für Kernphysik, KIT - Karlsruher Institut für Technologie, Germany*

³ *Universidad Michoacana, Instituto de Física y Matemáticas, Morelia, Mexico*

⁴ *Institut für Experimentelle Kernphysik, KIT - Karlsruher Institut für Technologie, Germany*

⁵ *National Institute of Physics and Nuclear Engineering, Bucharest, Romania*

⁶ *Fachbereich Physik, Universität Siegen, Germany*

⁷ *Istituto di Fisica dello Spazio Interplanetario, INAF Torino, Italy*

⁸ *Universidade São Paulo, Instituto de Física de São Carlos, Brasil*

⁹ *Fachbereich Physik, Universität Wuppertal, Germany*

¹⁰ *Dept. of Astrophysics, Radboud University Nijmegen, The Netherlands*

¹¹ *Soltan Institute for Nuclear Studies, Lodz, Poland*

¹² *Department of Physics, University of Bucharest, Bucharest, Romania*

¹³ *now at: Max-Planck-Institut Physik, München, Germany;* ¹⁴ *now at: Institute Space Sciences, Bucharest, Romania;* ¹⁵ *deceased;* ¹⁶ *now at: Univ Trondheim, Norway*
cantoni@to.infn.it, achiavas@to.infn.it

Abstract: The KASCADE-Grande experiment, located at Karlsruhe Institute of Technology, is a multi-component Extensive Air Shower (EAS) detector studying primary cosmic rays in the $10^{16} - 10^{18}$ eV energy range. In this contribution a measurement of the cosmic ray chemical composition, based on the comparison of the experimental distributions of the ratio between the EAS muon size and the total charged size (N_μ/N_{ch}) with those expected from a complete EAS simulation based on the QGSJet II-03 interaction model, is presented. It has already been shown that, in the frame of this interaction model, the detector performances allow to separate three different mass groups: light, intermediate and heavy. With the employed technique, the relative abundances of the three mass groups are derived and their evolution as a function of the charged particle size is observed. The differential spectra of the three mass groups are then inferred and discussed

Keywords: Composition, KASCADE-Grande

1 Introduction

The energy range from 10^{16} to 10^{18} eV is very important to deeply investigate the details of the knee of the primary energy spectrum. In the last ten years different experiments (e.g KASCADE [1] and EAS-TOP [2]) have shown that this feature can be attributed to the light component of the primaries (i.e. H or He). A definitive confirmation of the astrophysical origin of the knee can only be obtained by

the detection of the foreseen change of slope of the heavy component at a primary energy $\sim 10^{17}$ eV.

In this contribution we present a study of the primary cosmic ray chemical composition in the $10^{16} - 10^{18}$ eV energy range performed comparing the KASCADE-Grande experiment [3] data with the results of a full Extensive Air Shower simulation based on the CORSIKA [4] code and on the QGSJet II-03 [5] interaction model.

The KASCADE-Grande experiment is located at the Campus North of the Karlsruhe Institute of Technology, 110

m a.s.l. It consists of an array of 37 plastic scintillator modules 10 m^2 each (Grande) spread over an area of $700 \times 700 \text{ m}^2$, working jointly with the co-located and formerly present KASCADE experiment [6], consisting of 252 electron and muon scintillation detectors placed over a $200 \times 200 \text{ m}^2$ area. All events triggering a sevenfold coincidence of Grande array detectors, arranged on an hexagonal grid (mean side length of 130 m), are reconstructed. The charged particle size N_{ch} is determined by the Grande array and the muon number N_μ by the KASCADE array. Both (N_{ch}) and (N_μ) are measured with an accuracy $\leq 15\%$; a detailed description of the reconstruction procedure can be found in [3].

2 The Chi Square Method

The present analysis is performed, to minimize effects of a possible incorrect description (in the simulation) of the EAS evolution in atmosphere, on vertical events ($0^\circ \leq \theta \leq 24^\circ$). Data are divided in twelve N_{ch} intervals (from $\text{Log } N_{ch}=6.0$ to $\text{Log } N_{ch}=8.0$) and the N_μ/N_{ch} experimental distributions are fitted with a linear combination of those obtained by a complete simulation of events generated with a power law distribution in the $10^{15} - 10^{18} \text{ eV}$ energy range for five different primaries (H, He, C, Si, Fe). We have already shown that the KASCADE-Grande experiment performances allow us to separate, with such algorithm, events into three samples originated by different mass groups [7]. The combination giving the best fits (examples for two of the twelve N_{ch} intervals are shown in figures 1 and 2) is the one composed by the following mass groups: light, 100% hydrogen; intermediate, 50% helium and 50% carbon; heavy, 50% silicon and 50% iron. The linear combination of the simulated mass groups is expressed as follows:

$$F_{sim}(i) = \sum_j \alpha_j f_{sim,j}(i) \quad (1)$$

where $F_{sim}(i)$ is the total theoretical fraction of simulated events falling in the histogram channel i , $f_{sim,j}(i)$ is the fraction for the single component j ($j = 1, 2, 3$), $\sum_j(i)$ is the sum over the different components and α_j is the fit parameter representing the relative abundance of the component j . The fit parameters fulfill the conditions

$$0. \leq \alpha_j \leq 1. \quad (2)$$

and

$$\sum_j \alpha_j = 1. \quad (3)$$

The fit is performed minimizing the following Chi Square function:

$$\chi^2 = \sum_i \frac{(F_{exp}(i) - F_{sim}(i))^2}{\sigma(i)^2} \quad (4)$$

where $F_{exp}(i)$ is the fraction of experimental events falling in the histogram channel i and $\sigma(i)$ is the error on the theoretical

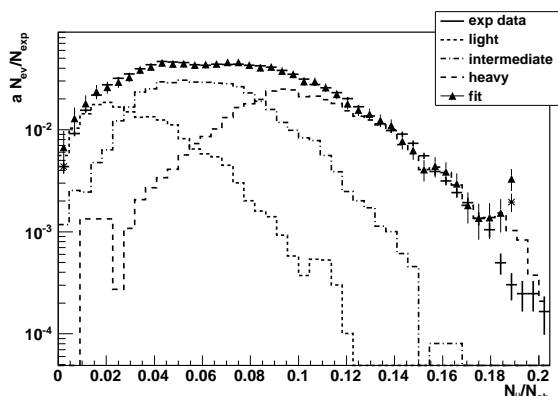


Figure 1: The experimental N_μ/N_{ch} distribution (solid line) measured in the $6.24 \leq \text{Log}(N_{ch}) < 6.36$ interval for vertical events ($0^\circ \leq \theta \leq 24^\circ$) fitted by a combination of Hydrogen (thin dashed line), Helium + Carbon in a 50% mixture (dot dashed line) and Silicon + Iron in a 50% mixture (thick dashed line). The triangles show the fit result. The experimental plot is normalized to 1 and every simulated component is normalized to its relative abundance. The tails of the experimental distribution are treated summing the events (the corresponding value is shown by a star) in a single bin, in order to have at least 5 events in each of them. In the shown example, the results for the abundances and the fit are: $\alpha_{light} = 0.14 \pm 0.02$; $\alpha_{intermediate} = 0.59 \pm 0.02$; $\alpha_{heavy} = 0.27 \pm 0.01$. The chi square and the cumulative function values are: $\chi_0^2/\nu = 56.52/46 = 1.23$, $P(\chi^2 > \chi_0^2) = 0.14$

expression (1). A fit is validated and the relative abundances of the mass groups are accepted if the cumulative function, $P(\chi^2 > \chi_0^2)$, is included in the $0.05 < P < 0.95$ interval.

The choice of sampling events in bins of the charged particle size is made in order to have a selection depending only on the performances of the experiment and not being influenced by an EAS simulation (as could be in the case of reconstructed energy bins).

The behavior of the relative abundances versus the charged particle size is shown in figure 3. The light and intermediate components show a trend with bigger fluctuations with respect to the heavy mass group. The relative abundance of the light mass group is almost independent on the charged particle shower size, while the heavy one shows a sudden change at $\log N_{ch} \sim 6.8$. The intermediate mass group seems to be more abundant near (in N_{ch} bins) the threshold, decreasing for higher N_{ch} and becoming nearly similar to those of light elements.

3 Spectra of the single mass groups

From the number of events measured in each $\Delta \log(N_{ch})$ interval ($N_{exp}(k)$, $k = 1, 12$) and having determined the

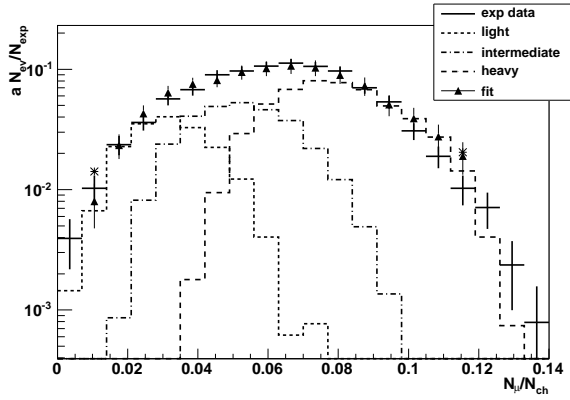


Figure 2: The experimental N_μ/N_{ch} distribution (solid line) measured in the $7.15 \leq \text{Log}(N_{ch}) < 7.24$ interval for vertical events ($0^\circ \leq \theta \leq 24^\circ$) fitted by a combination of light (thin dashed line), intermediate (dot dashed line) and heavy (thick dashed line). The triangles show the fit results. In the shown example, the results for the abundances and the fit are: $\alpha_{light} = 0.16 \pm 0.02$; $\alpha_{intermediate} = 0.30 \pm 0.04$; $\alpha_{heavy} = 0.52 \pm 0.03$. The chi square and the cumulative function values are: $\chi_0^2/\nu = 9.66/14 = 0.69$, $P(\chi^2 > \chi_0^2) = 0.79$

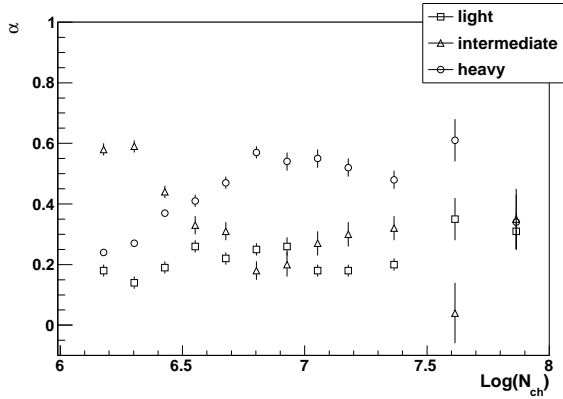


Figure 3: Relative abundances of the three mass groups versus the charged particle size N_{ch} measured for vertical events.

relative abundance of each mass group (j) we can calculate the number of events that are originated by primaries belonging to the j^{th} mass group ($N_j(k) = \alpha_j \cdot N_{exp}(k)$). The three mass group fluxes in each charged particle size bin are then derived:

$$\Phi_j(k) = N_j(k)/(A\Omega\Delta t)(m^{-2}sr^{-1}s^{-1}) \quad (5)$$

where $A = 1.52 \times 10^4 m^2$, $\Omega = 0.52 sr$ and $\Delta t = 1.1 \times 10^8 s$.

From a full EAS (based on the QGSJet II-03 interaction model) and detector simulation we derive, for each mass group, a power law relation ($E_0 = 10^b \cdot N_{ch}^a$) between the charged particle size and the primary energy (the values of the a and b parameters are reported in table 1). With these

	light	intermediate	heavy
a	0.99 ± 0.01	0.93 ± 0.004	0.91 ± 0.01
b	0.75 ± 0.06	1.30 ± 0.02	1.61 ± 0.03

Table 1: a , b parameters of the power law correlating, for each mass group, the charged particle size N_{ch} and the primary energy E_0

relations we convert the N_{ch} intervals into the corresponding energy bins (that are thus not the same for the three mass groups) and from the measured fluxes we derive the differential flux at the central energy of each interval.

To verify if, through the described algorithm, we are able to reproduce the spectra of the single mass groups we have performed the same analysis on test spectra: half of the simulated data set is used as fake experimental data while the other half is used as reference for the fitting procedure. With the goal of identifying possible spectral distortions artificially introduced by the analysis we have chosen the test spectra with a slope $\gamma = -3$ and without breaks for all elements. The results are shown in figure 4: the heavy mass group shows good agreement between test and reconstructed spectra in the whole energy range. The light and intermediate mass groups are in good agreement for energies greater than 4×10^{16} eV while near the threshold the reconstructed spectra are lower than the test ones. This result is not unexpected as shower and experimental fluctuations (that are bigger for low masses and originate an event migration from bin to bin) are not yet corrected for in the conversion from N_{ch} to energy. This procedure is under development, its results will be shown soon. It is worthwhile to point out that the uncorrected reconstructed test spectra show, for all mass groups, no artificial breaks.

Another hint of the correct behavior of the described analysis algorithm can be derived from figure 5 showing the relative abundances reconstructed for the previously described test spectra. These abundances show no dependence on N_{ch} in the whole range, even if fluctuations (mainly of the light and intermediate mass groups) around the expected value can be seen.

4 Conclusions

The performances of the algorithm aiming at the measurement of the evolution of the primary chemical composition of cosmic rays are described. We have shown how, with the KASCADE-Grande experiment performances, we are able to separate three mass groups and that all of them are needed to reconstruct the measured N_μ/N_{ch} distributions. The measured chemical composition gets heavier as the shower size N_{ch} increases as can be inferred from the evolution of the relative abundances of the three mass groups with N_{ch} .

The measured spectra of the three mass groups are shown in figure 6 as obtained in the frame of the QGSJet II-03

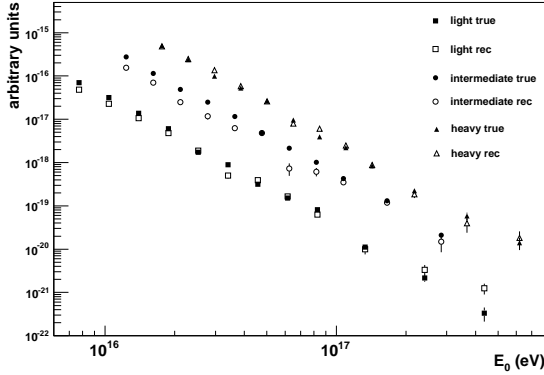


Figure 4: Comparison between test and reconstructed spectra for the three mass groups. In the fake spectrum all mass groups have equal abundance, in the plot the fluxes of light and heavy mass groups are multiplied by arbitrary factors for clarity.

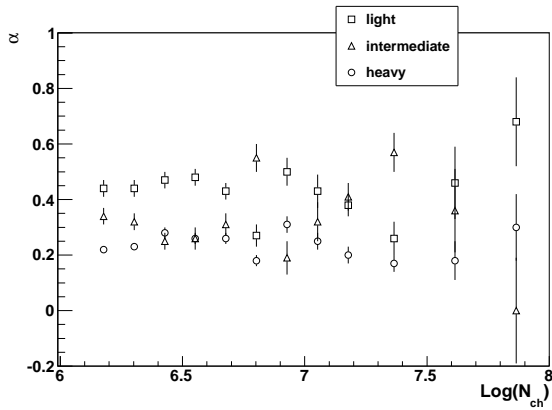


Figure 5: Reconstructed relative abundances of the three mass groups versus the charged particle size N_{ch} obtained analyzing test spectra with constant and equal slope for all elements.

interaction model. The spectrum of the heavy mass group shows a distinct change of slope and cannot be described by a single power law. This reconstructed spectrum is fitted with a function [8] describing a spectral shape with two different slopes interconnected by a smooth knee at energy E_k . The results, shown by the solid line in figure 6, are: $\gamma_1 = 2.67 \pm 0.02$, $\gamma_2 = 3.29 \pm 0.02$ and $\log E_k (eV) = 17.79 \pm 0.04$. The statistical significance of the change of slope is $\sim 4\sigma$. At a similar energy a (weaker) steepening is also observed in the all particle spectrum measured by KASCADE-Grande [9].

In contrast both the intermediate and light mass groups spectra are describable by a single power law due to the low event numbers. These spectra are dominated by statistical fluctuations, and no significant conclusion can thus be derived at the moment.

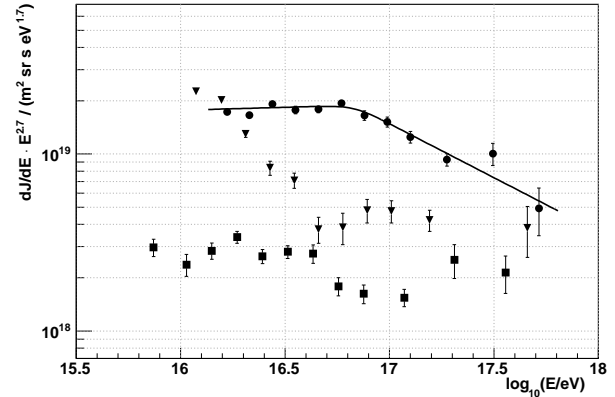


Figure 6: Differential energy spectra of the three mass groups: heavy (Si+Fe, dots), intermediate (He+C, triangles) and light (H, squares) elements.

All shown spectra do not yet take into account effects of event-to-event shower fluctuations at the energy assignment: a procedure to unfold them is under development.

It is important to emphasize that the present results, and in particular the relative abundances of the mass groups, heavily depend on the choice of QGSJet II-03 as interaction model. The entire analysis will be, in near future, repeated on basis of a complete EAS simulation based on a different interaction models, i.e. EPOS [10].

Acknowledgement: KASCADE-Grande is supported by the BMBF of Germany, the MIUR and INAF of Italy, the Polish Ministry of Science and Higher Education and the Romanian Authority for Scientific Research.

References

- [1] W.-D. Apel *et al.* (KASCADE Collaboration), *Astrop. Phys.* **24** (2005) 1.
- [2] M. Aglietta *et al.* (EAS-TOP Collaboration), *Astrop. Phys.* **21** (2004) 583.
- [3] W.-D. Apel *et al.* (KASCADE-Grande Collaboration), *NIM A* **620** (2010) 202.
- [4] D. Heck *et al.*, Report FZKA 6019, Forschungszentrum Karlsruhe (1998).
- [5] S.S. Ostapchenko, *Nucl. Phys. B (Proc. Suppl.)* **151** (2006) 143&147; S. Ostapchenko, *Phys. Rev. D* **74** (2006) 014026.
- [6] T. Antoni *et al.* (KASCADE Collaboration), *NIM A* **513** (2003) 429.
- [7] E. Cantoni *et al.* (KASCADE-Grande Collaboration), *Proc. 31st ICRC, Lodz (Poland) 2009*, #0524
- [8] W.-D. Apel *et al.* (KASCADE Collaboration), *Astrop. Phys.* **16** (2002) 245.
- [9] M. Bertaini *et al.* (KASCADE-Grande Collaboration), *Proc. 31st ICRC, Lodz (Poland) 2009*, #0323
- [10] K. Werner, F.M. Liu, T. Pierog, *Phys. Rev. C* **74** (2006) 044902.



KASCADE-Grande measurements of energy spectra for elemental groups of cosmic rays

D. FUHRMANN⁹, W.D. APEL¹, J.C. ARTEAGA-VELÁZQUEZ², K. BEKK¹, M. BERTAINA³, J. BLÜMER^{1,4}, H. BOZDOG¹, I.M. BRANCUS⁵, P. BUCHHOLZ⁶, E. CANTONI^{3,7}, A. CHIAVASSA³, F. COSSAVELLA^{4,13}, K. DAUMILLER¹, V. DE SOUZA⁸, F. DI PIERRO³, P. DOLL¹, R. ENGEL¹, J. ENGLER¹, M. FINGER⁴, P.L. GHIA⁷, H.J. GILS¹, R. GLASSTETTER⁹, C. GRUPEN⁶, A. HAUNGS¹, D. HECK¹, J.R. HÖRANDEL¹⁰, D. HUBER⁴, T. HUEGE¹, P.G. ISAR^{1,14}, K.-H. KAMPERT⁹, D. KANG⁴, H.O. KLAGES¹, K. LINK⁴, P. ŁUCZAK¹¹, M. LUDWIG⁴, H.J. MATHES¹, H.J. MAYER¹, M. MELISSAS⁴, J. MILKE¹, B. MITRICA⁵, C. MORELLO⁷, G. NAVARRA^{3,15}, J. OEHLISCHLÄGER¹, S. OSTAPCHENKO^{1,16}, S. OVER⁶, N. PALMIERI⁴, M. PETCU⁵, T. PIEROG¹, H. REBEL¹, M. ROTH¹, H. SCHIELER¹, F.G. SCHRÖDER¹, O. SIMA¹², G. TOMA⁵, G.C. TRINCHERO⁷, H. ULRICH¹, A. WEINDL¹, J. WOCHLE¹, M. WOMMER¹, J. ZABIEROWSKI¹¹

¹ *Institut für Kernphysik, KIT - Karlsruher Institut für Technologie, Germany*

² *Universidad Michoacana, Instituto de Física y Matemáticas, Morelia, Mexico*

³ *Dipartimento di Fisica Generale dell' Università Torino, Italy*

⁴ *Institut für Experimentelle Kernphysik, KIT - Karlsruher Institut für Technologie, Germany*

⁵ *National Institute of Physics and Nuclear Engineering, Bucharest, Romania*

⁶ *Fachbereich Physik, Universität Siegen, Germany*

⁷ *Istituto di Fisica dello Spazio Interplanetario, INAF Torino, Italy*

⁸ *Universidade São Paulo, Instituto de Física de São Carlos, Brasil*

⁹ *Fachbereich Physik, Universität Wuppertal, Germany*

¹⁰ *Dept. of Astrophysics, Radboud University Nijmegen, The Netherlands*

¹¹ *Soltan Institute for Nuclear Studies, Lodz, Poland*

¹² *Department of Physics, University of Bucharest, Bucharest, Romania*

¹³ *now at: Max-Planck-Institut Physik, München, Germany;* ¹⁴ *now at: Institute Space Sciences, Bucharest, Romania;* ¹⁵ *deceased;* ¹⁶ *now at: Univ Trondheim, Norway*
fuhrmann@physik.uni-wuppertal.de

Abstract: The KASCADE-Grande experiment, located at KIT-Karlsruhe, Germany, consists of a large scintillator array for measurements of charged particles, N_{ch} , and of an array of shielded scintillation counters used for muon counting, N_{μ} . KASCADE-Grande is optimized for cosmic ray measurements in the primary energy range 10^{16} eV to 10^{18} eV, thereby enabling the verification of a possible second knee expected at approximately 10^{17} eV. Exploring the composition in this energy range is of fundamental importance for understanding the transition from galactic to extragalactic cosmic rays. Following earlier studies of elemental spectra reconstructed in the first knee energy range from KASCADE data, we shall now extend these measurements to beyond 10^{17} eV. By analyzing the two-dimensional shower size spectrum N_{ch} vs. N_{μ} , we reconstruct the energy spectra of different mass groups by means of unfolding methods. The procedure and its results, which yield a strong indication for a kink in the iron spectrum at around 80 PeV, will be presented.

Keywords: Cosmic ray, energy spectrum, composition, knee, iron knee, KASCADE-Grande

1 Introduction

The spectrum of cosmic rays follows a power law over many orders of magnitude in energy, overall appearing rather featureless. However, there are a few structures observable. In 1958 Kulikov and Khristiansen [1] discovered a distinct steepening in the spectrum at around 10^{15} eV. Three years later Peters [2] concluded that the position of this kink, also called the cosmic ray “knee”, will depend on the atomic number of the cosmic ray particles if their acceleration is correlated to magnetic fields. Round about

half a century later, the KASCADE experiment [3] clarified that this change in spectral index is caused by a decrease of the so far dominating light¹ component of cosmic rays [4]. This result was achieved by means of an unfolding analysis disentangling the manifold convoluted energy spectra of five mass groups from the measured two-dimensional shower size distribution of electrons and muons at observation level. Based on the high energy interaction model QGSJET 01 [5] it was shown, that the kink in the all-

1. The description “light” refers to the atomic mass of the cosmic ray particles, which are primarily nuclei.

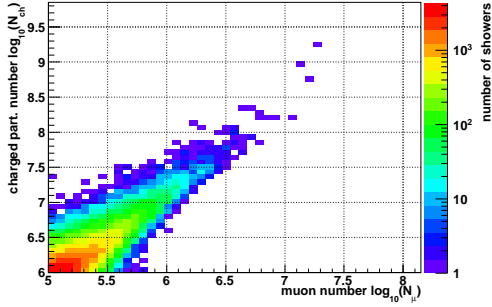


Figure 1: Measured shower size distribution.

particle spectrum at around 5×10^{15} eV corresponds to a knee observed in the hydrogen flux.

Nowadays, there are numerous theories about the origin and acceleration of cosmic rays. Concerning the knee position, some of them predict in contrast to the rigidity dependence considered by Peters a correlation with the mass of the particles. Hence, it is of great interest to verify whether also the spectra of heavy components exhibit analogous structures and if, at what energies. The KASCADE-Grande experiment [6] extends the accessible energy range of KASCADE to higher energies up to 10^{18} eV and allows by this to investigate the cosmic rays composition at regions where the possible, so-called iron knee is expected. The determination of this “second” knee enables the validation of the various theoretical models. Following this purpose, the KASCADE-Grande measurements have been analyzed similar to the afore-mentioned studies [4] of the KASCADE data. The applied unfolding method will be outlined in the next section. Thereafter, the uncertainties of the analysis and the resulting elemental energy spectra will be shown and studied. A more comprehensive description can be found in [7].

2 Outline of the analysis

The analysis’ objective is to compute the energy spectra of five² cosmic ray mass groups, represented by hydrogen (H), helium (He), carbon (C), silicon (Si) and iron (Fe) nuclei, from 10^{16} eV beyond primary energies of 10^{17} eV. The two-dimensional shower size spectrum $\lg N_{ch}$ vs. $\lg N_{\mu}$ of charged particles and muons measured with KASCADE-Grande is used as starting point for the unfolding analysis (Fig. 1). All measured³ air showers have to pass certain quality cuts to ensure good reconstructed shower sizes. Particularly, only air showers with zenith angles less than 18° are used exhibiting at least 10^6 charged particles and 10^5 muons. The measurement time covers approximately 1 318 days resulting in 78 000 accepted events passing all quality cuts. This corresponds to an exposure of $164\,709 \text{ m}^2 \text{ sr yr}$.

The convolution of the sought-after differential fluxes $dJ_n/d\lg E$ of the primary cosmic ray nuclei n into the measured number of showers N_i contributing to the cell i of shower size plane, and thus to the content of this specific

charged particle and muon number bin $(\lg(N_{ch}), \lg(N_{\mu}))_i$, can be described by an integral equation:

$$N_i = \sum_{n=1}^{N_n} \int_{T_m} \int_{\Omega_{tot}} \int_{A_f} \int_E \frac{dJ_n}{d\lg E} p_n d\lg E \cos \theta dA d\Omega dt, \quad (1)$$

with

$$p_n = p_n((\lg N_{ch}, \lg N_{\mu})_i | \lg E).$$

One has to sum over all N_n elements contributing to the all-particle cosmic ray spectrum, in this analysis the five representative primaries. T_m is the measurement time, Ω_{tot} the total solid angle accessible for the experiment and used for the analysis, and A_f the chosen fiducial area. The term p_n represents the conditional probability to reconstruct a certain combination of charged particle and muon number, respectively to get an entry in the cell $(\lg(N_{ch}), \lg(N_{\mu}))_i$, if the air shower inducing particle was of the type n and had an energy of E . More precisely, p_n itself is a convolution combining the intrinsic shower fluctuations occurring whilst the air shower development, the detection and reconstruction efficiency as well as the properties of the observables’ reconstruction process. The cosine term in $\cos \theta dA$ accomplishes the transformation from the horizontal surface element to the effective detection area.

Equation (1) can mathematically be understood as a system of coupled integral equations referred to as Fredholm integral equation of first kind. There are various methods to solve such an integral equation, albeit a resolvability often doesn’t *per se* imply uniqueness. In some preliminary tests it was found, that the unfolding algorithm of Gold [8] yields appropriate and robust solutions. It is a iterative procedure and *de facto* related to a minimization of a chi-square function. For countercheck purposes all results are validated by means of two additional algorithms, an also iterative method applying Bayes’ theorem [9] performing very stable, too, and a regularized unfolding based on a combination of the least-squares method with the principle of reduced cross-entropy [10], that yields slightly poorer results. All these solution strategies have in common that the response⁴ function p_n of Eq.(1) has to be known *a priori*. It is parametrized based on Monte Carlo simulations. The air shower development is simulated by means of CORSIKA [11] 6.307 based on the interaction models QGSJET-II-02 [12] and FLUKA 2002.4 [13]. The experiment’s response is simulated using CRES⁵ 1.16/07, which bases on GEANT 3.21 [14] detector description and simulation tool.

2. Due to effects of limited resolution not any number of mass groups can be treated.

3. Most of the cuts, e.g. the chosen zenith angle range, are also applied to the simulated air showers.

4. Also named kernel or transfer function; and more precisely it is rather a matrix than a simple function.

5. Cosmic Ray Event Simulation, a program package developed for the KASCADE [3] detector simulation.

3 Error analysis

The determination of the elemental energy spectra will be subjected to influences of different error sources. They can roughly be classified in two categories: uncertainties induced, or at least appearing whilst the deconvolution process and those embedded in the computed response function caused by the limited Monte Carlo statistics.

3.1 Uncertainties whilst the deconvolution

Firstly, the used data set is only a small sample based on a limited exposure, and hence suffering from statistical uncertainties. They are propagated through the unfolding algorithm and affect the quality of the solution. Furthermore, the used deconvolution method itself can introduce a systematic bias. The influences of both sources can be evaluated by means of a frequentist approach. Assuming appropriate⁶ spectral indices some trial elemental energy spectra are specified based on which a test data sample can be generated using Eq.(1). Subsequently, these data samples are unfolded. Since the true solution is *a priori* known, the deconvolution result can be compared to it to reveal statistical fluctuations induced by the limited measurement time and a possible systematic bias induced by the unfolding method.

3.2 Influences of limited Monte Carlo statistics

The amount of simulated air showers is strongly limited by reason of computing time. Due to the limited Monte Carlo statistics, the computation of the response function, i.e. the parametrization of the intrinsic shower fluctuations as well as of the detector properties, will only be possible under certain uncertainties resulting in an systematic error of the finally unfolded solution. In Fig. 2 exemplarily the simulated charged particle number distribution in case of hydrogen induced air showers with primary energy of 2×10^{15} eV is shown. A scattering around the used parametrization (“normal”) can be observed. This statistical uncertainty will be treated conservatively: Considering the computed fit parameters and their errors some new sets of parameters are calculated by means of a random generator. Based on each set, new response functions can be computed and used to unfold the data. Comparing the results reveals the caused systematic uncertainty in the solution. The distributions’ tails have to be inspected in more detail. Because of the very low statistics, the tails can vary within a certain range without worsen the fit result. In particular the right tail describing the fluctuations in direction to higher energies can have an important impact on the unfolded solution due to the steeply falling flux of cosmic rays. The systematic influence of the tails will conservatively be estimated by computing two additional response functions assuming in contrast to the standard case, in agreement with the statistical uncertainties, either a very fast decreasing or an elongated tail (cf. Fig. 2). Using both for a deconvolution and comparing the results yields the maximal sys-

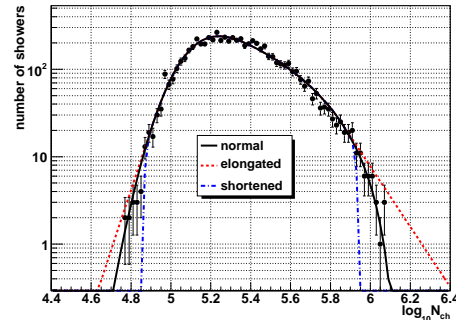


Figure 2: The simulated charged particle number distribution of 2×10^{15} eV hydrogen induced air showers with angles of incidence less than 18° . The distribution is fitted based on different approaches (see text).

tematic error range caused by the uncertainty in the tails description.

4 Results and conclusion

In Fig. 3 left panel the unfolded differential energy spectra of hydrogen and iron as well as the sum⁷ of the three single spectra of helium, carbon, and silicon are shown, representing respectively the fluxes of the light, heavy, and intermediate mass groups of cosmic rays. In addition, all five unfolded spectra are summed up to the all-particle flux, which is compatible to the results of other experiments (right panel) and agrees very well with the KASCADE-Grande all-particle spectrum published in [15]. The shaded band indicates the methodical uncertainties while the error bars represent the statistical error originating from the limited measurement time. With increasing energy the heavy component gets the dominant contributor to the cosmic ray composition. This agrees with the results of KASCADE [4] where a reduction of the light component beyond the first knee was found.

Both in the all-particle and the iron spectrum there is by eye a slight bending discernible at around 10^{17} eV. However, the change in the all-particle spectrum reveals not to be significant. In this context, one should keep in mind that this spectrum is the sum of all five elemental spectra unfolded separately, and by this is affected by their uncertainties. For the determination of the all-particle spectrum with KASCADE-Grande, there are more precise methods available, e.g. that one introduced in [15] stating a high significance for a change in the spectral index of the all-

6. Spectral indices close to those estimated by KASCADE are used in order to have realistic ones. However, some unlikely spectra are tested, too.

7. The intermediate component was combined because of the poorer results suffering from low statistics and making the plot confusing without giving further insights.

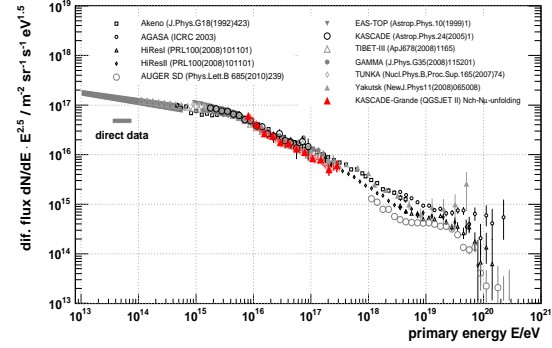
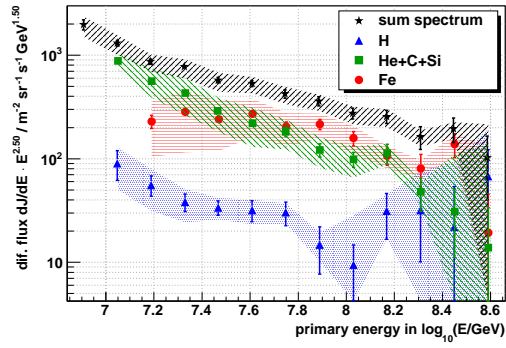


Figure 3: Depicted are the unfolded energy spectra for H and Fe, a combined spectrum for He, C and Si, as well as the all-particle spectrum (left panel). The all-particle spectrum conforms well to those of other experiments (right panel).

particle spectrum at around 1×10^{17} eV.

In order to judge the possible structures in the unfolded iron spectrum, it was fitted preliminarily by a single power law. However, the resulting chi-square probability for such a featureless single power law was below 1% ($\chi^2/ndf = 18.9/7$). In Fig. 4, the residual flux between the iron spectrum shown in Fig. 3, left panel, and such a spectrum that was derived by a single power law fit is depicted in order to emphasize the deviations between the single power law and the unfolded spectrum. Additionally, the iron spectrum is now fitted by a double power law:

$$\frac{dJ(E)}{d \lg E} = p_0 \times E^{p_2} \times \left(1 + \left(\frac{E}{p_1}\right)^{p_4}\right)^{(p_3 - p_2)/p_4}, \quad (2)$$

where $p_1 = \lg(E_{\text{knee}}/\text{GeV}) = 7.9 \pm 0.1$ corresponds to the knee position, while $p_2 = -2.62 \pm 0.02$ and $p_3 = -3.7 \pm 0.4$ are the spectral indices below and above the knee. The sharpness of the knee structure is encoded in $p_4 = 7.0$ and was fixed without worsening the fit's quality, while p_0 is a free normalization parameter. This fit describes the spectrum significantly better (chi-square probability at around 30% with $\chi^2/ndf = 6.2/5$), giving strong indications for a kink in the iron flux at around 80 PeV.

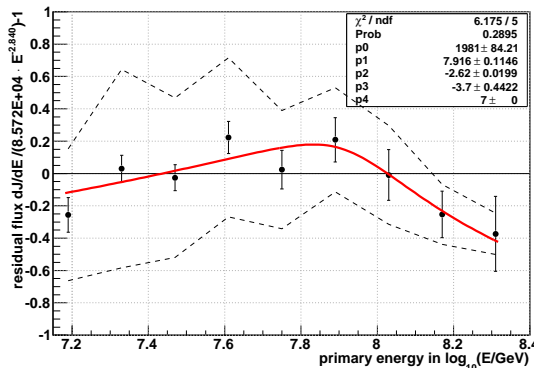


Figure 4: Residual flux between the iron spectrum shown in Fig. 3 and a spectrum that was derived by a single power law fit to that iron spectrum. Additionally, the iron spectrum is now fitted by a double power law.

Comparing⁸ the position of this potential iron knee to that for hydrogen (at around 2 PeV to 4 PeV) gives indications for a scaling of the knee positions with the charge of the nuclei rather than with their atomic mass number. This would encourage the cosmic ray acceleration models based on magnetic fields.

To summarize, there is a strong indication for a kink in the iron-like spectrum at around 80 PeV as well as for a dependence of the cosmic ray acceleration process on the charge of the nuclei, both on the premise that especially the used model QGSJET-II-02 describes the physics of hadronic interactions at these energies with a high level of reliability.

References

- [1] G. V. Kulikov et al., *Sov. Phys. JETP* **8** (1959) 441.
- [2] B. Peters, *Il Nuo. Cim.* **22** (1961) 800.
- [3] T. Antoni et al., *NIM A* **513** (2003) 490.
- [4] T. Antoni et al., *Astropart. Phys.* **24** (2005) 1.
- [5] N. N. Kalmykov et al., *Phys. At. Nucl.* **56** (1993) 346.
- [6] W.-D. Apel et al., *NIM A* **620** (2010) 202.
- [7] D. Fuhrmann, PhD thesis (in prep.), University Wuppertal (2011).
- [8] R. Gold, Report ANL-6984, Argonne (1964).
- [9] G. D'Agostini, *NIM A* **362** (1995) 487.
- [10] M. Schmelling, *NIM A* **340** (1994) 400.
- [11] D. Heck et al., Report FZKA 6019, Karlsruhe (1998).
- [12] S. Ostapchenko, *Nucl. Phys. Proc. Suppl.* **151** (2006) 143; S. Ostapchenko, *Phys. Rev. D* **74** (2006) 014026.
- [13] A. Fassò et al., Report CERN-2005-10, INFN/TC-05/11, SLAC-R-773 (2005).
- [14] R. Brun et al., Report CERN DD/EE/84-1, Geneva (1987); S. Giani et al., CERN W5013, Geneva (1994).
- [15] J. C. Arteaga-Velázquez et al., arXiv:1009.4716 (2010).

⁸ And assuming that the mass groups represented by H and Fe actually consist only, or at least primarily, of that two primaries.



Primary energy reconstruction from the S(500) observable recorded with the KASCADE-Grande array

G. TOMA¹, W.D. APEL², J.C. ARTEAGA-VELÁZQUEZ³, K. BEKK², M. BERTAINA⁴, J. BLÜMER^{2,5}, H. BOZDOG², I.M. BRANCUS¹, P. BUCHHOLZ⁶, E. CANTONI^{4,7}, A. CHIAVASSA⁴, F. COSSAVELLA^{5,13}, K. DAUMILLER², V. DE SOUZA⁸, F. DI PIERRO⁴, P. DOLL², R. ENGEL², J. ENGLER², M. FINGER⁵, D. FUHRMANN⁹, P.L. GHIA⁷, H.J. GILS², R. GLASSTETTER⁹, C. GRUPEN⁶, A. HAUNGS², D. HECK², J.R. HÖRANDEL¹⁰, D. HUBER⁵, T. HUEGE², P.G. ISAR^{2,14}, K.-H. KAMPERT⁹, D. KANG⁵, H.O. KLAGES², K. LINK⁵, P. ŁUCZAK¹¹, M. LUDWIG⁵, H.J. MATHES², H.J. MAYER², M. MELISSAS⁵, J. MILKE², B. MITRICA¹, C. MORELLO⁷, G. NAVARRA^{4,15}, J. OEHLISCHLÄGER², S. OSTAPCHENKO^{2,16}, S. OVER⁶, N. PALMIERI⁵, M. PETCU¹, T. PIEROG², H. REBEL², M. ROTH², H. SCHIELER², F.G. SCHRÖDER², O. SIMA¹², G.C. TRINCHERO⁷, H. ULRICH², A. WEINDL², J. WOCHLE², M. WOMMER², J. ZABIEROWSKI¹¹

¹ National Institute of Physics and Nuclear Engineering, Bucharest, Romania

² Institut für Kernphysik, KIT - Karlsruher Institut für Technologie, Germany

³ Universidad Michoacana, Instituto de Física y Matemáticas, Morelia, Mexico

⁴ Dipartimento di Fisica Generale dell' Università Torino, Italy

⁵ Institut für Experimentelle Kernphysik, KIT - Karlsruher Institut für Technologie, Germany

⁶ Fachbereich Physik, Universität Siegen, Germany

⁷ Istituto di Fisica dello Spazio Interplanetario, INAF Torino, Italy

⁸ Universidade São Paulo, Instituto de Física de São Carlos, Brasil

⁹ Fachbereich Physik, Universität Wuppertal, Germany

¹⁰ Dept. of Astrophysics, Radboud University Nijmegen, The Netherlands

¹¹ Soltan Institute for Nuclear Studies, Lodz, Poland

¹² Department of Physics, University of Bucharest, Bucharest, Romania

¹³ now at: Max-Planck-Institut Physik, München, Germany; ¹⁴ now at: Institute Space Sciences, Bucharest, Romania; ¹⁵ deceased; ¹⁶ now at: Univ Trondheim, Norway
gabriel.toma@nipne.ro

Abstract: We present a method to reconstruct the primary energy spectrum of cosmic rays from the charged particle densities recorded with the KASCADE-Grande detector. The KASCADE-Grande is hosted by the Karlsruhe Institute for Technology (KIT), Germany and is operated by an international collaboration. It has been shown that the charged particle density becomes independent of the primary mass at certain fixed distances from the shower axis and that it can be used as an estimator of the primary energy. Such distance is a characteristic of the detector and in the case of the KASCADE-Grande experiment it was shown that it is 500 m, hence the notation S(500). A relation is established by means of simulations between the primary energy of cosmic rays and the S(500). We account for the attenuation of inclined showers by applying the CIC method. By using the simulation derived calibration we build the primary energy spectrum from the recorded S(500). Several sources of systematic uncertainties are identified and their contribution to the final result is evaluated. Additionally we apply an unfolding to account for statistical fluctuations. The features of the obtained spectrum are discussed in relation to the result of another independent technique that is applied at KASCADE-Grande.

Keywords: KASCADE-Grande, primary energy spectrum, S(500)

1 Introduction

Previous investigations have shown that the charged particle density in air showers becomes independent of the primary mass at large but fixed distances from the shower axis and that it can be used as an estimator for the primary energy [1]. Such a distance is characteristic for a given ex-

periment. Based on this property a method was derived to reconstruct the primary energy spectrum from the particular value of the charged particle density, observed at such specific radial distances. While in the AGASA experiment the technique was applied for a distance of 600 m to the shower axis [2], in the case of the KASCADE-Grande array, detailed simulations [4] have shown that the particular distance for which this effect takes place is about 500 m

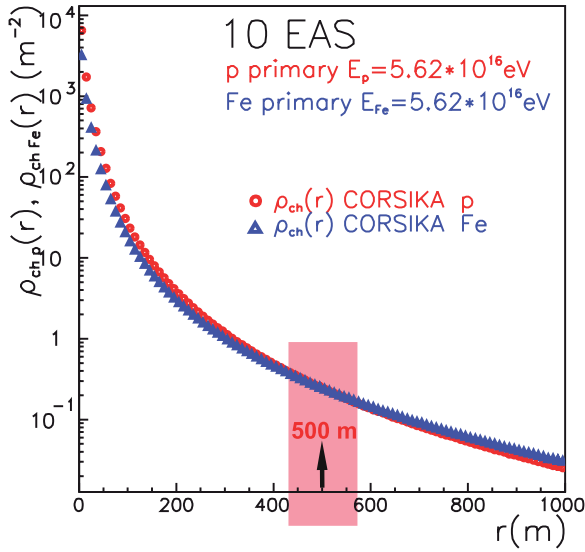


Figure 1: Simulations show that, for the case of the KASCADE-Grande experimental layout, the particle density becomes independent of the primary mass at around 500 m distance from the shower core; this plot shows averaged simulated lateral distributions for different primary types with equal energy.

(see Fig. 1 and Fig. 4). Hence the notation S(500) for the charged particle density at 500 m distance from the shower core. The distance is measured in a plane normal to the shower axis and containing the shower core. The data recorded in the detector plane is projected on the normal plane taking into account the attenuation effects characteristic to inclined events.

The study has been performed for both simulated (Fig. 5) and experimental (Fig. 6) events, using identical reconstruction procedures [5]. The CORSIKA Monte Carlo EAS simulation tool [6] is used to simulate air showers, with the QGSJETII model embedded for high energy interactions [7].

The energy deposits of particles in the KASCADE-Grande detector stations are recorded along with the associated temporal information (arrival times of particles). Using appropriate Lateral Energy Correction Functions (LECF), the energy deposits are converted into particle densities. The LECF functions are dependent on the shower zenith angle [8] and on the position of the station around the shower core (i.e. the LECF are dependent on the angle of incidence of particles in detectors). For every recorded event, a Linsley [9] Lateral Density Function (LDF) is used to evaluate the particle density at the radial range of interest, 500 m.

The described reconstruction is performed independently from the standard reconstruction applied at KASCADE-Grande, based on the $N_{ch}-N_{\mu}$ approach and described in [10].

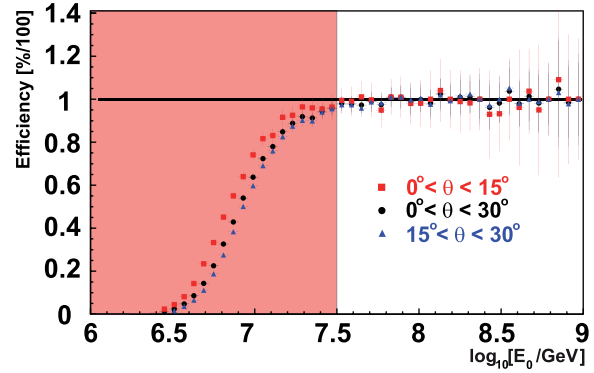


Figure 2: S(500) reconstruction efficiency for different zenith angular ranges and for the entire shower sample (all quality cuts applied); the reconstruction efficiency exceeds 95% at $\log_{10}[E_0/\text{GeV}] > 7.5$

2 KASCADE-Grande

In its general structure and operation, the KASCADE-Grande array [3] resembles other cosmic ray experiments. Hosted by the Karlsruhe Institute of Technology (KIT), Campus North, Germany at 110 m a.s.l and operated by an international collaboration, it is composed of many detector stations that are distributed over a wide area and it has been designed to record charged particle densities, without disentangling the type of secondary that is interacting in the sensitive medium. The shape of the array is rectangular with a length of ≈ 700 m. The lateral particle density distribution is subsequently inferred by adjusting the data registered with the detector stations to an a-priori assumed lateral distribution function.

Historically, the KASCADE-Grande detector array is an extension of a smaller array (the KASCADE array, operated since 1996). KASCADE was designed to record air showers initiated by primaries with energies in the $10^{14}-10^{17}$ eV range (including the knee range). The extension of the original KASCADE array was guided by the intention to extend the energy range for efficient EAS detection to $10^{16}-10^{18}$ eV (Fig. 2). This extended energy range provides various interesting aspects: the expected transition from galactic to extragalactic cosmic rays and, in particular the question whether there exists a "second knee" in the energy spectrum.

3 The constant intensity cut method (CIC)

For a given event sample, an EAS observable could have different values for events induced by identical primaries (E_0, A_0), but arriving from different zenith angles (due to EAS attenuation through the atmosphere). This is also the case for the S(500). To reach the detectors at ground level, an inclined event will propagate along an extended path

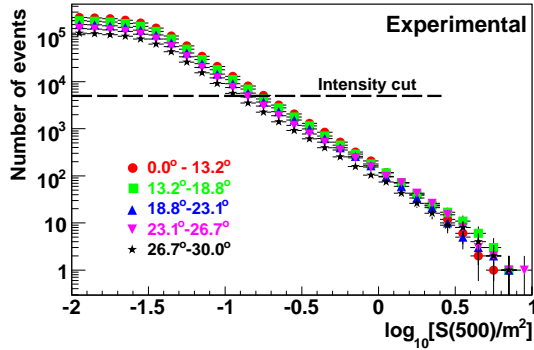


Figure 3: Integral $S(500)$ spectra; the horizontal line is a constant intensity cut at an arbitrarily chosen intensity; by assuming an exponential attenuation pattern the attenuation length of $S(500)$ was evaluated to $\lambda(500)=754 \pm 8 \text{ g}\cdot\text{cm}^{-2}$.

through the atmosphere compared to a vertical shower. The recorded particle densities at a given radial range for the two events will be different. One has to correct for this effect before performing an analysis simultaneously on all EAS events. This is achieved by applying the Constant Intensity Cut (CIC) method (Fig. 3) [11]. The method is based on the assumption that for a given minimum primary energy threshold we should record the same flux of events (i.e. primaries) from all zenith angles. Therefore we divide our shower sample in sub-samples corresponding to different zenith angular bins that subtend equal solid angles. Then we look in the integral $S(500)$ spectra of each sub-sample at a given arbitrary intensity. We establish a correlation between the $S(500)$ corresponding to the given intensity in each spectrum and the corresponding zenith angle. This correlation we use as a correction function. All reconstructed $S(500)$ values are corrected for attenuation by bringing them to the value they would have at a chosen reference angle. For the present study the reference angle is considered to be 21° , since the zenith angular distribution for the recorded EAS sample peaks at this value. The CIC correction is derived entirely from recorded experimental data and is independent from simulated studies.

4 Conversion to energy

For the experimental EAS sample, the total time of acquisition was 1173 days for a $500 \times 600 \text{ m}^2$ fiducial area. The same quality cuts were used for both simulated and experimental events. Only those events are accepted for which the zenith angle is below 30° , the reconstructed shower core is positioned inside the detector array and not too close to the border, and the event is triggered by more than 24 Grande stations (to ensure that density data is recorded close to the 500 m radial range, i.e. the shower is large enough). A good quality of the fit to the Linsley distribution is a further important criterion.

A calibration of the primary energy E_0 with $S(500)$ was

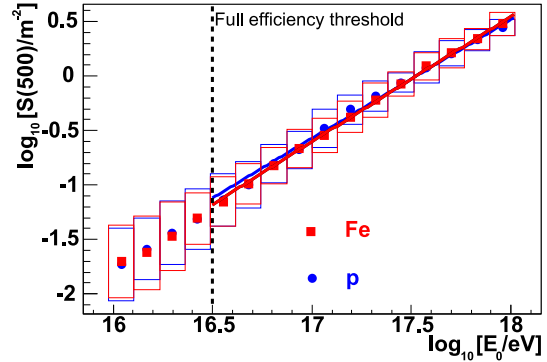


Figure 4: The dependence of $S(500)$ on the primary energy E_0 for two different primaries (showers in fairly equal proportions for the two masses); the box-errors are the errors on the spread; the errors on the mean are represented with bars and are dot-sized; straight lines represent power law fits.

derived from simulations (see Fig. 4). For the systematic contribution to the total error, several sources of systematic uncertainties have been identified: the spectral index of the simulated shower sample (which is different from the true one) is acting as a source of systematic uncertainty ($<1\%$ contribution), the $S(500)$ - E_0 calibration ($<1\%$ contribution), the CIC method ($<1\%$ contribution), the statistical fluctuations in the simulated shower sample (7%) and the choice of a certain reference angle at which to perform the $S(500)$ attenuation correction (7% contribution).

The energy resolution has also been evaluated from simulations by calculating the difference between the true and the reconstructed primary energy (applying CIC to the simulated data) and was found to be 22% for $E_0=10^{17} \text{ eV}$ (for all primaries) with a slight decrease with increasing energy.

5 The correction based on a response matrix

In the reconstruction of an observable, the final result may be under- or over-estimating the true value. When representing the energy flux as a histogram a particular reconstructed event may be stored in the wrong (neighboring) energy bin. Thus in every energy bin of our spectrum we will have the data correctly belonging to that bin, but also data that was migrating from neighboring bins. As the energy spectrum is very steep (spectral index $\gamma \approx -3$) we expect that for a given energy bin, the mis-reconstructed events falling into it will be coming predominantly from lower energy bins. This induces a shift of the reconstructed spectrum and a change of the spectral index (due to the variable energy resolution of the method with the energy). It is possible to account for the effect of fluctuations by calculating (from simulations) how many events migrate and where they add a contribution. Therefore a correction procedure based on a response matrix is derived and applied

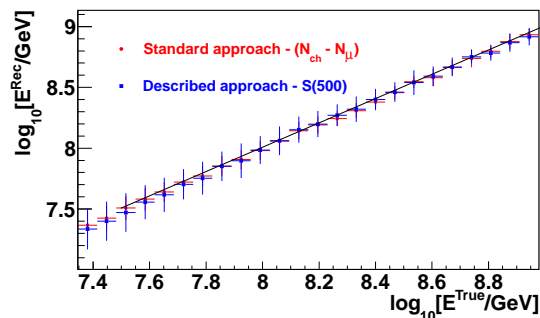


Figure 5: Comparison between the true (known) energy of primaries (five masses in fairly equal proportions) used in the simulated shower sample and the result of the reconstructions: the described reconstruction based on S(500) and the result of the standard KASCADE-Grande approach based on the $N_{ch} - N_{\mu}$ approach; the plot is a profile histogram, the error bars show the spread of data and the continuous line is the identity.

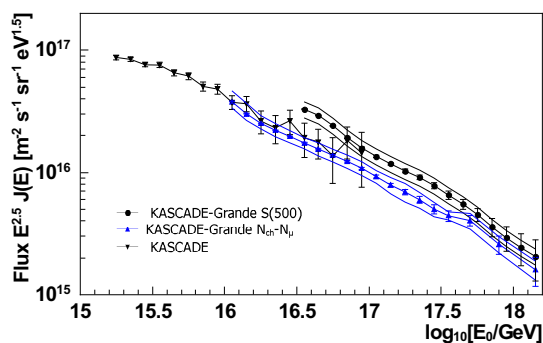


Figure 6: Reconstructed experimental energy spectrum by KASCADE-Grande from S(500)/CIC, multiplied by $E^{2.5}$ together with the result of the standard reconstruction procedure (based on the $N_{ch} - N_{\mu}$ correlation) and the results of KASCADE towards lower energies; the continuous lines above and below the spectrum show the systematic uncertainties.

to the experimental data. The spectrum presented in Fig. 6 includes the result of this correction.

6 Conclusions

The primary energy spectrum has been reconstructed from the particular case of charged particle densities recorded in the stations of the KASCADE-Grande array at 500 m distance from the shower axis, S(500). The study was performed for experimentally recorded events and also for simulated ones. The analysis of simulated events was needed in order to evaluate the reconstruction efficiency and quality and to derive a calibration curve $E_0 - S(500)$. The CIC method was applied on each shower in order

to correct for attenuation effects. Using the simulation-derived calibration the S(500) values are converted into primary energy. The S(500)-derived KASCADE-Grande spectrum is composition independent. An evaluation of the various uncertainty sources has been done and a correction based on a response matrix has been employed to account for the effects of the fluctuations on the spectral index of the reconstructed energy spectrum. The S(500)-derived all-particle primary energy spectrum (Fig. 6) shows a shift and a slightly different spectral index compared to an independently performed reconstruction approach based on the total number of charged particles and the muon number. In an event by event comparison, the profile plot in fig. 5 shows that when reconstructing simulated events with the two approaches there is good agreement between the methods. Present and future investigations are directed towards understanding the origin of the difference between the experimental results of the two methods. A possible source for this effect could be the shape of the lateral density distribution for simulated events that appears to be different from the shape of the experimental ones, although there could be additional sources for this shift.

Acknowledgement: The KASCADE-Grande experiment is supported by the BMBF of Germany, the MIUR and INAF of Italy, the Polish Ministry of Science and Higher Education (grant 2009-2011), and the Romanian Authority for Scientific Research, UEFISCSU, grant PNII-IDEI no. 461/2009 and grant PN 09370105. Part of the investigation was funded in the frame of the DAAD doctoral scholarship A/06/09016 Ref. 322 and by KIT Campus North in the frame of research visits.

References

- [1] A.M. Hillas *et al.*, Proc.12th ICRC, Hobart 3 (1971) 1001
- [2] D.M. Edge *et al.*, J. Phys. A: Math. Nucl. Gen. 6 (1973) 1612; M. Nagano *et al.*, J. Phys. G:Nucl.Part.Phys. 10 (1984) 1295; Y. Dai *et al.*, J.Phys.G: Nucl. Part. Phys. 14 (1998) 793
- [3] A. Haungs *et al.*, KASCADE-Grande collaboration, Nucl.Instr. and Meth. A 620 (2010) 202
- [4] H. Rebel and O. Sima *et al.* KASCADE-Grande collaboration, Proc. 29th ICRC Pune India 6 (2005) 297; I.M. Brancus *et al.* KASCADE-Grande collaboration, Proc. 29th ICRC Pune India 6 (2005) 361
- [5] O. Sima *et al.*, Report Forschungszentrum Karlsruhe 6985 (2004)
- [6] D. Heck *et al.*, Report Forschungszentrum Karlsruhe 6019 (1998)
- [7] N.N. Kalmykov, S.S. Ostapchenko and A.I. Pavlov, Nucl. Phys. B (Proc. Suppl.) 52B (1997) 17-28; S.S. Ostapchenko, Nucl. Phys. B-Proc. 151 (2006) 143-147; S.S. Ostapchenko, Phys. Rev. D 74 (2006) 014026
- [8] G. Toma *et al.*, Proc. 26th ECRS Lisbon Portugal so-134 (2006); GEANT users guide (1997)
- [9] J. Linsley *et al.*, Journ. Phys. Soc. Japan 17 (1962) A-III
- [10] M. Bertaina *et al.* - KASCADE-Grande Collaboration, Proc. 31th ICRC Łódź Poland (2009)
- [11] M. Nagano *et al.*, J.Phys G Nucl.Phys. 10 (1984) 1295



Tests of hadronic interaction models with the KASCADE-Grande muon data

J.C. ARTEAGA-VELÁZQUEZ¹, W.D. APEL², K. BEKK², M. BERTAINA³, J. BLÜMER^{2,4}, H. BOZDOĞ², I.M. BRANCUS⁵, P. BUCHHOLZ⁶, E. CANTONI^{3,7}, A. CHIAVASSA³, F. COSSAVELLA^{4,13}, K. DAUMILLER², V. DE SOUZA⁸, F. DI PIERRO³, P. DOLL², R. ENGEL², J. ENGLER², M. FINGER⁴, D. FUHRMANN⁹, P.L. GHIA⁷, H.J. GILS², R. GLASSTETTER⁹, C. GRUPEN⁶, A. HAUNGS², D. HECK², J.R. HÖRANDEL¹⁰, D. HUBER⁴, T. HUEGE², P.G. ISAR^{2,14}, K.-H. KAMPERT⁹, D. KANG⁴, H.O. KLAGES², K. LINK⁴, P. ŁUCZAK¹¹, M. LUDWIG⁴, H.J. MATHES², H.J. MAYER², M. MELISSAS⁴, J. MILKE², B. MITRICA⁵, C. MORELLO⁷, G. NAVARRA^{3,15}, J. OEHLISCHLÄGER², S. OSTAPCHENKO^{2,16}, S. OVER⁶, N. PALMIERI⁴, M. PETCU⁵, T. PIEROG², H. REBEL², M. ROTH², H. SCHIELER², F.G. SCHRÖDER², O. SIMA¹², G. TOMA⁵, G.C. TRINCHERO⁷, H. ULRICH², A. WEINDL², J. WOCHLE², M. WOMMER², J. ZABIEROWSKI¹¹

¹ *Universidad Michoacana, Instituto de Física y Matemáticas, Morelia, Mexico*

² *Institut für Kernphysik, KIT - Karlsruher Institut für Technologie, Germany*

³ *Dipartimento di Fisica Generale dell' Università Torino, Italy*

⁴ *Institut für Experimentelle Kernphysik, KIT - Karlsruher Institut für Technologie, Germany*

⁵ *National Institute of Physics and Nuclear Engineering, Bucharest, Romania*

⁶ *Fachbereich Physik, Universität Siegen, Germany*

⁷ *Istituto di Fisica dello Spazio Interplanetario, INAF Torino, Italy*

⁸ *Universidade São Paulo, Instituto de Física de São Carlos, Brasil*

⁹ *Fachbereich Physik, Universität Wuppertal, Germany*

¹⁰ *Dept. of Astrophysics, Radboud University Nijmegen, The Netherlands*

¹¹ *Soltan Institute for Nuclear Studies, Lodz, Poland*

¹² *Department of Physics, University of Bucharest, Bucharest, Romania*

¹³ *now at: Max-Planck-Institut Physik, München, Germany;* ¹⁴ *now at: Institute Space Sciences, Bucharest, Romania;* ¹⁵ *deceased;* ¹⁶ *now at: Univ Trondheim, Norway*
 arteaga@ifm.umich.mx

Abstract: The KASCADE-Grande experiment is an air-shower ground-based observatory designed to study in detail the energy spectrum and composition of primary cosmic rays in the region of $10^{16} - 10^{18}$ eV. These analyses are based on precise measurements of the charged, electron and muon numbers of the cosmic ray air-showers performed through different detector systems which come into play simultaneously in KASCADE-Grande during the data acquisition. Due to the quality of the data and the number of air-shower observables at disposal through the experiment the collected data proves to be also useful to test hadronic interaction models used for air-shower simulations. In this contribution, predictions of the QGSJET II-2, SIBYLL 2.1 and EPOS 1.99 hadronic models are confronted with the KASCADE-Grande muon data. Besides, the influence of these models on the all-particle energy spectrum derived from the muon size is also investigated.

Keywords: KASCADE-Grande, hadronic models, muons, simulations, energy spectrum

1 Introduction

The interpretation of high-energy cosmic ray data relies on the extensive air shower (EAS) simulations in which an important source of uncertainty is the description of hadronic interactions. The main problem is that for the physics of air showers the relevant processes lie in the kinematical region of small transverse momenta where QCD cannot be applied perturbatively and, in most of the cases, where no data is available. In this way, phenomenological models and parametrizations of accelerator data at low energies must

be invoked. These models are later extrapolated to high energies where they are used as valuable tools to understand the EAS observations at cosmic ray observatories [1]. Actually, air shower experiments can also help as laboratories to test and improve the modern hadronic interaction models in energy regions which at the moment are not reachable in particle accelerators. This task requires the measurement of as many EAS properties as possible with enough precision, such as the ones performed with the KASCADE experiment [2]. In the energy interval of $10^{14} - 10^{16}$, tests of early versions of the hadronic interaction models QGSJET,

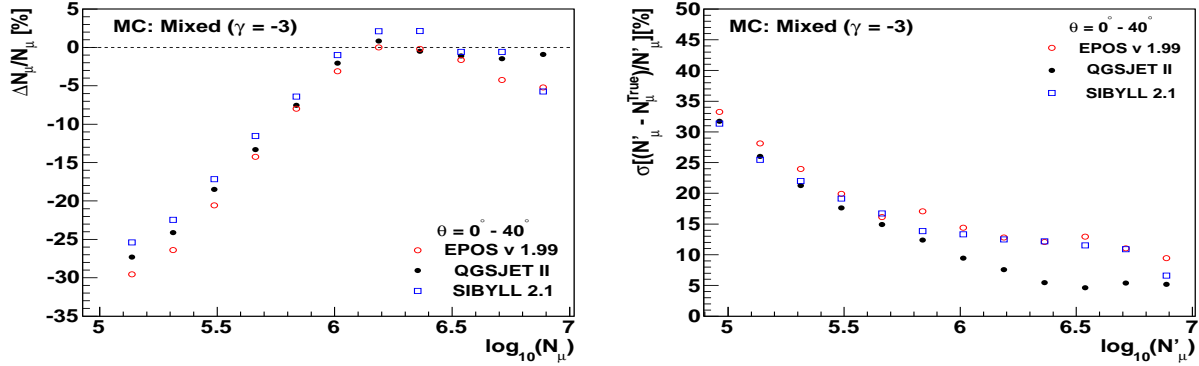


Figure 1: Left: Mean values of the muon correction function shown against the reconstructed muon number N_μ . Right: Fluctuations for the muon number after using the correction function versus the corrected muon number (N'_μ) assuming a mixed primary composition. MC results for different hadronic interaction models are presented.

EPOS, DPMJET and SIBYLL have been carried out with the KASCADE observatory (see [3] and references therein) through detailed studies involving the hadron, electron and muon contents of air showers. None of the above models was able to describe simultaneously all the KASCADE EAS data in the energy region around 1 PeV. Now, with the enhanced detector KASCADE-Grande [4], the possibility to extend these tests to the $10^{16} - 10^{18}$ eV interval is opened.

First investigations on this subject have been already performed with KASCADE-Grande. For example, in [5] it has been shown that predictions with QGSJET II about the muon production height (H_μ) distributions for EAS with zenith angles below $\theta < 18^\circ$ show a discrepancy compared to the measured data. On the other hand, in [6] measurements on the muon lateral distributions (ρ_μ) of EAS performed with KASCADE-Grande were confronted with the expected results of QGSJET II-2 and EPOS 1.99 finding an agreement between experiment and model predictions [6]. Some tests regarding the sensitivity of the KASCADE-Grande results to the QGSJET II-2 and EPOS 1.99 hadronic models have also been done, in particular, associated with the composition and the all-particle energy spectrum of cosmic rays derived from the ρ_μ and the charged particle number (N_{ch}) analyses, respectively [6]. EPOS 1.99 favors an abundance of light primary particles in the data and predicts a higher flux ($\sim 33\%$) in comparison with QGSJET II-2 [6].

In this work, the hadronic interaction models QGSJET II-2 [7], SIBYLL 2.1 [8] and EPOS v1.99 [9] are tested with the KASCADE-Grande muon data. The advantage of using muons is that in an air shower these particles undergo less atmospheric interactions than the electromagnetic component and, in consequence, they reflect directly the physics of the first hadronic interactions in EAS. Other tests and comparisons employing the ρ_μ distributions and the all-particle energy spectrum, derived by combining the information from the $N_{ch} - N_\mu$ observables, are performed in [10, 11].

In KASCADE-Grande, measurements of the total muon number in EAS (N_μ , number of muons greater than 230 MeV) are performed with an array of $192 \times 3.2 \text{ m}^2$ shielded scintillator detectors belonging to the former KASCADE experiment [2]. On the other hand, arrival times and charged particle densities, employed for estimations of the EAS arrival direction, N_{ch} content and core position, are measured with an enhancement called the Grande array, which is composed by $37 \times 10 \text{ m}^2$ plastic scintillator detectors scattered on a surface of 0.5 km^2 [4].

2 Description of data sets

For the present analysis, all air shower simulations were performed with CORSIKA [12] using Fluka [13] to treat hadronic interactions in the low energy regime. At high energies, the hadronic interaction models QGSJET II-2, SIBYLL 2.1 and EPOS v1.99, subjects of this investigation, were employed. The response of the detector was simulated with a GEANT 3.21 based code. Sets with spectral indexes $\gamma = -2.8, -3, -3.2$ were produced for several primary particle assumptions: H, He, C, Si, Fe and a mixed composition scenario (all single primaries in equal abundances).

Selection cuts were applied to both experimental and MC data. They were chosen according to MC studies to avoid as much as possible the influence of systematic uncertainties in the measurements of the EAS parameters. The selected data were composed of events with more than 11 triggered stations in Grande, shower cores inside a central area of $1.52 \times 10^5 \text{ m}^2$ and arrival directions confined to the zenith angle interval of $\Delta\theta = 0^\circ - 40^\circ$. These events were registered during stable periods of data acquisition and passed successfully the standard reconstruction procedure of KASCADE-Grande [4]. Additionally, only showers with $\log N_\mu > 5.1$ were considered for this work. Both the experimental and simulated data were analyzed and reconstructed with the same algorithms. With the above quality cuts, the effective time of observation with KASCADE-

Model	$\gamma = -2.8$			Λ_μ (g/cm ²) $\gamma = -3.0$			$\gamma = -3.2$		
	H	Mixed	Fe	H	Mixed	Fe	H	Mixed	Fe
EPOS 1.99	445 ± 26	624 ± 31	636 ± 37	459 ± 23	607 ± 30	624 ± 31	476 ± 25	614 ± 30	604 ± 30
QGSJET II	824 ± 33	832 ± 31	690 ± 43	900 ± 40	833 ± 31	693 ± 42	897 ± 100	825 ± 50	750 ± 62
SIBYLL 2.1	546 ± 44	657 ± 29	681 ± 46	637 ± 39	672 ± 29	688 ± 38	725 ± 44	681 ± 29	699 ± 40

Table 1: Muon attenuation lengths extracted from Monte Carlo data. The first column represents the hadronic interaction model. The corresponding composition scenario and spectral index, γ , of the MC sample under study are specified at the upper lines of the table.

Grande was equivalent to 1424 days. The threshold for full efficiency was found at $\log_{10} N_\mu \approx 5.4$.

3 Description of the analysis and results

To start with, all muon data was corrected for systematic uncertainties using muon correction functions derived from MC simulations for each hadronic interaction model assuming mixed composition and $\gamma = -3$. The functions were parametrized with respect to core position, azimuthal and zenithal angles, and muon size. In Fig. 1 the mean value of the muon correction function for different hadronic interaction models is plotted against the uncorrected N_μ . In general, after correction the systematic error on the muon number above threshold is found to be almost independent of the corrected muon size, N'_μ , and smaller than 6%. Fluctuations on N'_μ were also investigated. They are shown in Fig. 1 for a scenario with mixed composition and $\gamma = -3$. Note that although fluctuations exhibit the same tendency independently of the hadronic model under consideration, they present slight differences in magnitude, as it is the case for the correction functions. Therefore, some differences are expected when interpreting the same muon experimental data with the hadronic interaction models under consideration.

In a second step, to test the hadronic interaction models with the KASCADE-Grande muon data, predictions on the evolution of the muon content with the arrival zenith angle of the EAS were confronted with observations. The task was done comparing the expected and observed values of the muon attenuation length, Λ_μ . This quantity was extracted by applying the Constant Intensity Cut (CIC) method to the data as described in reference [14] but using a global fit to the attenuation curves, $\log_{10} N'_\mu(\theta)$, with the known formula

$$N'_\mu = N_\mu^0 \exp[-X_0 \sec(\theta) / \Lambda_\mu], \quad (1)$$

where $X_0 = 1023 \text{ g/cm}^2$ is the average atmospheric depth for vertical showers and N_μ^0 is a normalization parameter to be determined for each attenuation curve. The results for Λ_μ are presented in Tables 1 and 2. Discrepancies between the experimental values and the simulation results can be observed for the studied models. The differences do not disappear when modifying the primary composition or spectral index. As a consequence, the predicted evolution of the muon component with the zenith angle, $N'_\mu(\theta)$

Model	Λ_μ (g/cm ²)
EPOS 1.99	1851 ± 142
QGSJET II	1383 ± 84
SIBYLL 2.1	1443 ± 86

Table 2: Muon attenuation lengths extracted from KASCADE-Grande data under the framework of different hadronic interaction models. When comparing MC and experimental data it should be understood that the same N_μ correction function was employed.

(see equation 1) shows also a disagreement with the observations. The percentage of deviation for $N'_\mu(\theta)$ between experiment and simulations (mixed composition scenario with $\gamma = -3$) inside the frameworks of QGSJET II-2, EPOS 1.99 and SIBYLL 2.1 is presented in Fig. 2. Formula 1 was employed to calculate the curves of Fig. 2 using the values for Λ_μ of Tables 1 and 2 and normalizing data in such a way that the predicted N'_μ at $\theta = 0^\circ$ agrees with the measured value. Several factors, which are model dependent, may come into play in the observed differences: from the predicted muon correction function (see graphs in Fig. 1), up to the description of the production, evolution and fluctuations of the shower, therefore one should be cautious when extracting conclusions from these differences.

To finalize this analysis, the KASCADE-Grande energy spectra were reconstructed using QGSJET II-2, EPOS 1.99 and SIBYLL 2.1, under the assumption of a mixed compo-

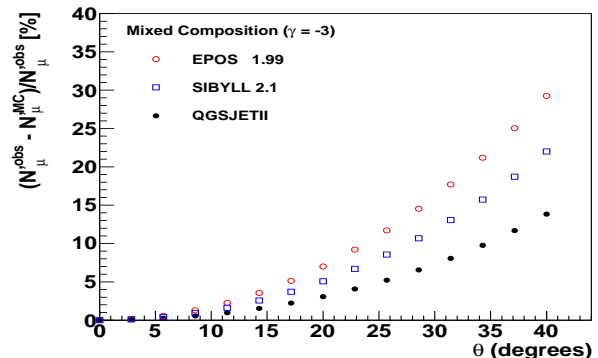


Figure 2: Relative deviation of measured data from model predictions for the dependence of the muon content with the zenith angle in the framework of three hadronic interaction models.

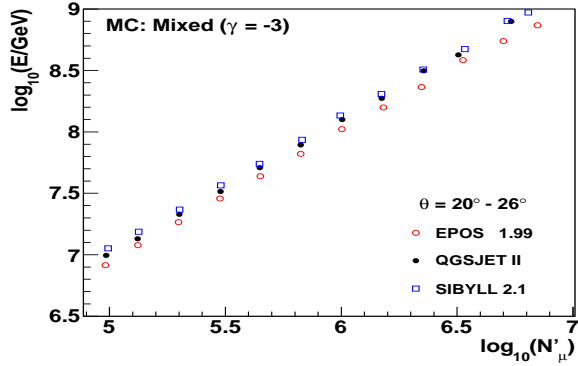


Figure 3: Primary energy as a function of the corrected muon number estimated from MC simulations for a mixed composition scenario with $\gamma = -3$ using QGSJET II-2, EPOS 1.99 and SIBYLL 2.1.

sition scenario and a spectral index $\gamma = -3$, and were compared with each other to test the influence of the hadronic interaction model on the KASCADE-Grande muon data. Details about the method of reconstruction can be found in [14]. One important difference with respect to reference [14] is that in the present work, the energy spectra were unfolded using the Gold algorithm [15]. As it was the case in [14] the primary energy was calculated using a calibration function of the form $E = \alpha_\mu [N'_\mu(\theta_{ref})]^{\beta_\mu}$, where $N'_\mu(\theta_{ref})$ is the corrected muon number of the EAS that is expected at θ_{ref} according to the CIC method. $\theta_{ref} = 23.3^\circ$ is a zenith angle of reference. On the other hand, α_μ and β_μ are model dependent parameters, which are determined from a fit to the MC data presented in Fig. 3. Note that at a fixed energy, the predictions of EPOS 1.99 for the mean number of muons in the interval $\theta = 20^\circ - 26^\circ$ give values higher by 14% compared to QGSJET II-2, and 21% to SIBYLL 2.1. The reconstructed energy spectra are shown in Fig. 4 for the full efficiency region.

As seen in Fig. 4, the all-particle energy spectrum derived with QGSJET II-2 is lower than the spectra calculated with SIBYLL 2.1 but larger than the flux estimated with EPOS 1.99. In particular, at $E = 10^8$ GeV, the above differences are of the order of 23% and 36%, respectively. These values are comparable to those derived from reference [6] ($\sim 30\%$) where the charged particle number is used instead to reconstruct the energy spectra within the QGSJET II-2 and the EPOS 1.99 frameworks. In the latter case, however, the EPOS 1.99 fluxes are shifted to higher energies in comparison with those estimated with QGSJET II-2.

4 Conclusions

Three hadronic interaction models: QGSJET II-2, EPOS 1.99 and SIBYLL 2.1 were tested in this paper by comparing their predictions for the attenuation of the muon content of EAS in the atmosphere with the observations of KASCADE-Grande. It was found that the above hadronic

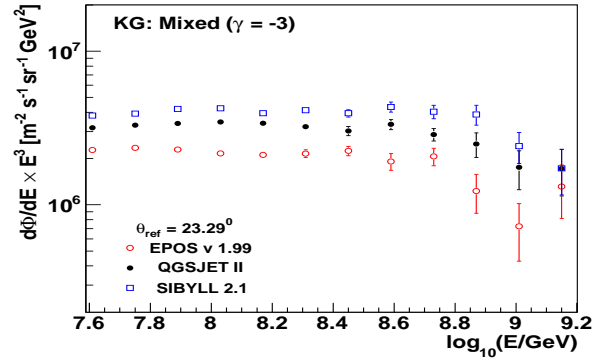


Figure 4: Energy spectra derived from KASCADE-Grande muon data using several hadronic models and assuming a mixed composition scenario with $\gamma = -3$.

interaction models do not describe this aspect of the measured muon data. The sensitivity of the all-particle energy spectrum derived from the N_μ measurements to the hadronic interaction models was investigated. The spectrum reconstructed using EPOS 1.99 is lower ($\sim 36\%$) in comparison with that from QGSJET II-2. The latter being smaller ($\sim 23\%$) than the spectrum derived with SIBYLL 2.1.

Acknowledgment: KASCADE-Grande is supported by the BMBF of Germany, the MIUR and INAF of Italy, the Polish Ministry of Science and Higher Education (in part by grant for 2009-2011) and the Romanian Authority for Scientific Research. This study was partly supported by the DAAD-Proalmex program (2009-2010) and CONACYT.

References

- [1] J. Knapp *et al.*, *Astrop. Phys.* **19** (2003) 77.
- [2] T. Antoni *et al.*, *NIM A* **513** (2003) 429.
- [3] W. D. Apel *et al.*, *J. Phys. G: Nucl. Part. Phys.* **36**, 035201 (12pp) (2009).
- [4] W.-D. Apel *et al.*, *NIM A* **620**, 202 (2010).
- [5] W.-D. Apel *et al.*, *Astrop. Phys.* **34**, 476 (2011).
- [6] Donghwa Kang *et al.*, KASCADE-Grande Coll., *Proc. XVI ISVHECRI*, astro-ph/1009.4902 (2010).
- [7] S.S. Ostapchenko, *Nucl. Phys. B (Proc. Suppl.)* **151** (2006) 143&147; S. Ostapchenko, *Phys. Rev. D* **74**, 014026 (2006).
- [8] E.J. Ahn *et al.*, *Phys. Rev D* **80**, 094003 (2009).
- [9] T. Pierog *et al.*, Report FZKA 7516, Forschungszentrum Karlsruhe 133, (2009).
- [10] V. de Souza *et al.*, KASCADE-Grande Coll., these proceedings.
- [11] M. Bertaina *et al.*, KASCADE-Grande Coll., these proceedings.
- [12] D. Heck *et al.*, Report FZKA 6019, Forschungszentrum Karlsruhe (1998).
- [13] A. Fassò *et al.*, Report CERN-2005-10, INFN/TC-05/11, SLAC-R-773 (2005).
- [14] J.C. Arteaga *et al.*, *Proc. 31st ICRC*, icrc0805, (2009).
- [15] R. Gold, AEC Research and Development Report ANL-6984, Argonne National Laboratory, Argonne, IL, 1964.



A direct measurement of the muon component of air showers by the KASCADE-Grande Experiment

V. DE SOUZA⁸, W.D. APEL¹, J.C. ARTEAGA-VELÁZQUEZ², K. BEKK¹, M. BERTAINA³, J. BLÜMER^{1,4}, H. BOZDOG¹, I.M. BRANCUS⁵, P. BUCHHOLZ⁶, E. CANTONI^{3,7}, A. CHIAVASSA³, F. COSSAVELLA^{4,13}, K. DAUMILLER¹, F. DI PIERRO³, P. DOLL¹, R. ENGEL¹, J. ENGLER¹, M. FINGER⁴, D. FUHRMANN⁹, P.L. GHIA⁷, H.J. GILS¹, R. GLASSTETTER⁹, C. GRUPEN⁶, A. HAUNGS¹, D. HECK¹, J.R. HÖRANDEL¹⁰, D. HUBER⁴, T. HUEGE¹, P.G. ISAR^{1,14}, K.-H. KAMPERT⁹, D. KANG⁴, H.O. KLAGES¹, K. LINK⁴, P. ŁUCZAK¹¹, M. LUDWIG⁴, H.J. MATHES¹, H.J. MAYER¹, M. MELISSAS⁴, J. MILKE¹, B. MITRICA⁵, C. MORELLO⁷, G. NAVARRA^{3,15}, J. OEHLISCHLÄGER¹, S. OSTAPCHENKO^{1,16}, S. OVER⁶, N. PALMIERI⁴, M. PETCU⁵, T. PIEROG¹, H. REBEL¹, M. ROTH¹, H. SCHIELER¹, F.G. SCHRÖDER¹, O. SIMA¹², G. TOMA⁵, G.C. TRINCHERO⁷, H. ULRICH¹, A. WEINDL¹, J. WOCHLE¹, M. WOMMER¹, J. ZABIEROWSKI¹¹

¹ *Institut für Kernphysik, KIT - Karlsruher Institut für Technologie, Germany*

² *Universidad Michoacana, Instituto de Física y Matemáticas, Morelia, Mexico*

³ *Dipartimento di Fisica Generale dell' Università Torino, Italy*

⁴ *Institut für Experimentelle Kernphysik, KIT - Karlsruher Institut für Technologie, Germany*

⁵ *National Institute of Physics and Nuclear Engineering, Bucharest, Romania*

⁶ *Fachbereich Physik, Universität Siegen, Germany*

⁷ *Istituto di Fisica dello Spazio Interplanetario, INAF Torino, Italy*

⁸ *Universidade São Paulo, Instituto de Física de São Carlos, Brasil*

⁹ *Fachbereich Physik, Universität Wuppertal, Germany*

¹⁰ *Dept. of Astrophysics, Radboud University Nijmegen, The Netherlands*

¹¹ *Soltan Institute for Nuclear Studies, Lodz, Poland*

¹² *Department of Physics, University of Bucharest, Bucharest, Romania*

¹³ *now at: Max-Planck-Institut Physik, München, Germany;* ¹⁴ *now at: Institute Space Sciences, Bucharest, Romania;* ¹⁵ *deceased;* ¹⁶ *now at: Univ Trondheim, Norway*
vitor@ifsc.usp.br

Abstract: The muon component of atmospheric air showers is a very important information in astroparticle physics because it is related to the primary particle mass and also because it depends on the hadronic interactions happening in the shower development. In this paper, we study the muon densities measured by the KASCADE-Grande experiment and illustrate its importance in composition studies and testing of hadronic interaction models. The data analysed here was measured by the KASCADE-Grande detector and lies in the $10^{16} - 10^{18}$ eV energy range. The measured muon density is compared to predictions of EPOS 1.99, QGSJet II and Sibyll 2.1 hadronic interaction models. This paper is an update of the results presented in [1]. The paper extends its scope by testing two extra hadronic models Sibyll 2.1 and EPOS 1.99.

Keywords: HE.1.2 Observations and simulations at energies 10^{16-18} eV

1 Introduction

Cosmic rays with energy range between 10^{16} and 10^{18} eV have the potential to reveal interesting astrophysical phenomena occurring in the Universe. In this energy range the transition between galactic to extragalactic predominance of the flux might occur. This transition is expected to cause an evolution of the mean mass of primary particles.

The KASCADE-Grande experiment (see figure 1) has been set up to measure primary cosmic rays in this energy range in order to help in the understanding of these

questions. The experiment is located at the Karlsruhe Institute of Technology, Campus North, Germany, where, besides the existing KASCADE [2] array, two new detector set ups (Grande and Piccolo) have been installed. The experiment is able to sample different components of extensive air showers (electromagnetic, muonic and hadronic) with high accuracy and covering a surface of 0.5 km^2 . For an overview of the actual setup of the KASCADE-Grande Experiment see ref. [3].

Muons are the messengers of the hadronic interactions of the particles in the shower and therefore are a powerful

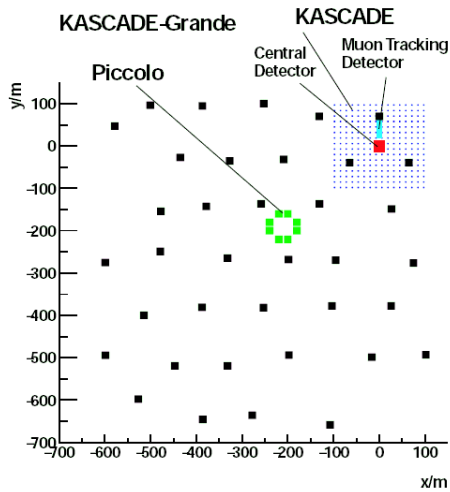


Figure 1: Representation of the KASCADE-Grande detectors.

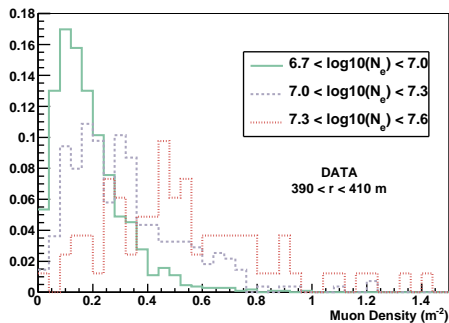


Figure 2: Distribution of the density of muons for three cuts in the total number of electrons.

tool to determine the primary particle mass and to study the hadronic interaction models.

In this article we present studies of the muon component of the showers. This paper is an update of a previous publication [1] in which the KASCADE-Grande Collaboration has shown the muon densities for the first time. In this contribution, we analyse two more years of data representing an substantial increase in the number of events. In this publication two extra hadronic interaction models are also tested: EPOS 1.99 and Sibyll 2.1.

2 Reconstruction

As explained in [1] and repeated here, the main parameters used in this study are the density of muons and the total number of electrons in the shower for which the reconstruction accuracy is going to be discussed below. For the reconstruction accuracy of the shower geometry see ref. [4].

The density of muons is directly measured by the KASCADE 622 m^2 scintillators. These detectors are shielded by 10 cm of lead and 4 cm of iron, corresponding to 20

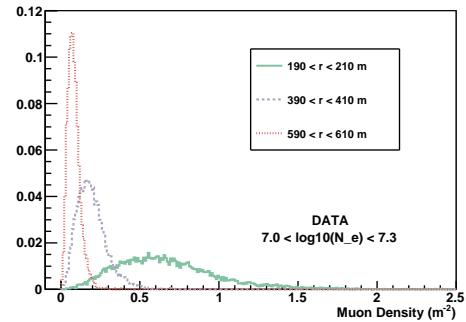


Figure 3: Distribution of the density of muons for three distances from the shower axis.

radiation lengths and a threshold of 230 MeV for vertical muons. The error in the measurement of the energy deposit was experimentally determined to be smaller than 10% [2].

For each shower, the density of muons is calculated as follows. The muon stations are grouped in rings of 20 m distance from the shower axis. The sum of the signals measured by all muon stations inside each ring is divided by the effective detection area of the stations. Therefore the muon density as a function of the distance from the shower axis is measured in a very direct way. No fitting of lateral distributions is needed in these calculations.

The total number of electrons in the shower is reconstructed in a combined way using KASCADE and KASCADE-Grande stations. A lateral distribution function (LDF) of the Lagutin type can be fitted to the density of muons measured by the KASCADE detector [5]. After that, using the fitted function, the number of muons at any distance from the shower axis can be estimated. The KASCADE-Grande stations measure the number of charged particles. The number of electrons at each KASCADE-Grande stations is determined by subtracting from the measured number of charged particles the number of muons estimated with the LDF fitted to the KASCADE stations.

At this stage, the number of electrons at each KASCADE-Grande station is known. Finally, a modified NKG [6] function is fitted to this data and the total number of electrons is determined in the fit.

Quality cuts have been applied to the events in this analysis procedure. We have required more than 19 KASCADE-Grande stations with signal. The showers used in all analyses along this paper were reconstructed with zenith angle between 0 and 42 degrees. The same quality cuts were applied to the simulated events used for reconstruction studies and to the data presented in the following section. After the quality cuts, the total number of electrons can be estimated with a systematic shift smaller than 10% and a statistical uncertainty smaller than 20% along the entire range considered in this paper [4].

Figure 2 shows the measured density of muons at three distances from the shower axis for events with a total number of electrons (N_e) in the range $7.0 < \text{Log}_{10}(N_e) < 7.3$

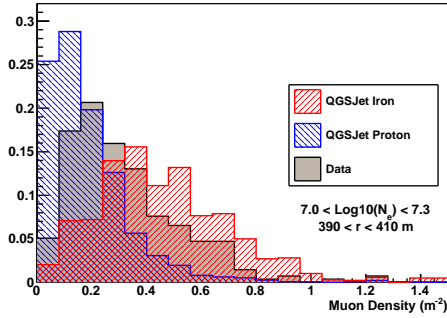


Figure 4: Measured distribution of the density of muons at 400 m compared to the predictions of QGSJet II.

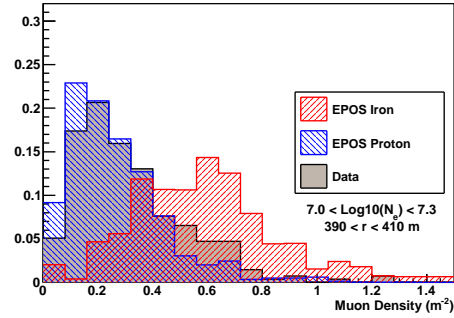


Figure 6: Measured distribution of the density of muons at 400 m compared to the predictions of EPOS 1.99.

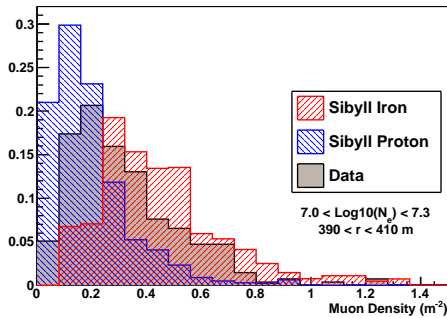


Figure 5: Measured distribution of the density of muons at 400 m compared to the predictions of Sibyll 2.1.

($\approx 10^{17}$ eV). Similar plots were obtained for other N_e ranges.

Figure 3 shows the density of muons at 400 m from the shower axis for events with total number of electrons (N_e) in the range $6.7 < \text{Log}_{10}(N_e) < 7.0$, $7.0 < \text{Log}_{10}(N_e) < 7.3$ and $7.3 < \text{Log}_{10}(N_e) < 7.6$. Similar plots were obtained for other distances from the shower axis.

Figure 2 and Figure 3 show the general expected trend: a) decrease of the muon density with increasing distance from the shower axis and b) increase of the muon density with increasing total number of electrons. In the next sections we explore these relations in order to show the capabilities of the KASCADE-Grande experiment for a composition study and for tests of the hadronic interaction models.

We present data for $7.0 < \text{Log}_{10}(N_e) < 7.3$ and $390 < r < 410$ m, these cuts have been chosen in order to minimize the fluctuation of the signal and the reconstruction inaccuracy and to maximize the number of showers for which we have data, however the same conclusions would be drawn for all parameter cuts.

3 Simulation

For all studies in this paper we have used the CORSIKA [7] simulation program with the FLUKA [8] option for low energy hadronic interactions. Three high energy hadronic

interaction models were used EPOS 1.99 [9], QGSJet II [10] and Sibyll 2.1 [11]. No thinning is used [7].

CORSIKA showers are simulated through the detectors and reconstructed in the same way as the measured data, such that a direct comparison between data and simulation is possible.

Figures 4, 6 and 5 show the comparison of the measured density of muons to values predicted by QGSJet II, EPOS 1.99 and Sibyll 2.1, respectively. For the three hadronic interactions models we show the limiting cases of proton and iron nuclei as primary particles. It can be seen in figures 4, 6 and 5 that the data lie well within the proton and iron limits for QGSJet II, EPOS 1.99 and Sibyll 2.1. These graphics are going to be further discussed in the next sections.

4 Analysis

Figure 7 shows the mean muon density as a function of the distance from the shower axis compared to the predictions of QGSJet II, EPOS 1.99 and Sibyll 2.1. The three hadronic interaction models bracket the data within the proton and iron limits for the entire range of distances from 100 to 720 meters. For distances further than 720 meters the statistics is not enough for a conclusion.

Interesting to note is also the slope of the LDF. Considering an equal probability trigger for protons and iron primaries as a function of distance from the shower axis, one can analyse the slope of the LDF as a test of the hadronic interaction models or as a composition parameters.

The intermediate distance from 200 to 600 m is the most significant range. For larger distance the statistical fluctuations dominates and at short distances the accuracy of the core position reconstruction impacts the measurements of the LDF resulting in a steeply falling curve as seen in figure 7.

It is clear that the measured LDF is not parallel to the QGSJet, nor EPOS 1.99 nor Sibyll 2.1 curves. That shows that the slope of the LDF cannot be well described by neither models if the composition is supposed to be dominated by only one light or only one heavy primary. If the compo-

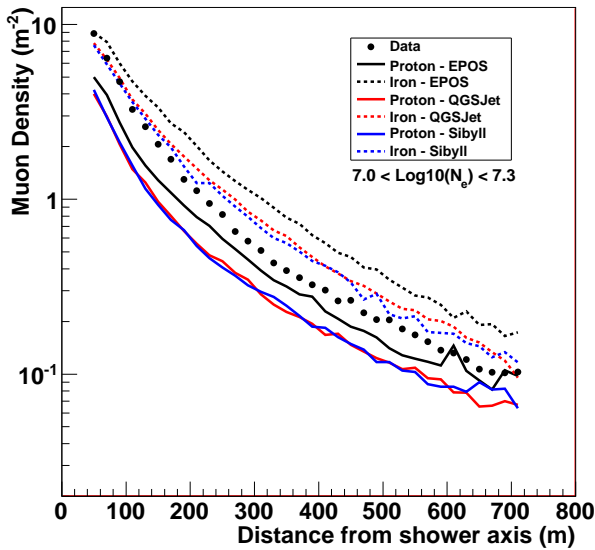


Figure 7: Lateral distribution of muons compared to the predictions of QGSJet II, EPOS 1.99 and Sibyll 2.1.

sition is mixed the slope varies with distance and the interpretation depends on the exact composition.

Figure 8 shows the evolution of the mean muon density as a function of N_e . The calculations done with QGSJet II, EPOS 1.99 and Sibyll 2.1 using proton and iron nuclei as primary particles bracket the data in the entire range of $5 < \text{Log}_{10}(N_e) < 8$.

Nevertheless, both figures 7 and 8 show that EPOS 1.99 would require a very light primary composition in order to fit the data. On the other hand, QGSJet II and Sibyll 2.1 could fit the data with an intermediate primary abundance between proton and iron nuclei.

Besides that, in figure 8 it is possible to analyse a possible transition of the primary component with increasing total number of electrons. The analysis done with both models show no abrupt change in the composition in the entire energy range.

5 Conclusions

The Grande array is in continuous and stable data taking since December 2003. The quality of the detector can be illustrated by the smooth data curve and small fluctuations in figures 7 and 8.

In this article, we have briefly described the procedure used to measure the density of muons with the KASCADE array and we have studied its correlation with the distance from the shower axis and the total number of electrons in the shower.

The density of muons in the shower is measured directly by the KASCADE detectors. We have used this data to study the hadronic interaction models QGSJet II, EPOS 1.99 and

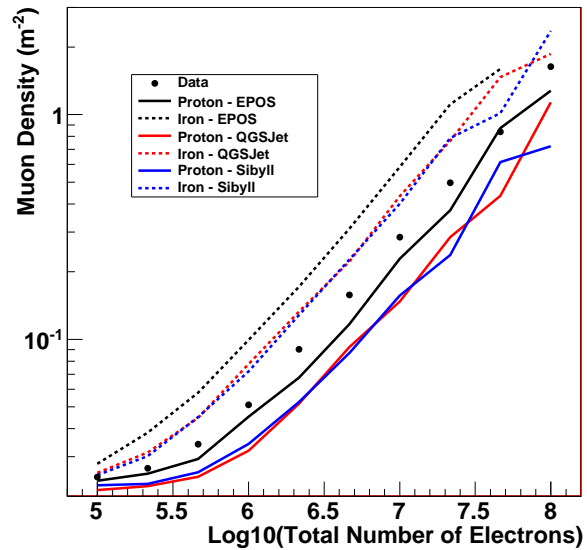


Figure 8: Muon density as a function of the total number of electrons compared to the predictions of QGSJet II, EPOS 1.99 and Sibyll 2.1.

Sibyll 2.1. The plots shown here are an update of the previous publication [1]

Figure 8 shows no abrupt change with increasing total number of electrons up to $\text{Log}_{10}(N_e) = 7.5 \approx 5 \times 10^{17}$ eV. The mean primary mass estimation would depend on the hadronic interaction model used.

References

- [1] V. de Souza *et al.* KASCADE-Grande Coll., Proc. 31th ICRC, Lodz (2009).
- [2] T. Antoni *et al.* KASCADE Coll., Nucl. Instr. and Meth. A 513, (2003) 490.
- [3] KASCADE-Grande Coll., Nucl. Instr. and Meth. A620 (2010) 202-216.
- [4] F. di Piero *et al.* KASCADE-Grande Coll., Proc. 31th ICRC, Lodz (2009).
- [5] D. Fuhrmann *et al.* KASCADE-Grande Coll., Proc. 31th ICRC, Lodz (2009)
- [6] K. Greisen, Progress in Cosmic Ray Physics 3 (1956) 1. K. Kamata and J. Nishimura, Suppl. Prog. Theor. Phys. 6 (1958) 93.
- [7] D. Heck *et al.*, Report FZKA 6019 (1998).
- [8] G. Battistonia *et al.*, ISVHECRI (2006) hep-ph/0612075v1.
- [9] K. Werner, M.F. Liu, and T. Pierog Phys. Rev. C 74 (2006) 044902.
- [10] S.S. Ostapchenko, Phys. Rev. D 74 (2006) 014026.
- [11] Eun-Joo Ahn *et al.*, Phys.Rev.D 80 - 094003 (2009).



On the primary mass sensitivity of muon pseudorapidities measured with KASCADE-Grande

J. ZABIEROWSKI¹ P. ŁUCZAK¹, P. DOLL², W.D. APEL², J.C. ARTEAGA-VELÁZQUEZ³, K. BEKK², M. BERTAINA⁴, J. BLÜMER^{2,5}, H. BOZDOG², I.M. BRANCUS⁶, P. BUCHHOLZ⁷, E. CANTONI^{4,8}, A. CHIAVASSA⁴, F. COSSAVELLA^{5,13}, K. DAUMILLER², V. DE SOUZA⁹, F. DI PIERRO⁴, R. ENGEL², J. ENGLER², M. FINGER⁵, D. FUHRMANN¹⁰, P.L. GHIA⁸, H.J. GILS², R. GLASSTETTER¹⁰, C. GRUPEN⁷, A. HAUNGS², D. HECK², J.R. HÖRANDEL¹¹, D. HUBER⁵, T. HUEGE², P.G. ISAR^{2,14}, K.-H. KAMPERT¹⁰, D. KANG⁵, H.O. KLAGES², K. LINK⁵, M. LUDWIG⁵, H.J. MATHES², H.J. MAYER², M. MELISSAS⁵, J. MILKE², B. MITRICA⁶, C. MORELLO⁸, G. NAVARRA^{4,15}, J. OEHLISCHLÄGER², S. OSTAPCHENKO^{2,16}, S. OVER⁷, N. PALMIERI⁵, M. PETCU⁶, T. PIEROG², H. REBEL², M. ROTH², H. SCHIELER², F.G. SCHRÖDER², O. SIMA¹², G. TOMA⁶, G.C. TRINCHERO⁸, H. ULRICH², A. WEINDL², J. WOCHLE², M. WOMMER²,

¹ *Soltan Institute for Nuclear Studies, Lodz, Poland*

² *Institut für Kernphysik, KIT - Karlsruher Institut für Technologie, Germany*

³ *Universidad Michoacana, Instituto de Física y Matemáticas, Morelia, Mexico*

⁴ *Dipartimento di Fisica Generale dell' Università Torino, Italy*

⁵ *Institut für Experimentelle Kernphysik, KIT - Karlsruher Institut für Technologie, Germany*

⁶ *National Institute of Physics and Nuclear Engineering, Bucharest, Romania*

⁷ *Fachbereich Physik, Universität Siegen, Germany*

⁸ *Istituto di Fisica dello Spazio Interplanetario, INAF Torino, Italy*

⁹ *Universidade São Paulo, Instituto de Física de São Carlos, Brasil*

¹⁰ *Fachbereich Physik, Universität Wuppertal, Germany*

¹¹ *Dept. of Astrophysics, Radboud University Nijmegen, The Netherlands*

¹² *Department of Physics, University of Bucharest, Bucharest, Romania*

¹³ *now at: Max-Planck-Institut Physik, München, Germany;* ¹⁴ *now at: Institute Space Sciences, Bucharest, Romania;* ¹⁵ *deceased;* ¹⁶ *now at: Univ Trondheim, Norway*
janjab@zpk.u.lodz.pl

Abstract: With the Muon Tracking Detector in the KASCADE-Grande experiment mean EAS muon pseudorapidities are investigated. Here we report on the results of studying the sensitivity of this quantity to the mass of primary cosmic ray particles. Obtained values of the mean logarithmic mass in the 10^{16} eV - 10^{17} eV range of primary energies, based on the QGSJetII - FLUKA interaction model combination, are compared with the results of other experiments. The validity of the model in reproducing experimentally measured pseudorapidity values and its comparison with the EPOS 1.99 is discussed.

Keywords: muons; air showers; pseudorapidity; mass composition; model tests.

1 Introduction

The Muon Tracking Detector (MTD) [1] is one of the detector components in the KASCADE-Grande EAS experiment [2] (see Fig.1), operated at the Karlsruhe Institute of Technology (KIT) - Campus North, in Germany, by an international collaboration. The MTD measures directions of muon tracks in EAS with excellent angular resolution of $\approx 0.35^\circ$. These directional data allow to investigate the longitudinal development of the muonic component in showers which is a signature of the development of the hadronic EAS core, being in turn dependent on the mass of the primary cosmic ray particle initiating a shower. Such

studies can be done either by the determination of a mean muon production height [3] or by using the mean pseudorapidity (η) of EAS muons, expressed in terms of their tangential (τ) and radial (ρ) angles (quantities reconstructed in the experiment) [4], [5]. In this work we investigate to what extent one can use the muon pseudorapidity for the determination of primary mass.

2 Muon pseudorapidities in KASCADE-Grande

In KASCADE-Grande muons can be registered up to 700 m from the shower core, but normally different anal-

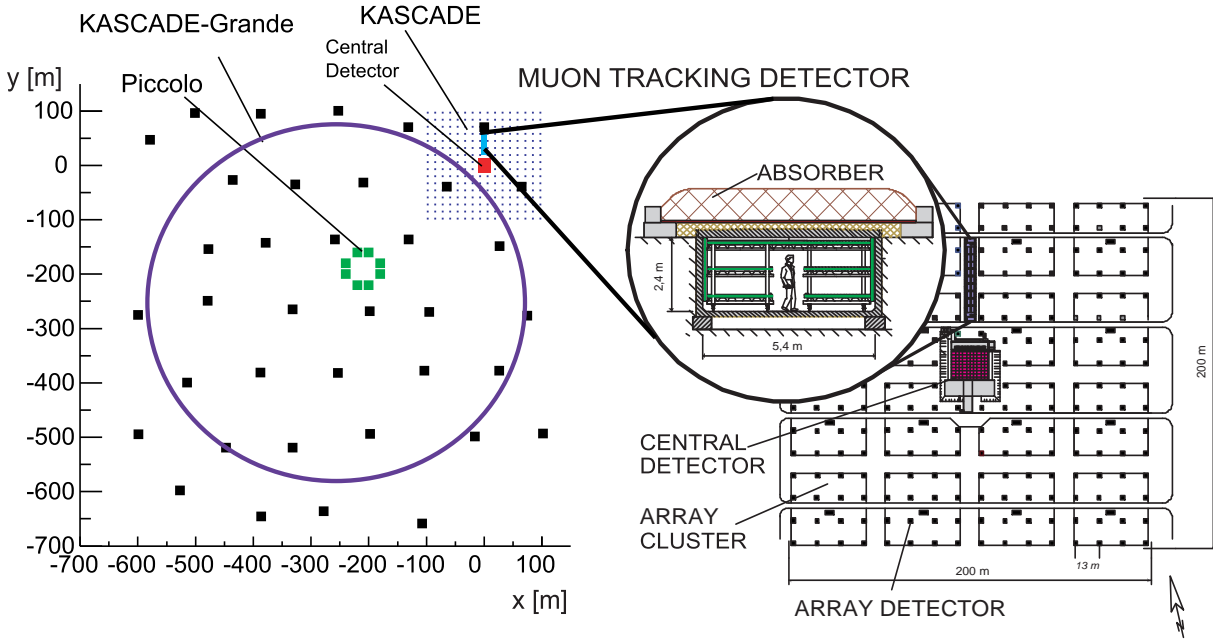


Figure 1: Layout of the KASCADE-Grande experiment distributed over the KIT - Campus North area. KASCADE is situated in the North-East corner of the Campus; note the position of the Muon Tracking Detector.

yses are carried out in specific distance ranges. In Fig. 2 lateral distribution of mean EAS muon pseudorapidities

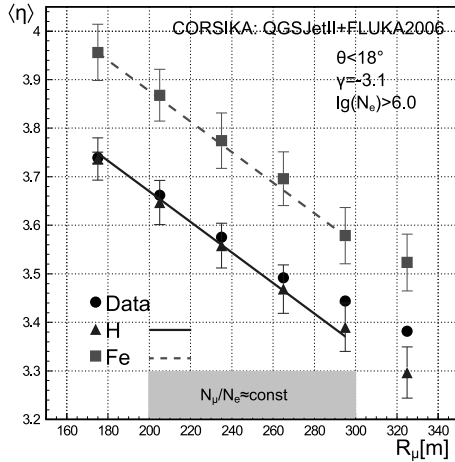


Figure 2: Lateral distribution of mean muon pseudorapidity in the limited distance range (see text) measured in KASCADE-Grande and compared with the CORSIKA simulation values for proton and iron primaries.

measured with the MTD in KASCADE-Grande are shown, together with the results of CORSIKA [6] Monte-Carlo simulations, employing a QGSJetII [7] and FLUKA2006 [8] model combination. Requirement of shower size $\log N_e > 6$ ensures full experiment trigger efficiency for registration, both, proton- and iron-initiated showers. Muons from iron showers are, per average, produced higher than those from proton showers, and this leads to the observed difference in the mean pseudorapidities on

ground, i.e., to the primary mass sensitivity of muon pseudorapidities. In Fig. 2 one can notice in the experimental data, below 200 m, a bias towards proton mass, resulting (for showers above 10^{16} eV) from some saturation effects in the MTD close to the shower core. Above 300 m, an increasing bias towards iron mass is observed, caused by non-equal MTD trigger efficiency for all types of primaries there. Therefore, all subsequent investigations are done in the distance range 200 m - 300 m, where, as it was checked with the N_μ/N_e ratio of showers used in the analysis, registration efficiency of the MTD is primary mass independent.

3 Mean logarithmic mass calculated with muon pseudorapidities

The distribution of measured muon pseudorapidity in the range 200-300 m from the shower core shows, that its mean value is contained between the simulated values for proton and iron primaries (Fig. 3).

In order to assess the average mass composition of cosmic rays with the standard $\langle \ln A \rangle$ procedure one has to be sure, that the mean muon pseudorapidity linearly depends on primary mass. The results of the linearity check are shown in Fig. 4. Here, the $\langle \ln A \rangle$ was calculated from η distribution for simulated carbon showers and compared with the known value $\ln 12 = 2.49$. The mean value of calculated $\ln A$ differs here by less than 2% from the true value for carbon primary, justifying the use of muon pseudorapidity for the determination of $\langle \ln A \rangle$ of cosmic rays above 10^{16} eV.

$\log[E_0/\text{GeV}]$ range	$\langle E_0 \rangle$ [GeV]	$\langle \ln A \rangle$ (QGSJetII-FLUKA)	$\langle \ln A \rangle$ EPOS1.99-FLUKA
7.0 – 7.3	$(1.38 \pm 0.01) \times 10^7$	0.4 ± 0.3	1.0 ± 0.5
> 7.0	$(2.23 \pm 0.01) \times 10^7$	1.1 ± 0.2	1.2 ± 0.3
7.3 – 7.6	$(2.69 \pm 0.01) \times 10^7$	1.6 ± 0.3	-
> 7.3	$(3.92 \pm 0.03) \times 10^7$	2.0 ± 0.2	1.5 ± 0.5
7.6 – 7.9	$(5.34 \pm 0.02) \times 10^7$	2.2 ± 0.5	2.4 ± 1.3
> 7.6	$(7.12 \pm 0.08) \times 10^7$	2.7 ± 0.4	3.5 ± 1.1
> 7.9	$(13.20 \pm 0.26) \times 10^7$	2.5 ± 1.4	-

Table 1: Results of the $\langle \ln A \rangle$ calculated in the $10^{16} - 10^{17}$ eV primary energy range for two high-energy interaction models.

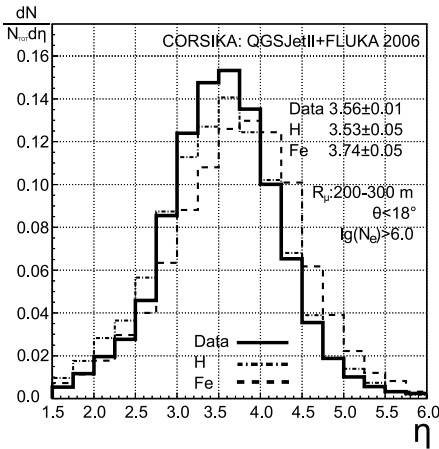


Figure 3: Distribution of measured muon pseudorapidity in the range 200-300 m from the shower core together with the simulation results for proton and iron initiated showers.

In the following the results for the primary energy decade $10^{16} - 10^{17}$ eV will be given. The primary energy was calculated using total number of charged particles and total number of muons in showers, with a procedure described in [9]. The energy ranges in which the $\langle \ln A \rangle$ was calculated are shown in the first column of Table 1. In the second column mean energy values, taking into account the spectrum with an index -3.1, are given. Columns 3 and 4 contain calculated $\langle \ln A \rangle$ values for QGSJetII and EPOS 1.99 [10], respectively. Due to the very limited statistics of available simulations with EPOS not in all energy bins the calculation was possible. In those, where it was possible, the errors (only statistical were considered) are, anyway, much larger than in case of the QGSJetII.

The results from columns 3 and 4 of Table 1 are presented in Fig. 5, together with a collection of $\langle \ln A \rangle$ values (taken from Fig. 14 (top) in Ref. [11]) derived from the average depth of the shower maximum by various experiments.

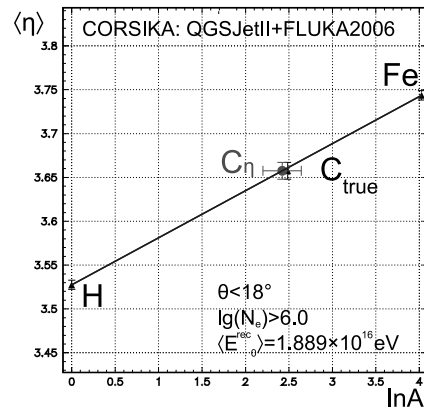


Figure 4: Test of the linear dependence of mean EAS muon pseudorapidity on the logarithm of primary mass. Triangles - simulated $\langle \eta \rangle$ values for H, C and Fe versus true $\ln A$ on the x-axis. A full circle - $\langle \ln A \rangle$ calculated for carbon, using its $\langle \eta \rangle$ value.

4 Discussion and conclusions

As seen in Fig. 5 our results, obtained with EAS muons pseudorapidity measured on ground level, are compatible with the collection of mean logarithmic mass values derived from the average depth of the shower maximum. They show similar rise of $\langle \ln A \rangle$ with energy in the investigated primary energy range. This compatibility, rather with the results obtained from measurement of the light generated during the shower development than the ones measured on ground (e.g. electron/muon ratio) is because the mean muon pseudorapidity is also a signature of shower development.

Obtained values are generally lower than those from other experiments. The main reason for this can be, that the QGSJetII model, despite improvement with respect to QGSJet01, gives still too high mean pseudorapidity values compared with the measurements.

It was found in previous studies (e.g. [12]), that in the investigated distance range from the core about 40 % of the registered muons is produced in the hadronic interactions above 200 GeV, i.e., they are modeled in the simulations

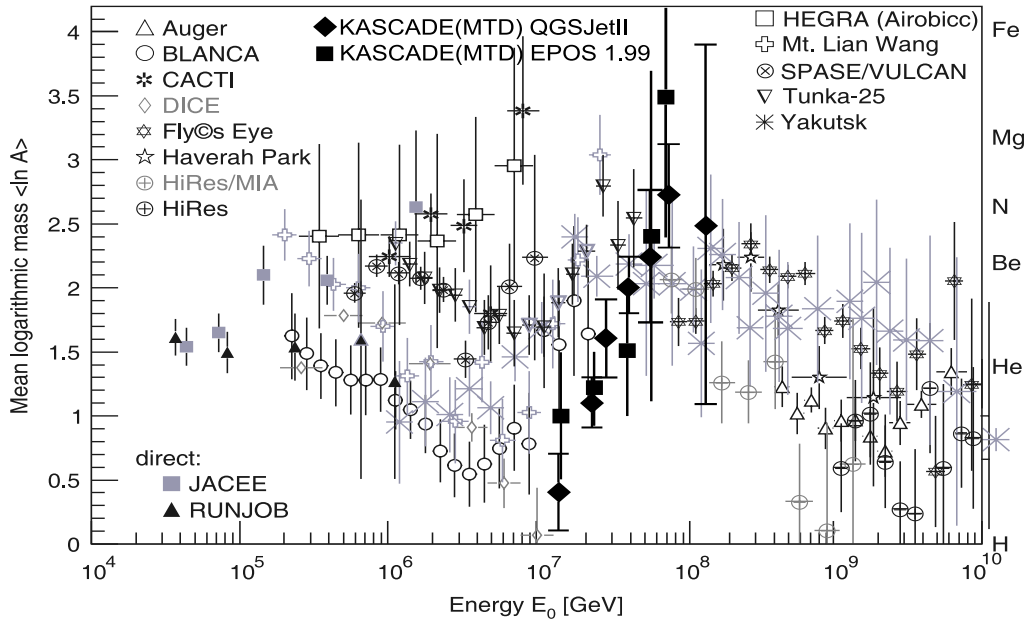


Figure 5: Results of mean logarithmic mass values obtained with mean muon pseudorapidities, shown together with the values derived from the average depth of the shower maximum by different experiments, from Fig. 14 (top) of Ref. [11].

by QGSJetII. And this model creates more muons at the heights above 4-5 km, than observed experimentally [3]. Such muons have higher mean muon pseudorapidity than the ones created deeper in the atmosphere [13], thus affecting the determination of the $\langle \ln A \rangle$.

The mean pseudorapidity values obtained in simulations suffer from the insufficient shower statistics in the simulations. A standard approach is to use the same simulated shower 5 or 10 times over the detector area in order to reduce the time needed for simulations to acceptable value. In this particular investigation such an approach creates additional, systematic error in the determination of $\langle \ln A \rangle$, impossible to be quantified without using each simulated shower once, what would require very significant increase of the simulation time.

In Fig. 5 some $\langle \ln A \rangle$ values obtained with the EPOS 1.99 model are shown for the comparison. Due to the much smaller number of simulated data the statistical errors are much larger than in case of QGSJetII (see also Table 1). Moreover, the above mentioned effect of shower statistics is influencing the results even more.

One can say that the general behaviour showing rise of the primary mass with the energy is also seen with this model, however it is not possible to compare the values of the logarithmic mass predicted by the two models in question.

In conclusion, the mean muon pseudorapidity in EAS is a primary mass sensitive parameter and, providing the large enough number of simulated showers is available for the analysis, the $\langle \ln A \rangle$ of primary cosmic rays can be derived. However, the small difference between $\langle \eta \rangle$ values for proton and iron initiated showers (≈ 0.2) would require a significant increase in the number of simulated showers and, even then, the remaining uncertainties would prohibit

to make a convincing mass composition studies with, at least, 3 mass groups.

Acknowledgement: KASCADE-Grande is supported by the BMBF of Germany, the MIUR and INAF of Italy, the Polish Ministry of Science and Higher Education (this work by grant for 2009-2011) and the Romanian Authority for Scientific Research.

References

- [1] P. Doll et al., NIM A **488** (2002) 517.
- [2] W.D. Apel et al. (KASCADE-Grande Collaboration), NIM A **620** (2010) 202.
- [3] W.D. Apel et al., (KASCADE-Grande Collaboration), Astrop. Phys. **34** (2011) 476.
- [4] J. Zabierowski, K. Daumiller and P. Doll, Nucl. Phys. B (Proc. Suppl.) **122** (2003) 275.
- [5] J. Zabierowski et al. (KASCADE Collaboration), Nucl. Phys. B (Proc. Suppl.) **151** (2006) 291.
- [6] D. Heck et al., Report FZKA 6019, Forschungszentrum Karlsruhe, 1998.
- [7] S.S. Ostapchenko, Nucl. Phys. B (Proc. Suppl.) **151** (2006) 143&147; S. Ostapchenko, Phys. Rev. D **74** (2006) 014026.
- [8] A. Fassò et al., Report CERN-2005-10, INFN/TC-05/11, SLAC-R-773 (2005).
- [9] M. Bertaina et al.,(KASCADE-Grande Collaboration), Proc.22nd ECRS, Turku, Finland, 3-6.08.2010, Astrophys. Space Sci. Trans.,7,XX-XX,2011
- [10] K. Werner, F.M. Liu, T. Pierog, Phys. Rev. C **74** (2006) 044902.
- [11] J. Blümer, R. Engel and J.R. Hörandel, Prog. Part. and Nucl. Phys., **63** (2009) 293.
- [12] J. Zabierowski et al. (KASCADE-Grande Collaboration), Nucl. Phys. B (Proc. Suppl.) **196** (2009) 114.
- [13] J. Zabierowski et al.,(KASCADE-Grande Collaboration), Proc.31th ICRC, Lodz, Poland (2009) #171, FZKA Report 7516, Forschungszentrum Karlsruhe (2009) 37.



Gamma-Ray Source Studies using a Muon Tracking Detector (MTD)

P. DOLL¹, K. DAUMILLER¹, J. ZABIEROWSKI¹¹, W.D. APEL¹, J.C. ARTEAGA-VELÁZQUEZ², K. BEKK¹, M. BERTAINA³, J. BLÜMER^{1,4}, H. BOZDOG¹, I.M. BRANCUS⁵, P. BUCHHOLZ⁶, E. CANTONI^{3,7}, A. CHIAVASSA³, F. COSSAVELLA^{4,13}, V. DE SOUZA⁸, F. DI PIERRO³, R. ENGEL¹, J. ENGLER¹, M. FINGER⁴, D. FUHRMANN⁹, P.L. GHIA⁷, H.J. GILS¹, R. GLASSTETTER⁹, C. GRUPEN⁶, A. HAUNGS¹, D. HECK¹, J.R. HÖRANDEL¹⁰, D. HUBER⁴, T. HUEGE¹, P.G. ISAR^{1,14}, K.-H. KAMPERT⁹, D. KANG⁴, H.O. KLAGES¹, K. LINK⁴, P. ŁUCZAK¹¹, M. LUDWIG⁴, H.J. MATHES¹, H.J. MAYER¹, M. MELISSAS⁴, J. MILKE¹, B. MITRICA⁵, C. MORELLO⁷, G. NAVARRA^{3,15}, J. OEHLISCHLÄGER¹, S. OSTAPCHENKO^{1,16}, S. OVER⁶, N. PALMIERI⁴, M. PETCU⁵, T. PIEROG¹, H. REBEL¹, M. ROTH¹, H. SCHIELER¹, F.G. SCHRÖDER¹, O. SIMA¹², G. TOMA⁵, G.C. TRINCHERO⁷, H. ULRICH¹, A. WEINDL¹, J. WOCHLE¹, M. WOMMER¹

¹ *Institut für Kernphysik, KIT - Karlsruher Institut für Technologie, Germany*

² *Universidad Michoacana, Instituto de Física y Matemáticas, Morelia, Mexico*

³ *Dipartimento di Fisica Generale dell' Università Torino, Italy*

⁴ *Institut für Experimentelle Kernphysik, KIT - Karlsruher Institut für Technologie, Germany*

⁵ *National Institute of Physics and Nuclear Engineering, Bucharest, Romania*

⁶ *Fachbereich Physik, Universität Siegen, Germany*

⁷ *Istituto di Fisica dello Spazio Interplanetario, INAF Torino, Italy*

⁸ *Universidade São Paulo, Instituto de Física de São Carlos, Brasil*

⁹ *Fachbereich Physik, Universität Wuppertal, Germany*

¹⁰ *Dept. of Astrophysics, Radboud University Nijmegen, The Netherlands*

¹¹ *Soltan Institute for Nuclear Studies, Lodz, Poland*

¹² *Department of Physics, University of Bucharest, Bucharest, Romania*

¹³ *now at: Max-Planck-Institut Physik, München, Germany;* ¹⁴ *now at: Institute Space Sciences, Bucharest, Romania;* ¹⁵ *deceased;* ¹⁶ *now at: Univ Trondheim, Norway*
paul.doll@kit.edu

Abstract: A large area ($128m^2$) streamer tube detector, located within the KASCADE-Grande experiment, has been built with the aim to identify muons and their directions from extensive air showers by track measurements. We discuss the possibility of observation of Gamma-Ray sources by means of single isolated muons above the background of cosmic-ray muons using a muon tracking detector (MTD) exhibiting good angular resolution. Properties of the pion photo-production process and of the MTD which support the identification of Gammas are discussed. Preliminary Gamma spectrum accumulated from Crab and the Mkn421 flux correlation with X-ray (RXTE/PCA) are presented.

Keywords: gamma ray sources, muon tracking

1 Introduction

A reliable understanding of the muon production by primary gamma-rays is mandatory to gauge the sensitivity of the experiment to gamma primaries. The Vector Meson Dominance Model is usually employed for photo-nuclear interactions at gamma energies above a few GeV. To illustrate the critical role played by the event generators in predicting the muon content of showers, the Feynman-x distribution of charged pions (in the laboratory frame) as calculated by the FLUKA code demonstrates [1] a basic difference between gamma and proton-induced collisions: The gamma primaries lead to a much larger fraction of

high-x secondaries than the proton primaries, therefore, focussing the pions to very forward direction, and, therefore, compensating for the much smaller pion photo-production cross section.

High energy gamma rays produce muons in the Earth's atmosphere that can be detected and reconstructed in relative shallow underground muon detectors. Such detectors are sensitive to muon energies of a few GeV. Although muons of such low energy compete with a large background of cosmic ray muons, they can be identified provided the detector has sufficient effective area and resolution. Unlike air-Cherenkov telescopes [2, 3, 4] muon detectors cover a large fraction of the sky with a large duty cycle. The advan-

tage is considerable in studying the emission from highly variable sources. Moreover, background multi-muon bundles can be conveniently rejected without suppression of the predominantly single-muon gamma signal.

Detected muons originate in gamma induced pion production with some 20 times higher gamma energies [5]. A low energy threshold for muon detection provides for the correspondingly low energy gammas a deep view into the Universe. Muons of $E_\mu > 1 \text{ GeV}$ associated with primary photons of several GeV provide an almost attenuation-free window into the depth of the universe suffering little from flux losses due to collisions with IR and CMB radiation via pair production.

2 Muons from Gammas

Gamma rays initiate atmospheric cascades of mostly electrons and photons, but also some muons. Muons originate from the decay of charged pions which are also photo-produced by high energy shower photons [6] albeit with much smaller cross section.

The signal-to-noise ratio, defined as the number of events divided by the square root of the number of background events in a resolution pixel of $\sigma^\circ \times \sigma^\circ$, depends on the detector area A and the zenith angle Θ as [6]: $S/N^{1/2} = A^{1/2}/\cos\Theta^{0.9}\sigma$. The formula simply expresses that the signal-to-noise ratio is improved for increased area A , better resolution σ and sources observed at larger zenith angle Θ , where the cosmic ray background muon rate is reduced.

The MTD [7] is sensitive to the gamma energy region above $\sim 10 \text{ GeV}$ while the muon energy cut equals to 0.8 GeV .

As mentioned above the background includes some fraction of multi-muon events. Rejecting multi-muon events not only improves the signal-to-noise ratio, it also improves the angular resolution which may be degraded by less reliable reconstruction of complex muon bundles initiated by high energy cosmic ray particles which are accompanied by other shower particles. MTD with its detection area of $A_{MTD} = 128\text{m}^2$ has below the shielding an average rate of 2.5kHz which results above an energy of 0.8 GeV in $\sim 10^7$ tracks from background muons per year in a $1^\circ \times 1^\circ$ pixel. Assuming a further reduction because of the strong focusing of the gamma induced muons by about 10, this rate may lead for Crab [6] to $S/N^{1/2} = 40$ for one year of running.

3 Muon Tracking Detector (MTD)

The MTD [7] is built out of Streamer Tube (ST) chambers of 4 m length and located in the KASCADE-Grande experiment [9]. The ST chambers are grouped in, so called, *modules*. Four modules, three positioned on horizontal planes (top, middle, bottom) and one arranged vertically (wall), form a muon telescope. The whole detector comprises 16

telescopes arranged in two rows. The low mass structure of the detector design reduces secondary interactions in the sensitive detector part.

To deal with clean muon tracks an efficient filter absorbing a large fraction of the low energy electromagnetic component of proton induced showers is mandatory. The larger Bethe-Heitler cross-section induced showers for gammas leading to pair production and subsequent electromagnetic cascade are readily absorbed by the filter. The energy threshold (0.8 GeV) is suitable for background reduction. Following the characteristic energy $\epsilon_\mu = m_\mu c^2 6.4\text{km}/\tau_\mu c \sim 0.8 \text{ GeV}$ muons from proton induced showers do not survive over the path length of 6.4 km and with energies close to the MTD threshold but decay to electrons which are readily absorbed. Photo-nuclear produced muons survive more easily because of comparatively lower production height. This situation improves the S/N ratio for photon detection. The stability of the MTD [7] is very good. The detector gas system follows precisely the atmospheric gas pressure.

The first-level γ /proton discrimination is mostly achieved by the characteristics of the MTD. The ratio of the number of hits in the top module to the track number N_{hit}^{top}/N_{track} in each tower is a powerful tool in discriminating against hadron induced air showers. Only tracks with one hit in each module are accepted. Only hits with small cluster size 'cls' (clusters of readout wires or readout strips) are accepted. The background of high energy electrons or hadrons is further reduced by cuts in the track quality Q^2 (see [7]). Showering electrons or hadrons lead to larger 'cls' and, therefore, smaller Q^2 .

For the subsequent analysis the following cuts in the data have to be employed: 1) Only data over one full sidereal day (86163 solar seconds) are considered. 2) Only sidereal days where all 16 telescopes are functioning are used. 3) The daily rate should follow a Gaussian distribution, and only days with rate within $\pm 4\sigma$ are accepted. 4) Only data corrected for pressure and temperature in the atmosphere and in the detector are included.

4 Gamma-Source Search

To identify sources which emit high energy gammas and which are with small probability converted to single muons deep in the atmosphere, we have the possibility to restrict the arrival direction and arrival time. The restriction in time and direction has the task to reduce other disturbing sources like the Sun. We have to cope with about 3 orders of magnitude larger background from cosmic ray muons in a canonical $1^\circ \times 1^\circ$ window in the sky.

The optimal square bin size for the search of a point gamma-ray source with the MTD is 1° on a side, corresponding to a Gaussian angular resolution of about 0.3° .

For the search of point sources, the fluctuation of events in a fixed direction of the sky is investigated. When examining the fluctuation of the number of muon events bin by bin and

searching for possible sources with a muon event excess, we employ the numbers N_{on} , T_{on} , N_{off} , T_{off} . We use Li-Ma [10] formula to examine the fluctuation of the number of muon events bin by bin and to search for possible muon event excess. In the current analysis this procedure is used with bin size $\Delta\delta = 0.25^\circ$ and $\Delta\alpha = \Delta\delta/\cos\delta$, confined to specific regions on the sky to investigate the MTD sensitivity to specific gamma-ray sources. Only specific track directions in Θ and Φ and only specific arrival time intervals, where the corresponding source is high (winter months for Crab) ($\Theta_{source} < 35^\circ$) are chosen to accumulate clean single muon events in the δ versus α (declination versus right ascension) plane.

The analysis shows that the strong requirements of only 1 hit in each detector module and all $cls < 3$ give good profiles for Crab and Mkn421.

Observation of Mkn421 with the ARGO-YBJ experiment is reported by S.Vernetto et al. [11]. The FERMI view of the TeV blazar Mkn421 is given in [12] and the MAGIC observations of Mkn421 and related optical/X-ray/TeV multiwavelength studies are reported in [13]. Mkn421 is a very active Galaxy nucleus showing strong variation in the X-ray and TeV Gamma-ray fluxes and appears at 38.3° , $11.08 h$ which is 0.1° closer to the zenith and 0.15° later in time than the nominal position. The muon intensity is sampled and weighted with the actual MTD efficiency and smoothed afterwards. Again, only data epochs are considered when Mkn421 is high. Interestingly, the source profile is improved when employing days (properly matched in time) for which appreciable X-ray flux ($> 2.5 photons/day$) is reported [15]. For the Mkn421 source a correlation analysis with the X-ray flux measurements by the All-Sky-Monitor (ASM) onboard the RXTE-satellite [15] was performed providing the correlation as shown in Fig. 1. The picture exhibits a clear correlation between the time averaged (1 day) high energy muon flux and the time averaged X-ray flux above $2 keV$. A narrow window around the nominal Mkn421 position improves the correlation in Fig. 1. Also a correlation between the muon flux from the MTD in the region of Mkn421 and the gamma flux in the GeV range recorded by FERMI satellite [16] is observed. The dashed line in Fig. 1 represents a fit to the correlation and deserves further studies. Employing days with almost constant X-ray activity from Mkn421, the conversion of GeV gammas into muons in the atmosphere above the MTD can be investigated. Fig. 2 shows the correlation of the muon rate with the atmospheric pressure overburden. It shows the strong gain of photo-produced pions with pressure especially after correction (solid points in Fig. 2) for the pressure dependent track detection efficiency of the MTD [7]. The strong dependence of the muon rate on the atmospheric pressure suggests the pion photo-production to occur in the lower atmosphere.

Fig. 3 shows for Crab a two-dimensional multi-quadric interpolation [8] of the data points in the δ versus α (declination versus right ascension) plane (in the boundaries of a MAGIC presentation). The contour scale is in units of

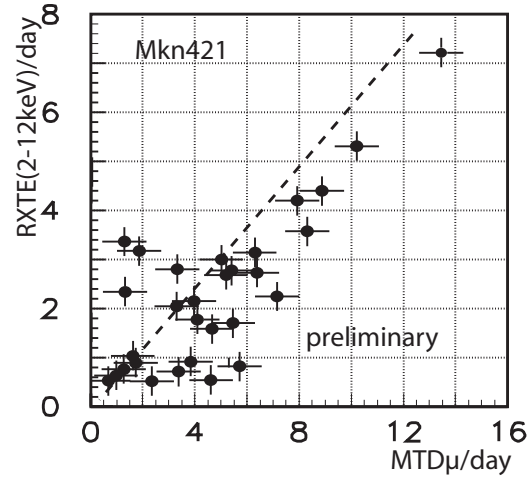


Figure 1: Correlation of the X-ray flux with the muon rates in a narrow window around the nominal Mkn421 position. Data were taken in a high flux period during February 2010. The dashed line emphasizes a linear dependence between the X-ray flux and the GeV gamma ray flux. So far, only fraction of all data are considered.

excess counts per smoothing radius. The position of the source as quoted by the MAGIC group [14] is given by the cross. The displacement of the source to larger zenith Θ , and smaller azimuth Φ , and possible deformation is due to the geomagnetic field B_{geo} and is expected to depend on the momentum of the muons and their orientation with respect to the geomagnetic field components.

Gamma-ray induced muons in the deep atmosphere we expect to be almost charge symmetric. Therefore, the spread of the source profile is reproducing the muon momentum distribution. Muons are considered to exhibit negative charge if they are deflected towards the East from the line connecting the actual Crab position with the geomagnetic field direction. Mean deflection of about 0.6° is expected for 1 GeV muons created 1 km above ground. Only negatively charged muons to the East side of the source are considered for accumulating an angle-distance spectrum. The frequency of muon tracks as function of $1/distance$ to the nominal Crab source position is plotted in the Fig. 4. resulting in steep falling spectrum. The inverse angle-distance is expressed in muon momentum, assuming a $\sim p_\mu \times B_{geo}$ dependence. Assuming further that muons at threshold ($0.8 GeV$) stem from gammas about 10 times higher in momentum would provide a preliminary gamma energy scale. The preliminary flux normalization considers the gamma flux attenuation in the air, the small $\sigma_{\gamma\pi}$ cross section on air, the mass density of the atmosphere and the momentum dependence of the $\pi \Rightarrow \mu$ conversion rate and the exposure of the MTD. The dashed line represents a $flux_\mu \sim p_\mu^{-2}$ flux dependence. A more detailed unfolding of the gamma source spectrum has still to be carried out.

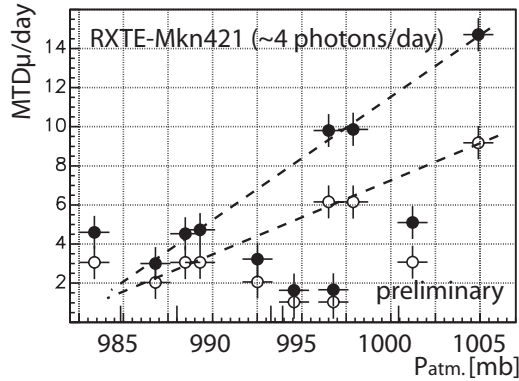


Figure 2: Variation of the photo-pion production yielding muons with atmospheric pressure for a window of almost constant X-ray flux from Mkn421 (see Fig. 1, dashed region). The full symbols consider the effect of the MTD track detection efficiency.

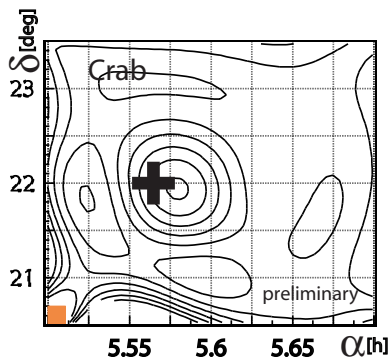


Figure 3: Muon yield close to the nominal Crab position in a $3^\circ \times 3^\circ$ field of view. The cross represents the Crab position after MAGIC [14]. The contour lines vary in 25% steps. So far, only fraction of all data are considered.

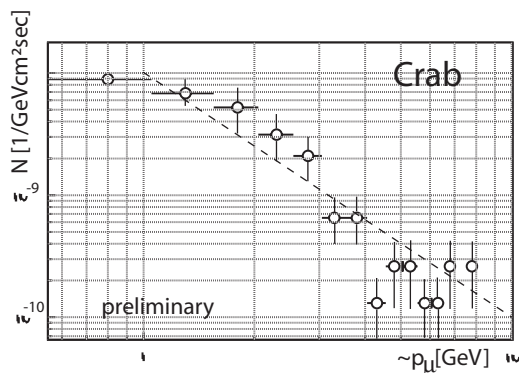


Figure 4: Muon flux variation derived as function of the inverse distance from the nominal source position and expressed in momentum units above the muon momentum threshold of the MTD (0.8 GeV). So far, only fraction of all data are considered.

5 Outlook

The high resolution muon tracking detector MTD in the KASCADE-Grande experiment demonstrates to be capable to identify gamma point sources in the sensitivity range of Crab fluxes. The highly variable gamma source Mkn421 provides in its 'high' state a test beam to study the efficiency of $\gamma \Rightarrow \mu$ conversion in the atmosphere depending on the atmospheric parameters, and further tuning of the MTD response to gammas. Future analysis of a larger data sample will provide more detailed information on the nature of high energy gamma source muons. There is a common understanding that the high energy gamma source muons serve as sensitive probes to investigate the high energy photon interactions in the atmosphere, providing a gamma detector in the multi-GeV range.

Acknowledgement: KASCADE-Grande is supported by the BMBF of Germany, the MIUR and INAF of Italy, the Polish Ministry of Science and Higher Education (this work in part by grant for 2009-2011) and the Romanian Authority for Scientific Research.

References

- [1] A.Fasso and J.Poirier, *Phys.Rev.* **D63** (2001) 036002
J. Gress *et al.*, *Nucl. Instr. and Meth.* **A302** (1991) 368.
- [2] V.A. Acciari *et al.*, VERITAS Coll. arXiv:1012.2200
- [3] S. Klepser *et al.*, MAGIC Coll. arXiv:1104.0863
- [4] A. Abramowski *et al.*, HESS Coll. arXiv:1104.2548
- [5] P.Achard *et al.*, L3 Coll., *Astrop. Phys.* **25** (2006) 298
P.LeCoultre *et al.*, *Nucl.Phys. B (Proc.Suppl.)* **122** (2003) 161
- [6] T.K.Gaisser,F.Halzen,T.Stanev and E.Zas, *Phys.Lett.***B243** (1990) 444
F.Halzen,T.Stanev and G.B. Yodh, *Phys.Rev.* **D55** (1997) 4475
T.K.Gaisser,F.Halzen and T.Stanev, *Phys. Reports* **258** (1995) 173.
- [7] P. Doll *et al.*, *Nucl. Instr. and Meth.* **A488** (2002) 517.
W.-D. Apel *et al.*, (KASCADE-Grande Coll.), *Astrop. Phys.* **34** (2011) 476.
- [8] J. Allison , *Comp. Phys. Comm.***A 77** (1993) 377.
- [9] W.-D. Apel *et al.*, *Nucl. Instr. and Meth.* **A620** (2010) 202.
- [10] Ti-Pei Li and Yu-Qian Ma, *The Astroph.Jour.*, **272** (1983) 317.
- [11] S. Vernetto *et al.*, ARGO-YBJ Coll. Proceed. 31th. ICRC (2009), Lodz, Poland
M. Amenomori *et al.*, Tibet AS γ Coll. *ApJ* **580** (2002) 887.
- [12] D. Paneque *et al.*, FERMI-LAT Coll. Proceed. 31th. ICRC (2009), Lodz, Poland
- [13] G. Bonnoli *et al.*, MAGIC Coll. Proceed. 31th. ICRC (2009), Lodz, Poland
- [14] E. Aliu *et al.*, MAGIC Coll. *Science* **322** (2008) 1221
- [15] <http://www.swift.psu.edu/monitoring>
- [16] <http://fermi.gsfc.nasa.gov/ssc/data/policy/>
- [17] <http://xte.mit.edu/asmlc/ASM>